ENERGY LEVELS IN Pt^{192} and Pt^{194}

ENERGY LEVELS IN Pt^{192} and Pt^{194}

by

JOHN DUNCAN MacARTHUR, B.Sc.

A Thesis

Submitted to the Faculty of Graduate Studies

in Partial Fulfilment of the Requirements

for the Degree

Doctor of Philosophy

McMaster University

October 1962

DOCTOR OF PHILOSOPHY (1962) McMASTER UNIVERSITY
Hamilton, Ontario

(Physics)

TITLE: Energy Levels in Pt^{192} and Pt^{194}

AUTHOR: John Duncan MacArthur, B.Sc. (University of Western Ontario)

SUPERVISOR: Professor M. W. Johns

NUMBER OF PAGES: (ix), 193

SCOPE AND CONTENT:

The technique of recording coincidence events has been applied in the study of several nuclei.

Two platinum nuclides have been investigated experimentally through the use of two types of coincidence spectrometers. For both these nuclei, Pt^{192} and Pt^{194}, the investigation included beta-gamma experiments which measured the intensities of the beta groups feeding some of the levels in these nuclei and directional correlation experiments which determined the spins of some of their excited states. A study of the gamma-gamma coincidences of Pt^{194} confirmed the decay scheme proposed by previous workers.

The directional correlation of the one cascade in Co^{58} forms the part of the paper present in Chapter IV.

Finally, the appendices contain a description of an apparatus for the preparation of beta sources and an explanation of a set of experiments designed to calibrate the gamma-gamma coincidence spectrometer for its tasks.

ACKNOWLEDGEMENTS

I wish to thank Professor M.W. Johns for his guidance and enthusiastic support during my endeavours at this university.

To the members of my Supervisory Committee, Dr. M. W. Johns, Dr. H. Petch and Dr. M. A. Preston, I should like to express my thanks for their help.

Without the financial assistance of the Woodrow Wilson Fellowship Foundation and the National Research Council, the years spent at this university would not have been possible. Therefore I gratefully acknowledge their generosity.

Finally, to my wife who deciphered my writing and edited this thesis, and to Miss Josephine Donovan, who bravely typed the final manuscript, I wish to express my sincere appreciation.

TABLE OF CONTENTS

	Page
INTRODUCTION	1
CHAPTER I - RADIATION AND ANGULAR DISTRIBUTIONS	4
Introduction	4
Spin and Parity	4
Electromagnetic Transitions	6
Internal Conversion	10
Angular Correlations	12
Beta Decay	17
CHAPTER II - NUCLEAR MODELS	22
Introduction	22
A. Shell Model	23
Introduction	23
Independent Particle Model	24
Shell Model with Residual Internucleon Forces	26
B. Collective Model	28
Introduction	28
Vibrational Model	29
Beta and Gamma Vibrations	33
Deformed Shell Model	34
Asymmetric Rotator	37
CHAPTER III - THE EQUIPMENT AND THE EXPERIMENTAL METHOD	40
Introduction	40
Scintillation Spectrometer	41
Directional Correlation Experiment	44
Double Lens Magnetic Spectrometer	50
Coincidence Circuitry	51
Theory of Coincidence Counting	59
Chance	64
CHAPTER IV - Co^{58}	67
Introduction	67

Page

The Paper - The Decay of Co^{58} 68
Abstract 68
Introduction 69
Coincidence Measurements 69
Angular Correlation Function for δ_1 and δ_2 73
Intensity of δ_2 from the Coincidence Measurements 75
Intensity and Energy of Cross-Over Gamma Ray 77
Magnetic Spectrometer Measurements 77
Experimental Results 80
The Fermi Admixture in the Decay of Co^{58} 81
References 84
Acknowledgements 84
Discussion 85

CHAPTER V - Pt^{192} 88

Introduction 88
A. Directional Correlation 91
Introduction 91
Experimental Method 92
Results 96
(1) The 1065-316 kev Cascade 96
(2) The 885-316 kev Cascade 98
(3) The 478-316 kev Cascade 101
Discussion 102
(1) The 1201-kev Level 102
(2) The 1381-kev Level 102
B. Beta-Gamma Coincidences 104
Introduction 104
Experimental Method 104
Results 107
(1) Coincidences Between the 467-kev Gamma Rays and Beta Rays 107
(2) Coincidences Between the 600-kev Gamma Rays and Beta Rays 109
(3) Coincidences Between the 300-kev Gamma Rays and Beta Rays 111
(4) Intensities of the Beta Groups 111
Discussion 117
Conclusions 123

CHAPTER VI - Pt^{194} 125

Introduction 125

Page

A. Coincidence Experiments on the Decay Scheme of Ir^{194} 126
Introduction 126
Experimental Methods 128
Results 135
(1) Coincidence Relationships 136
(2) Gamma Ray Intensity Measurements 140
(3) Beta-Gamma Coincidence Experiments 144
Discussion 153
B. Directional Correlation Experiments 159
Introduction 159
Experimental Methods 160
Results 161
(1) The 940-328 kev Cascade 161
(2) The 1450-328 kev Cascade 161
(3) The 1160-328 kev Cascade 163
Discussion 166
(1) The 1267-kev Level 166
(2) The 1779-kev Level 166
(3) The 1480- and 1512-kev Levels 167
Conclusions 169

APPENDIX I - CATHODE SPUTTERING 171

Introduction 171
The Apparatus 171
Sputtering 172
Source Preparation 174

APPENDIX II - CALIBRATION OF THE NaI(Tl) DETECTORS 176

A. Photopeak Detection Efficiencies 176
Introduction 176
Experimental Method 177
Results 180
B. Directional Correlation Correction Factors 182
Introduction 182
Experimental Method 182
Results 183
Conclusions 186

REFERENCES 187

LIST OF FIGURES

Figure No.		Page
1.	Angular Momenta of a Deformed Nucleus	31
2.	Collective Motions of a Deformed Nucleus	35
3.	A Scintillation Spectrum	42
4.	Schematic Diagram of the Coincidence Spectrometers	45
5.	Correlation Table	46
6.	Magnetic Spectrometer	52
7.	Fast Coincidence Circuits	57
8.	Simple Coincidence Schemes	63
P1.	Decay Scheme of Co^{58}	70
P2.	Scintillation Spectra of Co^{58}	72
P3.	810-865 kev Directional Correlation	74
P4.	Conversion Spectra of Co^{58}	78
9.	Decay Scheme of Ir^{192}	90
10.	Ir^{192} Spectrum in Coincidence with the 300-kev Peak	94
11.	1065-316 kev Directional Correlation	97
12.	885-316 kev Directional Correlation	99
13.	Some Possible Spin Sequences Involving 2→0 Transitions	100
14.	Beta Spectrum in Coincidence with 467-kev Gamma Rays	108
15.	Beta Spectrum in Coincidence with 600-kev gamma rays	110

Figure No. Page

16. Beta Spectrum in Coincidence with 300-kev Gamma Ray 112

17. Decay Scheme of Ir^{194} 127

18. Ir^{194} Singles Spectrum in Gating Channel 130

19. Ir^{194} Spectra in Coincidence with Windows A,B, and C 137

20. Partial Spectrum in Coincidence with 300-kev Gamma Rays 139

21. Beta Spectrum in Coincidence with 300-kev Gamma Rays 145

22. Beta Spectrum in Coincidence with 600-kev Gamma Rays 146

23. Beta Spectrum in Coincidence with 940-kev Gamma Rays 147

24. Beta Spectrum in Coincidence with 1160-kev Gamma Rays 148

25. Beta Spectrum in Coincidence with 1450-kev Gamma Rays 149

26. Intensity Balance of Some Levels in Ir^{194} 157

27. 940-328 kev and 1160-328 kev Directional Correlation 162

28. 1450-328 kev Directional Correlation 164

A1. Sputtering Apparatus 173

A2. Curve of Photopeak Detection Efficiency 181

A3. Apparatus for Measuring Angular Efficiency 184

A4. Solid Angle Correction Factors 185

LIST OF TABLES

Table No.		Page
I	Shell Structure	25
PI	Transitions in Fe^{58}	83
II	Ground State Configurations of Co^{58} and Fe^{58}	85
III	Intensities of Relevant Gamma Rays in Pt^{192}	114
IV	Experimental Results	115
V	Beta Intensities	118
VI	Intensity Balance for the Levels of Pt^{192}	121
VII	Coincidence Cascades Observed	141
VIII	Intensities of Gamma Rays in Pt^{194}	143
IX	Intensities (%) of Beta Groups from Beta-Gamma Experiments	151

INTRODUCTION

At the beginning of this century, the scientific world was introduced to the field of nuclear physics through the discovery of Becquerel (1896) that some natural substances spontaneously emitted ionizing radiations. In the ensuing investigation of this phenomenon, the radioactivity of the natural substances was found to consist of three types of radiation - alpha, beta and gamma. The exact nature of these radiations was clarified when the alpha rays were identified as helium atoms stripped of their electrons (Rutherford and Royds (1909)), the beta rays were shown to be electrons (Becquerel (1900)), and the gamma rays to be similar to X-rays (Gray (1912)). Because alpha and beta rays are charged, they could be bent in a magnetic field. The latter of these was more easily deflected because of its smaller mass and the investigation of the energy distribution (Von Baeyer, Hahn and Meitner (1912)) of the beta rays from many atoms revealed that both continuous distributions and homogeneous groups of electrons were possible. The former were thought to arise from a nuclear process while the latter were deduced to result from the emission of an orbital atomic electron by the gamma rays coming from the nucleus (Rutherford, Robinson and Rawlinson (1914)).

Until after the Second World War, nuclear spectroscopy did not blossom into the vast field of endeavour, which it is today, for at

least two reasons. In the first place, the existing nuclear theory had not been developed in any detail and did not serve as a unification for the experimental data which had been accumulated, and in the second place, radioactive sources could not be made in sufficient strength for detailed studies to be undertaken. There was one exception to this dearth of physical understanding and that was Fermi's theory for the continuous beta spectrum (Chapter I).

With the development of powerful nuclear reactors, the lack of source material vanished and the experimentalists developed precision instruments and good techniques for the investigation of nuclear disintegrations. In order to consolidate the wealth of new information, Mayer (1948) and Haxel, Jensen and Suess (1948) revived with important modifications the shell model of Bethe and Bacher (1936). In addition, the auxiliary processes of internal conversion (Rose (1949)), of directional correlation (Hamilton (1940)), and of multipole radiation (Blatt and Weisskopf (1952)) were reinvestigated and the calculations of these effects extended.

The shell model represented only a beginning in the understanding of nuclear systematics. When research showed that it was not completely satisfactory, the co-operative effects of the nucleons in the nucleus were investigated and found to have important effects on the energy levels in nuclei.

The study of the merits of the different models requires knowledge of many levels in the same nucleus as well as general trends

throughout the nuclear mass table. To study the levels in a complex decay, the experimental techniques must be quite discriminating.

One of these techniques is the coincidence method in which the simultaneous occurrence of related events is detected. This method has been applied in a study of the platinum metals in this laboratory because it is thought that a decision about the relative merits of different approaches to collective motion might be possible in this region of the mass table.

This thesis describes a series of experiments on the decays of Ir^{192} and Ir^{194} designed to obtain the nature of the excited levels in the daughter nucleus. All of the experimental work was performed with two coincidence spectrometers. As a basis for the interpretation of the experimental results, the first three chapters present the necessary theoretical explanation of the experimentally observed phenomenon, a description of the models of nuclear structure and a description of the actual experimental equipment. In Chapter IV, a copy of a paper submitted to Nuclear Physics on Co^{58} is quoted; in addition to this paper, the chapter includes a discussion of the main beta transition. The results for the two iridium nuclides are presented separately in Chapters V and VI.

CHAPTER I

RADIATIONS AND ANGULAR DISTRIBUTIONS

Introduction

The radioactive disintegration of an unstable nucleus gives rise to several types of radiations. In beta decay, positive or negative electrons are emitted and a change in the nuclear species of one unit of charge results. Although the energies of these particles form a continuous distribution, they may be divided into groups of different maximum energy. The existence of these groups suggests that the daughter nucleus may have different excited states. Such is indeed the case. The daughter nucleus in an excited state emits further radiations - gamma rays or electrons of homogeneous energy - in order to arrive at its lowest energy state.

The experimentalist observes these radiations and performs different experiments with them. In order to make deductions from his measurements, he needs some theoretical understanding of the processes which he observes and a method of relating his measurements to the properties of the state. It is the purpose of this chapter to supply this information.

Spin and Parity

The angular momentum or spin of a particle in a nucleus consists of two parts. The first is the orbital angular momentum of integral

value (in units of $\hbar = 1.05 \times 10^{-27}$ erg-seconds) which the particle possesses because, in a classical sense, it is moving in a closed path about a centre; the second is the intrinsic spin of value, $\frac{1}{2}\hbar$, which it always possesses and which has no classical analogue. The spin, $I\hbar$, of the nucleus as a whole in any state is then the resultant of the orbital angular momentum and the intrinsic spin momentum of all the particles in the nucleus.

Associated with the spin are a number of electric and magnetic moments which, in principle, could be used to measure the spin. For example, through the magnetic moment a Zeeman splitting of a level's substates could be effected by an external magnetic field. Unfortunately except for a few rare cases, e.g. Fe^{57} (DePasquali et al. (1960)), the components of the gamma radiation between the levels are not separated in energy by more than 10^{-8} ev and so are not detectable. An alternative method of measurement utilizes the dynamic moments of the states linked by the radiation. The change in spin determines the values of the internal conversion coefficients or is reflected in the spatial distribution of the radiation (angular correlations). It is also important in determining the transition probability for beta transitions, although a measurement of this quantity is less indicative of the spin change than the other observations.

Empirically, it is found that the ground state spins of odd-A nuclei are half-integral, those of even-A nuclei are integral and those of even-even nuclei are zero. The shell model of the nucleus (Chapter II)

has been quite successful in predicting the ground state spins, but has not been as satisfactory for excited states.

The parity of a level is a characteristic of the wave function describing the state under spatial reflection. The wave function has odd or even parity depending on whether the wave function does, or does not, respectively, change sign under spatial inversion. All physical phenomena were believed to conserve parity until Lee and Yang (1956) questioned this fact and Wu et al. (1957) demonstrated the violation of parity conservation for the beta decay process.

In beta and gamma ray spectroscopy, the measurement of the parity of a level is made through a comparison with the parity of another level. The change in parity manifests itself in the multipole character and polarization of the electromagnetic transition or in the type of beta decay which occurs.

Electromagnetic Transitions

An excited state is an unstable configuration which returns to the stable ground state by the emission of energy. In nuclear de-excitation, this energy may be carried away either by particle emission or electromagnetic radiation. For excitation energies up to a few million volts, electromagnetic radiation is dominant.

The emission of a gamma ray is accomplished through the interaction of the electromagnetic field with the charges and currents in the nucleus. The probability for a transition between an initial (i)

and a final (f) state is then (Heitler (1947))

$$T_{i\to f} = \frac{2\pi}{\hbar}\left|\left\langle \psi_f \middle| H \middle| \psi_i \right\rangle\right|^2 \frac{dN}{dE}$$

where ψ_f and ψ_i are the final and initial state wave functions, H is the interaction Hamiltonian and dN/dE is the number of final states per unit energy interval for the radiation.

In general, the interaction causing the radiation will be of the form

$$H_{rad} = -\frac{1}{c}\int \underline{J}.\underline{A}\, d\tau$$

where $\underline{J}$ is the current density in the nucleus and $\underline{A}$ is the vector potential representing the radiation. The nature of this potential is clarified by an expansion in terms of the multipole fields representing the different quanta of angular momentum L carried away by the radiation. Classically, the fields correspond to those arising from charge and current distributions of order 2^L. Associated with each pole are two fields differing in parity. They are designated as electric when the parity is $(-1)^L$ and magnetic when it is $(-1)^{L+1}$. Thus, electromagnetic radiation is characterized as E1, M1, E2, M2, E3, M3, etc. in order of decreasing probability.

Because the gamma rays have a wave length very much longer than the nuclear radius, the expression for the fields can be simplified by using the asymptotic behavior of some of the functions. The transition probabilities can then be written (Goldhaber and

and Weneser (1955))

$$T_e(L) = \frac{8\pi c(L+1)}{L\left[(2L+1)!!\right]^2} k^{2L+1} \sum_M \sum_{M_f} \left| (I_f, M_f \left| \frac{1}{e} \int \rho r^L Y_L^M(\theta, \varphi) d\tau \right| I_i, M_i) \right|^2$$

and

$$T_m(L) = \frac{e^2}{hc} \frac{8\pi c(L+1)}{L\left[(2L+1)!!\right]^2} k^{2L+1} \sum_M \sum_{M_f} \left| (I_f, M_f \left| \frac{1}{L+1} \frac{1}{ec} \int \nabla r^L Y_L^M(\theta, \varphi) \; (\underline{r} \times \underline{J}) d\tau \right| I_i, M_i) \right|^2$$

where the initial and final states have been identified by $|I_i, M_i)$ and $(I_f, M_f|$ respectively and ρ is the charge density related to the current density, $\underline{J}$, by the continuity equation. If the initial and final states have an angular momentum dependence given by spherical harmonics, a selection rule for the possible L values arises naturally from the properties of these harmonics,

$$I_i + I_f \geq L \geq |I_i - I_f|.$$

In addition since each state has a definite parity, a second condition follows from parity conservation; the change in parity of the radiating system is given by $= (-1)^L$ for electric transitions

and $= (-1)^{L+1}$ for magnetic transtions.

The interpretation of a transition would be extremely difficult if all the angular momentum fields allowed by the selection rules were present. However, from a consideration of the transition probabilities with increasing L, it can be seen that successive poles differ by a factor of approximately $(kR)^2$ where k is the wave number of the radiation and R is the nuclear radius. This is very small for gamma rays

below 2.5 Mev so that normally the lowest pole compatible with other conditions is present. There is also a retardation of magnitude $(v/c)^2$ for magnetic as compared to electric transitions of the same pole because the nucleons in the nucleus are not moving at relativistic speeds (Wilkinson (1960)).

Partially because of these two facts, transitions are often of a dual nature, the most common being mixtures of M1 and E2.

The properties of the transitions discussed up to now have arisen primarily from the nature of the electromagnetic interaction. Further selection rules are predicted when recourse is made to specific models (Goldhaber and Weneser (1955), Wilkinson (1960)). To obtain a basis for the comparison of transition rates, the probability for a single particle transition in the shell model as calculated by Weisskopf (1951) is used. Empirically, it is found that the observed rates are within a factor of ten of these estimates for most E1 and M1 transitions, especially in the low mass region. Futhermore, when allowance is made for the influence of the other nucleons in the nucleus which may regroup when the transition occurs, the transition-probability distribution is found to follow the theoretical one remarkably well (Wilkinson (1960)). In contrast, the observed E2 transitions are considerably faster than the single particle estimates. This is one piece of evidence suggesting that there is co-operative motion in the nucleus, a situation which would enhance quadrupole radiation. Other higher order transitions are relatively rare so that generalizations are not

justified. An exception is the M4 transition which exists because of the larger angular momentum change between adjacent levels just before closed shells (Chapter II). Goldhaber and Sunyar (1951) have compiled the data to show that these transition probabilities are as predicted by Weisskopf's estimates.

Internal Conversion

In addition to the emission of a gamma ray, an excited nucleus may transfer its energy to one of the orbital electrons, ejecting it from the atom. This process, called internal conversion, acts through the electromagnetic field so that again there are electric and magnetic transitions of different orders.

The electromagnetic interaction couples the charges and currents of the nucleus to those of the electrons. The transition probability may be separated into electronic and nuclear factors, the latter being the same as is found in the gamma emission process of the same multipolarity. Under certain assumptions, the ratio of the number of conversion electrons to the number of gamma rays will not depend on the nuclear matrix elements but on the electronic wave functions only. These can be calculated with accuracy.

It is well known that the electrons surrounding the nucleus exist in different orbits. Thus it is possible for the conversion process to occur in any orbit allowed by the energy release in the nuclear decay and measurements can be made of the K-shell, L_I-shell, L_{II}-shell, L_{III}-shell, etc. conversion coefficients.

The calculation of these coefficients is tedious. This is reflected in the earliest ones (Hulme (1932)) which are very meagre in quantity. With the advent of digital computers, Rose et al. (1949) was able to extend these calculations. In his tabulations he ignored the fact that the nucleus has a finite extension which distorts the electron wave functions from those for a Dirac particle in the field of a point charge. The incorporation of the finite size of the nucleus into the theory had the greatest effect on those conversion coefficients which depend most strongly on the behavior of the wave function near the origin, namely, M1 (Sliv and Band (1956), (1958), Rose (1958)).

The finite size has a second effect on the internal conversion process. The inner electrons, especially for heavy nuclei, will penetrate into the nuclear matter and interact directly with the nucleons (Church and Weneser (1960), (1961)). The resulting matrix elements, which differ from the electromagnetic matrices, contribute insignificantly to the conversion process except when the gamma matrix element is small because of some selection rule. Many anomalous coefficients in odd nuclei have been found (Asaro et al.(1960)) and some have been related to the penetration matrix element (Gerholm et al. (1961), Pettersson et al.(1961)). In addition it is just these penetration matrix elements which allow $0 \rightarrow 0$ transitions; electromagnetic radiation is rigorously forbidden for these because of the transverse nature of light. E0 transitions may also contribute to the conversion process if $I_i - I_f = 0$ even when I is not zero. The

contribution is not thought to be large and it has been difficult to detect this effect with certainty (Nathan and Hultberg (1958), Gallagher and Thomas (1959)).

Angular Correlations

Besides the energy, the empirical data on nuclear excited states consists mainly of the spin and parity of the levels. The data is obtained by a study of the depopulating transition either through its dependence on the multipolarity of the transition or through the spatial distribution of its radiation field. For the latter measurement, the directional correlation between the successive absorption and emission of particles is an established technique. Angular correlations have also been important in determining the types of interaction responsible for beta decay (Konopinski (1959)) and in measuring nuclear matrix elements (Gerholm et al. (1961), Pettersson et al. (1961)).

The directional correlation experiment did not come of age until the advent of scintillation detectors with their intrinsically high efficiency for gamma ray detection (Kallmann (1947), Brady and Deutsch (1948)). Even then experimentalists were limited to simple decay schemes because of a lack of energy selection for the gamma rays. This deficiency was overcome by using pulse height analyzers to sort out the energy left in the scintillator.

The theory of angular correlations involves the description of the relationship between two or more directions of motion and three or

more angular momenta. There are several approaches to the problem (Devons and Goldfarb (1957)). The earliest was Hamilton's (1940) which applied the perturbation theory to describe the radiation coming from the second state in terms of its population characteristics as determined by the first transition. A second approach is that of the density matrix (Fano (1952), Frauenfelder (1955)). It incorporates the lack of knowledge about the several unobserved angular momenta in a statistical analysis. The analysis is applicable to radiations other than electromagnetic. Biedenharn (1960) has examined the correlation process in terms of the only observable quantity, the angle between the radiations.

Since some of the work in this thesis is concerned with correlations, a further description of the physical aspects is warranted, Following Biedenharn, the correlation function is expanded in terms of the orthonormal Legendre functions in the angle between the momentum vectors for the detected particles.

$$W(\theta) = \frac{1}{4\pi} \sum (2\nu + 1)\, B_\nu\, P_\nu(\cos\theta)$$

The coefficients B_ν will then be the average value of the Legendre polynomials over all possible configurations - the direction of the angular momentum for the intermediate state can be oriented in many ways with respect to the directions of the two observed radiations.

$$B_\nu = \left[P_\nu(\cos\theta)\right]_{Av}$$

The rest of the problem involves the evaluation of these coefficients.

Firstly, by a theorem from spherical trigonometry, the spherical angle between the particles is related to the angular momentum of the intermediate state, I.

$$\left[P_\gamma(k_i.k_f)\right]_{Av} = \left[P_\gamma(k_i .I)\right]_{Av} \left[P_\gamma(k_f .I)\right]_{Av}$$

It is immediately evident that the coefficients are products of factors which depend on one transition only. Each of these factors can be evaluated because the conservation of angular momentum couples the orbital angular momentum of the particle to other unobserved angular momentum, e.g. intrinsic spin, initial state angular momentum, etc. in a definite manner. The physical fact that the orbital angular momentum of the particle $\underline{\ell}$ is perpendicular to the linear momentum $\underline{k}$ completes the linkage from the direction of motion to the angular momentum of the intermediate state.

The coupling is an averaging process because, from a classical viewpoint, no information about the unobserved angular momentum is given, or, from a quantum mechanical viewpoint, the direction of a spin is not known - only its magnitude and component along some fixed axis. Classically, the mathematical form is an average of the Legendre polynomial in the angle between the coupling spins. Quantum mechanically, because there is a quantization, only discrete angles are allowed and the Legendre polynomial will not suffice. The quantum mechanical analogues are the Racah coefficient for the angle between two quantized vectors and the Wigner coefficient for the angle between one quantized vector

and a direction. The factors comprising the coefficients, B_ν, are then products of the Racah and Wigner coefficients suitably normalized. The property of the Racah coefficient that one of its numbers ν must satisfy the relation

$$\nu \leq \min(2I,\ 2\ell_i,\ 2\ell_f)$$

Where I, ℓ_i and ℓ_f are also numbers in the coefficients, limits the angular distribution expansion to a finite number of terms.

As mentioned above, the coefficients are products of two factors, each depending on one transition. To facilitate the tabulation of these factors a standard correlation - that for a gamma-gamma cascade - has been chosen and its factors for the possible transitions listed. For other types of cascades particle parameters have been introduced which convert the tabulated values to the particle transition involved (Nijgh, Wapstra and Van Lieshaut (1959)).

In terms of these quantities, the general expression for the correlation can be written

$$W(\theta,\ P_1,\ P_2) = \sum_\nu \left\{\sum_{L_1 L_1'} b_\nu(L_1,\ L_1',\ P_1)\ F_\nu(L_1,\ L_1',\ I_i,\ I)\right\} \left\{\sum_{L_2 L_2'} b_\nu(L_2,\ L_2',\ P_2)\ F_\nu(L_2,\ L_2',\ I_f,\ I)\right\} P_\nu(\cos\theta)$$

where each b_ν represents some particle parameter, each F_ν represents a tabulation value for a gamma ray transition, and P_1 and P_2 are the momenta of the particles involved.

In order to perceive the experimental importance of this expression, a gamma ray cascade in which the first transition is not pure, i.e. contains a mixture of multipole radiations, will be used as an example.

For gamma rays, the particle parameters become

$$b_\gamma(L, L+1, P_1) = \delta_L \delta_{L+1}$$

where the new quantities are the reduced matrix elements for the transition of multipole order L.

$$\delta_L = (I \,||L||\, I_1)$$

The angular distribution is then,

$$W(\Theta) = \sum_\gamma \Big[\delta^2_{L_1} F_\gamma(L_1, L_1, I_i, I) + 2\delta_{L_1}\delta_{L_1+1} F_\gamma(L_1, L_1+1, I_i, I) + \delta^2_{L_1+1} F_\gamma(L_1+1, L_1+1, I_i, I) \Big] \Big[\delta^2_{L_2} F_\gamma(L_2, L_2, I_f, I) \Big] P_2(\cos\Theta).$$

When it is recalled that the angular distribution is a relative measurement, the δ_{L_1} and δ_{L_2} may be combined with the non-appearing constant in front of the distribution expression. A ratio of $\delta_{L_1+1}/\delta_{L_1}$ will therefore appear. This is referred to as the mixing ratio of the transition, $\delta = \dfrac{(I\,||L+1||\,I_i)}{(I\,||L||\,I_i)}$

$$W(\Theta) = \sum_\gamma \Big[F_\gamma(L_1, L_1, I_i, I) + 2\delta F_\gamma(L_1, L_1+1, I_i, I) + \delta^2 F_\gamma(L_1+1, L_1+1, I_i, I) \Big] \Big[F_\gamma(L_2, L_2, I_f, I) \Big] P_\gamma(\cos\Theta)$$

or for experimental purposes,

$$W(\theta) = \sum_{\gamma} A_{\gamma}^{1} A_{\gamma}^{2} P_{\gamma}(\cos\theta).$$

Except for some distinctive distribution patterns from cascades composed of two pure transitions, the nature of the second transition and therefore A_{γ}^{2} must be known and used to obtain A_{γ}^{1} from the measured distribution. With the aid of graphs or of tables listing the A_{γ}'s as a function of δ for different cascades (Arns and Wiedenbeck (1958), Taylor and McPherson (1960), (1961)), a determination of the mixing ratio can be made.

Beta Decay

Along with electrons of definite energy, the nucleus is known to emit beta particles which have a continuous energy distribution. At the time when this was convincingly proved (Ellis and Wooster (1927)), physicists felt that many of the laws of physics were in jeopardy. In order to preserve these, Pauli (1934) boldly postulated the existence of a light neutral particle which Fermi named the neutrino. It was assumed to be emitted simultaneously with the beta particle and, although its existence was only hypothetical, Fermi (1934) incorporated it in his theory of the beta interaction. This mechanism, which allows for the emission of two particles with the total energy divided between them in a statistical manner, predicted a beta continuum of the proper shape, and suggested that the end-point of the continuum was associated with the energy release of the beta process. Other theoreticians (Gamow and Teller

(1936), Konopinski and Uhlenbeck (1941) investigated the general nature of Fermi's theory under Lorentz invariance and found that there were five possible types of interactions. Many experiments were designed to determine the particular types involved as well as the properties of the neutrino (Wu (1955), Kofoed-Hansen (1955)). Until 1956, these experiments tended to be inconclusive. In that year, Lee and Yang (1956) made the revolutionary suggestion that parity was not conserved in weak interactions, of which beta decay is one phenomenon, and the following year, Wu et al. (1957) performed a crucial experiment to show that, indeed, parity was not conserved in beta decay.

Fermi's original theory of beta decay was constructed in analogy with the electromagnetic interaction. In this particular choice of form, he picked one of the five possible Lorentz-invariant interactions, the vector form. The other four possibilities are the scalar, axial vector, tensor and pseudoscalar. The interaction Hamiltonian, which is a combination of all five interactions, may be written

$$H = \sum_x g(\psi_i\, Q_x\, \psi_f^\dagger)\ (\psi_e\, Q_x\, \psi_\nu^\dagger) + \text{Hermitian Conjugate}$$

where ψ_i and ψ_f are the initial and final nuclear states; ψ_e and ψ_ν are the electron and neutrino wave function; Q_x is the operator whose explicit form for the five interactions is given by Rose (1955); and g is the strength constant analogous to e in the electromagnetic transition. Three of the interactions, vector, axial vector and tensor, have two parts, the first produced by the charge density, and the second produced

by a current density. Because the nucleons do not move quickly in the nucleus, the second part is small compared to the first.

When the coulomb effect of the electrons clothing the nucleus is neglected, both the leptonic wave functions are those of plane waves. The usual expansion in terms of increasing angular momentum and decreasing magnitude is made producing transition probabilities of different orders. When the first term is retained and used with the larger nuclear term in any of the interactions, allowed transitions are calculated. First forbidden transitions occur through the product of the large nuclear matrix element and the second term of the expansion for the leptons or through the product of the small nuclear matrix elements and the first term in the expansion. The probabilities for the higher-ordered forbidden transitions are constructed in a similar manner.

A further classification is sometimes made. Those interactions which allow a spin flip, i.e. axial vector and tensor, are called Gamow-Teller, while those which do not, i.e. scalar and vector, are called Fermi. Now that the beta decay has been shown to be a V - A combination (Konopinski (1959)), it is seen that one of each type is present.

An examination of the matrix elements for the two interactions involved in beta decay reveals the following selection rules:

	Vector	Axial Vector
Allowed	$\Delta I = 0$ $\quad \Delta\pi$ = no	$\Delta I = 0, \pm 1$ $\quad \Delta\pi$ = no ($0 \rightarrow 0$ excluded)
First Forbidden	$\Delta I = 0, \pm 1$ $\quad \Delta\pi$ = yes ($0 \rightarrow 0$ excluded)	$\Delta I = 0, \pm 1, \pm 2$ $\quad \Delta\pi$ = yes
Second Forbidden	$\Delta I = \pm 2$ $\quad \Delta\pi$ = no	$\Delta I = \pm 2, \pm 3$ $\quad \Delta\pi$ = no

etc.

The distribution of energy for the continuum is found by summing the transition probabilities over all the unobserved quantities and is given by

$$N(W) = C\,|M|^2 F(Z, W)\, pW\, (W_o - W)^2\, S_N\, dW$$

where C is the strength constant, M is the nuclear matrix element, F is the Fermi function which adjusts the electron wave function for the presence of the orbital electrons, W_o (in units of $m_o c^2$) is the maximum disintegration energy, p (in units of $m_o c$) is the electron momentum $p = (W^2 - 1)^{\frac{1}{2}}$, S_N is the shape factor and N(W) is the number of electrons of energy between W and W + dW per unit time. For allowed and most first forbidden transitions the shape factor is a constant, while for other decays it is a function of the momentum of the leptons and may indicate the order of forbiddenness of the transition.

The total decay rate

$$\lambda = \frac{\ln 2}{t} = \int_1^W N(W)\, dW$$

$$= C|M|^2 f$$

provides a means of comparing different transitions. The product ft,

where t is the half-life, is a function of the nuclear matrix elements and its value is an indication of the forbiddenness of the transition.

The beta decay process applies to positron emission and electron capture when these are allowed by energy considerations. The expressions for the relevant quantities have minor changes related to the type of lepton involved (Rose (1960)).

In measuring a beta spectrum, it is desirable to know the maximum energy and intensity of the different beta transitions which may be present. Since these spectra are normally observed with a magnetic spectrometer, the distribution in momentum

$$N(p) = C|M|^2 F(Z, W) p^2(W_o - W)^2 S_N$$

is measured rather than an energy distribution. A plot of the quantity $(N(p) / p^2FS_N)^{\frac{1}{2}}$ as a function of energy is then a straight line whose intercept with the energy axis gives the value of the maximum energy of the beta disintegration. If several groups of beta rays are present, they appear as breaks in the linear plot and can be revealed by subtracting the higher energy groups as determined by their straight lines and replotting. This process is called the Fermi analysis of a beta spectrum.

CHAPTER II

NUCLEAR MODELS

Introduction

The discovery of the electron and of radioactivity suggested that the atom was not an indivisible constituent of nature but consisted of subatomic particles of opposite charge. The relationship in space of these charges was an object of speculation until Rutherford (1911) performed his experiment of scattering alpha particles from thin foils. His results, which showed that the positive charge was concentrated in a very small region of the atom, helped to establish the concept of the nuclear atom. In this picture, as further developed by Bohr (1913), the central region or nucleus contains nearly all of the mass of the atom, and the electrons move in orbits of discrete radii about the nucleus. Furthermore, the nucleus possesses a positive charge equal to the number of protons which it contains. When a comparison was made between the mass of the nucleus and the mass associated with the number of positive charges present in the nucleus, a great discrepancy was found. The additional mass was postulated to arise from protons whose charges had been neutralized by an equal number of electrons. However, the presence of these electrons in the nucleus created a dilemma, because

(a) their de Broglie wave length was much longer than the finite extension of the nucleus for any reasonable potential

and, (b) their intrinsic spin required that, contrary to fact, odd-odd nuclei, like N^{14}, have a half integral spin for their ground state. This situation was resolved by the discovery of the neutron (Chadwick (1932)) whose properties of mass, charge and spin satisfied the requirements for admission as a nuclear member. Its discovery and the concept that the electrons emitted in beta decay were created at the moment of emission by the transformation of a neutron into a proton, removed the electron from the nucleus.

Still to be resolved was the manner in which the neutrons and protons were placed in the nucleus. Until very recently, this structure was predicted on the basis of phenomenological models. The shell model and collective model have been greatly developed in order to facilitate the understanding of the low energy excitation of nuclei, while the optical model, the statistical model and the compound-nucleus model have found wide application in treating the higher excitation arising in nuclear reactions. The first two of these models are important in beta decay and will be described here in parts A and B respectively.

A. SHELL MODEL

Introduction The great success of a shell model for the electronic structure of atoms stimulated interest in a shell model for the nucleons. Indeed, many pieces of experimental evidence suggested

the existence of certain numbers of protons and neutrons which were particularly stable. However, a nuclear potential similar to that used in atomic structure fails to predict the observed "magic numbers". This is not too surprising when it is realized that the potential for the electrons is produced by an external agent, the massive nucleus, while the nucleons interact strongly with each other and not with a central body.

The potential between the electrons and the nucleus is electromagnetic in nature and the nucleus appears as a point charge to the electrons, In contrast to this, a potential for the nucleus would have to arise as an average effect of the nuclear interaction between many nucleons distributed over a volume. In addition, the nuclear force is short range and acts nearly always between pairs of nucleons. It is therefore surprising that the structure of the nucleus can be treated with a potential of any kind. However, the addition of a strong spin-orbit interaction - which couples the intrinsic spin and orbital angular momentum of each nucleon - to a central potential makes configurations with 2, 8, 20, 50, 82 and 126 nucleons of either type especially stable (Mayer (1948), Haxel, Jensen and Suess (1948)). These are just the "magic numbers" observed experimentally.

Independent Particle Model In a central potential, V(r), of square-well form, the energy levels available to a nucleon are found to group into shells. Each shell has a number of levels of different energies as determined by the orbital angular momentum, ℓ. The ℓ- values of

the levels in any one shell are found to be all even or all odd and thus no one shell contains both even and odd ℓ - values.

The potential of the nuclear shell model with spin-orbit coupling is

$$V = V(r) + f(r)\, \underline{\ell} \cdot \underline{s}$$

where V(r) and f(r) are the radial functions of the central and spin-orbit potentials respectively, and $\underline{\ell}$ and $\underline{s}$ are the orbital and spin angular momentum vectors. With this potential, the total angular momentum of a particle, $\underline{j} = \underline{\ell} + \underline{s}$, is a constant of the motion rather that the orbital angular momentum. The spin-orbit force separates the levels with the two possible j - values for each ℓ - value by an amount of energy proportional to the ℓ -value. When the sign of f(r) is negative, the level with the higher j - value is lowered in energy, so that, for sufficiently high values of ℓ, the level can be removed from one oscillator group and placed in the next lower one. This is illustrated in Table I.

TABLE I

Shell Structure

Oscillator group	0	1		2			3				4			
ℓ - value	1s	1p		1d	2s		1f	2p			1g	2d	3s	
j - value	$1s_{1/2}$	$1p_{3/2}$	$1p_{1/2}$	$1d_{5/2}$	$2s_{1/2}$	$1d_{3/2}$	$1f_{7/2}$	$1f_{5/2}$	$2p_{3/2}$	$2p_{1/2}$	$1g_{9/2}$	$1g_{7/2}$	$2d_{5/2}$	$2d_{3/2}$ ...
Number of nucleons in shell	2	6		12			30							

The orbital angular momentum does not lose its significance entirely, but determines the parity of the nucleon in any particular

level. For even values of l, the parity is even, and for odd values, odd. Thus, without a spin-orbit force the parity of all the levels in an oscillator shell are the same. However, the spin-orbit force in lowering a level from one shell to another has added to some shells a level of opposite parity. This added level appears at the top of the energy scale in the lower shell and produces a situation in which levels differing greatly in angular momentum and having opposite parities are close together. Electromagnetic transitions between such pairs of states have very small transition probabilities. Thus, just before the completion of the closed shells with high oscillator numbers, states with long lifetimes might be expected. It is in these regions of the periodic table that long-lived isomeric states are found (Goldhaber and Sunyar (1955)).

Besides determining the "magic numbers" and the islands of isomerism, the shell model is capable of predicting the ground state spins for nuclei having one particle or one hole outside of their closed shell. The prediction is based on Pauli's exclusion principle (1925) which requires that the spin of a closed shell be zero. The spin of the whole nucleus is therefore that of the extra nucleon or hole.

Shell Model with Residual Internucleon Forces In order to treat unfilled levels with more than one particle in them, it is necessary to introduce a residual interaction between individual nucleons. Two

effects arise from this force. Firstly, the pairs of particles in the same level tend to couple together to give a resultant spin of zero, and hence only the last odd nucleon need be considered in predicting the spin. Secondly, a pairing energy exists which increases directly with the value of j. Thus a nucleus may find that it is more economical to fill the levels of the higher j - values with pairs of particles even though this necessitates moving one particle from a state of lower energy to one of higher energy. As a consequence of this pairing energy, few nuclei are found with spins of 13/2, 11/2, 9/2 or even 7/2 for their ground states.

The above rules are useful in determining the spin and nucleon configuration of the ground state. Knowledge of the configuration makes it possible to calculate the magnetic moment of the nucleus for that state. Contributions to the magnetic moment arise from both the orbital and spin angular momenta so that the moments depend on the ℓ - value of the orbit, on the type of nucleon and on whether the nucleon is in the $j + \frac{1}{2}$ or $j - \frac{1}{2}$ level. Experimentally, it is found that these moments serve only as limiting values (the Schmidt Limits - Schmidt (1937)) and that nearly all moments lie between the values calculated for $j + \frac{1}{2}$ and $j - \frac{1}{2}$.

In order to improve the agreement with experimental values, nuclear configurations having the same spin value, but arising from different methods of coupling the particles' angular momenta, are introduced into the wave function describing the state. Even in the

supposedly simple cases, many configurations may be present in unknown amounts and the problem of calculating the moments becomes very complicated. Under these circumstances, the numerical results computed from the assumed configurations must generally be treated with skepticism, although for some cases the calculated values are in excellent agreement with the experimental values.

Excited states are also amenable to description in terms of the energy levels predicted by this model. For nuclei with closed shells plus a particle or a hole, the excitations should correspond to that required to transfer the particle from the ground state to the successively higher single particle states. For a few particles outside of closed shells, there are many ways in which nuclear excitation may occur; to illustrate, a pair of particles coupling to a spin of zero in the ground state may couple differently to form excited states; a pair may be broken with one going to a high single particle state of different angular momentum; or, a pair may be excited to a new level together. The energies and spins of the states so formed can be predicted in a few cases on the basis of particle states and reasonable assumptions (Kurath (1960)) about the internucleon force. Levels corresponding to these predictions have been found in the nuclear spectra of certain nuclei, e.g. Zr^{90} (Bjørnholm, Nielsen and Sheline (1959)).

B. COLLECTIVE MODEL

Introduction While the independent particle model is adequate for

the description of nuclear structures very near to closed shells, some properties, especially the large quadrupole moments and electric quadrupole transition probabilities, of nuclei removed from closed shells cannot be attributed to those of the last particle alone. Configuration mixing might help in the description, but calculations are so involved that the work is prohibitively complex. The nature of the properties cited suggests that many nucleons are involved. A description in terms of the deformation of the nuclear surface ignores the action of the individual particles, but incorporates the collective effects of many particles.

Nuclei with closed shells appear on both experimental and theoretical grounds to be spherical. If a nucleon is added, it will tend to distort and polarize such a nucleus (Rainwater (1950)). Although a second particle couples with the first to give a zero spin, it can still add its polarizing effect to that of the first. The stability of the core against deformation is gradually broken down as extra nucleons are added until a nucleus with a deformed shape has a lower energy than one with a spherical shape (Alder et al. (1956)). At this point the ground state of the nucleus will correspond to a non-spherical nuclear shape.

Vibrational Model Near closed shells, the nuclei are not strongly deformed. However, the stability against oscillations is reduced and vibrations of simple harmonic nature called phonons occur. The vibrations of lowest energy correspond to surface oscillations of a

quadrupole nature. Each of these phonons has an energy $\hbar\omega$, a spin 2, and even parity. Because the phonon energy is often less than that necessary for particle excitation, quadrupole oscillations are important in low energy spectra.

For even-even nuclei, the first excited state has the characteristics of a one-phonon excitation. When a second phonon is added, the two spins can couple to a resultant of 0, 2 or 4. This triplet will occur at an energy twice that of the single phonon excitation, but the members of the trio are likely to be split in energy due to the perturbation from other possible excitations. Examples of nuclei with this characteristic spectrum are the Sn and Cd isotopes (Scharenberg, Stewart and Wiedenbeck (1956), Mottelson (1958)).

For odd nuclei, there are a number of states of one-phonon excitation because the ground state angular momentum can couple with the spin of the phonon to give several states (Alder et al. (1956), Brink (1960)).

The radiation from these states is found to be predominantly electric quadrupole in nature although other multipoles might be allowed by the spin change. This situation is reasonable because the phonons cause the nucleus to have a quadrupole deformation, and therefore, a large quadrupole moment. Another requirement of the description in terms of phonon excitation is that the transition from the second spin-2 state is prohibited; this arises because only one phonon can be destroyed at a time. Experimentally, the ground

state transitions from such states are present because of perturbations, but occur with greatly reduced intensity.

Rotational Model The addition of several nucleons causes the nucleus to assume a permanently deformed shape. In this situation, the excitation of a nucleus can be divided into that associated with changes in intrinsic shape (vibrations) and that associated with changes in its orientation in shape (rotations). If the deformed nucleus is assumed to have an axis of symmetry, the latter excitations are describable by a rotational Hamiltonian

$$H = \frac{\hbar^2}{2J}\left[(I^2 - K^2)/J_1 + K^2/J_3\right]$$

where $\underline{I}$ is the total angular momentum, K its projection on the symmetry axis, and J_1 and J_3 are the moments of inertia about the axes perpendicular and parallel to the symmetry axis respectively. The relevant angular momentum quantum numbers are illustrated in Figure 1.

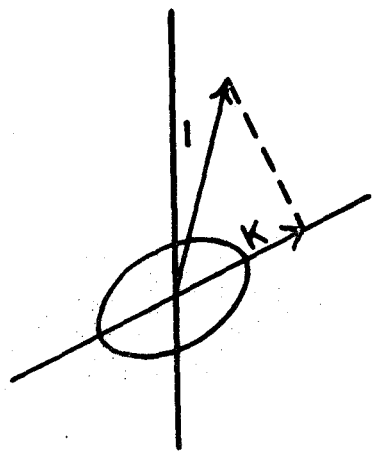

FIG 1

For even-even nuclei in their lowest rotational band, the eigenvalue K is zero so that the energy spectrum of the deformed nucleus is,

$$E = \frac{\hbar^2}{2J}\left[I(I+1)\right].$$

Because the deformation is symmetric about a plane perpendicular to the symmetric axis, a rotation of 180° does not change the intrinsic wave function. For this reason the rotations of odd angular momentum which have odd parity are effectively eliminated. For bands with K not equal to zero the energy relation is

$$E = \frac{\hbar^2}{2J}\left[I(I+1) - K^2\right]$$

with all values of I greater than K permissible. This description in terms of rotational excitation finds quantitative justification in several nuclides of the rare earth and actinide elements whose spectra are interpretable in terms of rotational bands, e.g. Dy^{160} (Preston (1962)) and Pu^{238} (Mottelson (1958)).

Odd-A nuclei have an intrinsic spin different from zero so that K is never zero. The rotational spectra of these nuclei will have, therefore, a structre given by the last equation. Intrinsic state spins of $\frac{1}{2}$ must be treated more fully because of a Coriolis interaction between the rotation and intrinsic motion associated with the spin $\frac{1}{2}$ nucleon. The energy spectrum is modified to

$$E = \frac{\hbar^2}{2J}\left[I(I+1) + a(-1)^{I+\frac{1}{2}}(I+\tfrac{1}{2})\right]$$

in which a is the so-called decoupling parameter which can be positive or negative and can be calculated in terms of the intrinsic wave function. The Coriolis interaction is present in other bands but its effect is less obvious; it merely causes moments of inertia to be increased and transition intensities to be altered (Kerman (1959)).

This model, because of its nature, requires that electromagnetic radiation between the levels be electric quadrupole, and it is empirically observed that these transitions are greatly enhanced. This property depends on the wave function of the nucleon states involved. Each wave function is separable into an intrinsic and collective part. When the assumption is made that the intrinsic state does not change from level to level within a band, ratios of reduced transition probabilities can be deduced. Measurements of these allow a determination of the nuclear deformation.

Beta and Gamma Vibrations Rotation is merely the simplest collective motion of deformed nuclei. The nucleon deformation is usually described in terms of two parameters, beta and gamma; beta is a measure of the total deformation, and gamma is a measure of the asymmetry from a spheroidal shape. In the Bohr and Mottelson picture (1953), the nucleus is axially symmetric so that gamma is zero or thirty

degrees. However, quadrupole vibrations which destroy the axial symmetry are possible. These are called gamma vibrations and have a K quantum number of 2. A second type of vibration which changes the total amount of the deformation but preserves the established symmetries occurs. It is called a beta vibration and has a K - value of zero.

Each of these vibrations may have rotational motion added to them giving rise to bands of levels. For even-even nuclei, a pictorial representation of these oscillations is given in Figure 2.

Collective excitation can also produce states of opposite parity. These do not result from quadrupole oscillations but from octupole vibrations. Such a vibration is shown in Figure 2 as a pear-shaped deformation which flips back and forth along the symmetry axis. Because it is an octupole deformation it has a spin of three and a spin projection K = 0. Its parity is opposite to that of the quadrupole vibrations because it is not symmetric about an axis perpendicular to the symmetry axis.

Deformed Shell Model The existence of a deformation for even-even nuclei in the region between closed shells raised the possibility that the deformation might have some effect on the individual particle states. In an investigation of the influence of this deformation, Nilsson (1955) used an axially symmetric central potential with the normal spin-orbit force of the shell model and included a term in the orbital angular momentum which made the potential intermediate between that of a square-well and a simple harmonic oscillator.

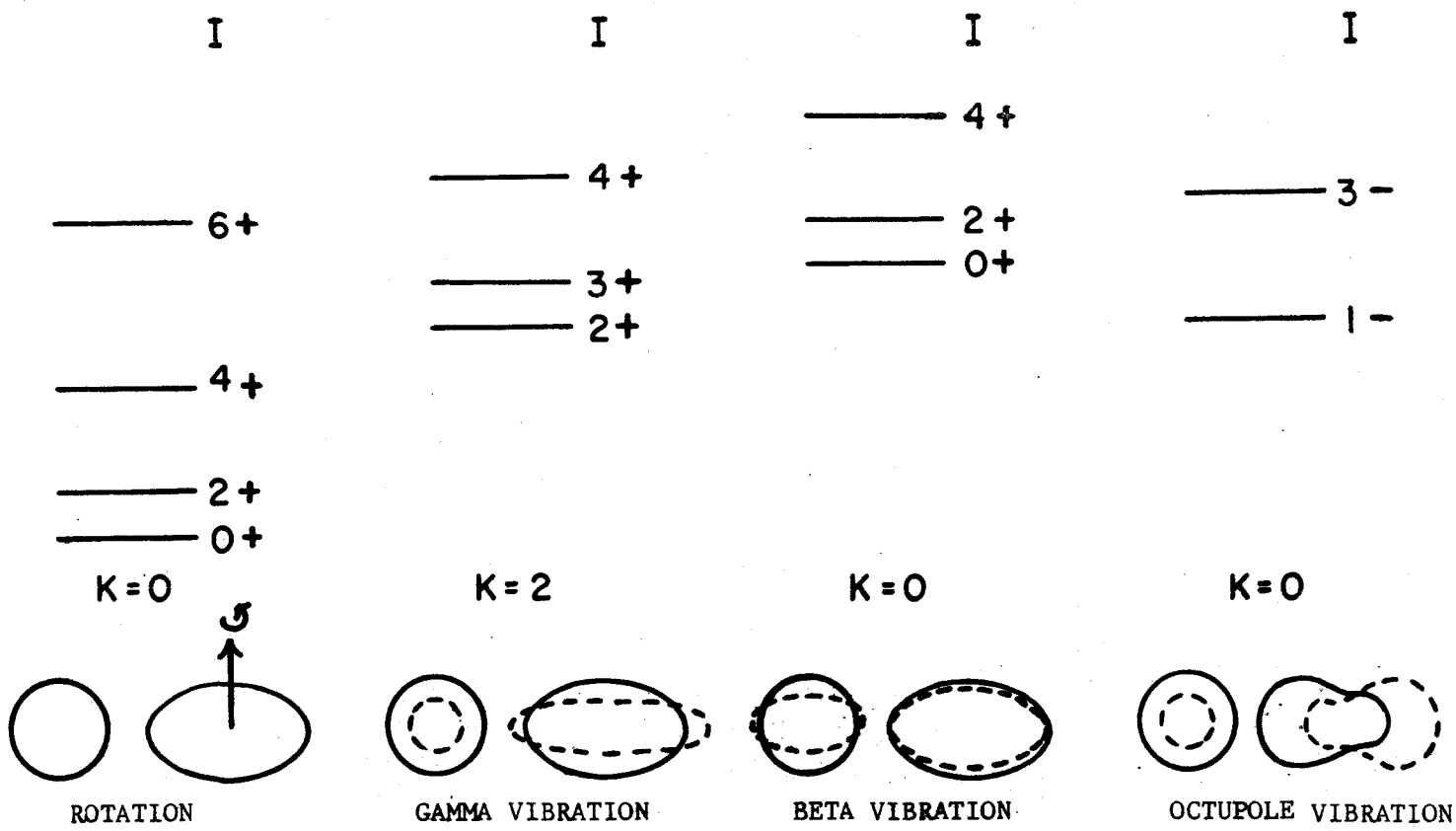

Fig. 2 Some possible spin values for the rotational bands built on the different types of collective motion. For each type of collective motion, cross-sectional views perpendicular and parallel to the symmetry axis are shown. The solid and dotted lines indicate the extremities of the nuclear shape reached in each type of vibration.

The strengths of the separate parts of his potential were adjusted to give the correct level spacings of the independent particle model. When the single particle levels were determined as a function of the deformation, any distortion was found to remove the degeneracy of the states with similar j - values and to form only doubly degenerate levels specified by the projection, Ω_p, of the angular momentum along the symmetry axis. The spins of the ground states and low-lying levels of deformed odd-A nuclei as predicted by this model are an improvement over those of the independent particle model, especially in the rare earth region.

For each level, rotational bands are possible whose level structure is given by

$$E = \frac{\hbar^2}{2J} \left[I(I+1) - I_o(I_o+1) \right]$$

where I_o is the spin of the ground state. When two intrinsic levels are close together, the two bands many intermingle and the simple formula for the two level structures will be modified. Dy^{161} illustrates the situation (Bohr and Mottelson (1960)).

The transitions between bands are slower than those within the band because of the change in intrinsic structure. The latter are governed by selection rules involving the quantum numbers peculiar to the levels of the deformed shell model (Alaga (1957)).

The other types of collective motion, i.e. beta and gamma, are not excluded from the low energy spectra in odd nuclei; however,

their energy as seen in neighbouring even-even nuclei is often higher than excited intrinsic states. Also, as pointed out earlier, the spin of the intrinsic state can couple in different ways to the collective angular momentum so that identification of these states is difficult.

Asymmetric Rotator Neither the vibrational model nor the model of rotational bands built on the different types of intrinsic states satisfactorily explains the empirical data observed in the region of nuclei where the deformation is not fully developed. In addition, the transition probabilities predicted are not verified, and complete violation of the selection rules does occur. One explanation for this situation is that K is a good quantum number but that a vibrational-rotational interaction occurs which distorts the simple picture. The exact nature of the interaction is not known so that predictions are difficult to make. A second approach is the asymmetric rotator in which the quantum number K loses its significance and the concept of axial symmetry no longer applies.

Davydov and his collaborators (1959, 1960, 1961) studied the spectra of such nuclei which possess no axis of symmetry. They used the same basic assumptions as many other investigators of collective motion and found that the three types of excitation - rotation, beta vibrations and gamma vibrations - follow naturally from the theory. However, for rotational motions, there are more levels than those found previously because there are more axes about which to rotate.

Thus, for even-even nuclei, there are two rotational levels with a spin of 2 instead of one, and a spin-3 level is predicted which has a definite energy relationship to the two spin-2 levels.

$$E_1(3) = E_1(2) + E_2(2)$$

Evidence for this type of behavior has been found in the transition region of the periodic table.

Oscillatory excitations are also predictable. For each type of vibration, there is a level with a spin of zero that has a relatively low energy and can be situated among the rotational states of the model. The existence of two zero-spin states contrasts with the one obtained in the symmetric model. Since particle excitations of about the same energy as that for these collective motions are possible, a distinction between the approaches is not feasible unless the nature of the levels in question can be deduced.

The nature of the levels can be investigated through a measurement of the transition probabilities from the particular levels. Both approaches furnish functions dependent on the type of deformation, so that the transition probabilities between different states can be calculated (Alaga et al. (1955), Davydov and Fillipov (1959)). Usually of greater use than the absolute rates are the ratio of the reduced transition probabilities to or from a pair of levels in the same band. In the theory of symmetric nuclei, the ratio is a quotient of two Clebsch-Gordon coefficients

$$\frac{B(L,\ I_i \rightarrow I_f)}{B(L,\ I_i \rightarrow I_f')} = \left(\frac{\langle I_i\ L\ K_i\ K_f - K_i \mid I_i\ L\ I_f\ K_f \rangle}{\langle I_i\ L\ K_i\ K_f - K_i \mid I_i\ L\ I_f'\ K_f \rangle} \right)^2$$

while for asymmetric nuclei the ratio involves the values of the stable nuclear deformation parameters. It is these ratios which provide a sensitive test of the nuclear behavior.

CHAPTER III

THE EQUIPMENT AND THE EXPERIMENTAL METHOD

Introduction

The theory of a physical phenomenon finds little acceptance unless its predictions can be verified. The various aspects of nuclear disintegration are not exceptions to this rule, and in order to investigate them many instruments and experimental techniques have been developed. In order to obtain the results of this thesis, two types of coincidence spectrometers have been employed. These two instruments differ in their design because they are used to detect two types of radiation, gamma rays and electrons.

It has long been known that a magnetic field can be used to measure the momentum of a charged particle. This fact has found wide application in the design of magnetic spectrometers to measure the momentum distribution of the beta particles and the momentum of the conversion electrons accompanying beta decay. In contrast, the detection of a gamma ray is difficult because of its small interaction with matter. Indeed, all the radiation that reaches a detector is not necessarily detected. The scintillator introduced by Kallmann (1947) has a relatively high detection efficiency. This property has made gamma rays much easier to observe and has increased the usefulness

of the coincidence technique, so powerful in unravelling complex decay schemes.

Scintillation Spectrometer

In order to utilize the properties of a phosphor, a scintillation spectrometer consists of the phosphor optically coupled to a photomultiplier, a stabilized high voltage power supply and a pulse sorting apparatus. The gamma ray entering the crystal suffers collisions with electrons and leaves ionized particles in its wake. In recombining at special lattice sites, the particles produce flashes of light. The crystals are transparent to this light and when a photomultiplier whose photocathode is sensitive to this spectral radiation is attached to the crystal, the gamma ray can be detected as an electrical pulse whose height is proportional to the energy lost in the crystal.

The electrical pulses from the photomultiplier are analyzed in a pulse height selecting device. Two types of apparatus are available, a single channel pulse height analyser and a multichannel pulse height analyser. The former sorts the electrical pulses with a pair of flip-flop discriminators triggered at different voltages. Those pulses which fire one flip-flop only are in the energy "window" and can be recorded with a scaler. In order to secure an energy spectrum, a narrow energy window is set above the lower energy discriminator and the latter is raised by discrete amounts. A plot of the number of counts against the discriminator setting will then give the energy

spectrum. In the multichannel analyser, an electrical pulse is converted to a pulse train whose length is determined by the pulse height, and the number of pulses in the train are counted to give the pulse height, i.e. the energy of the radiation. The advantage of this instrument is that every pulse arriving at the analyser is processed and recorded, whereas in the single channel analyser, only those pulses falling in the energy window are recorded.

Because there are three principal methods for gamma rays to interact with the crystal - photoelectric production of electrons, compton scattering and pair production - the energy of a monoenergetic gamma ray does not appear as a narrow peak in the energy distribution, but is a broad peak with a valley and then a higher flat compton region (Figure 3). The region where the large number of pulses cluster is called the photopeak and is produced by gamma rays which lose all of their energy in the crystal either by a photoelectric interaction or a multiple scattering process.

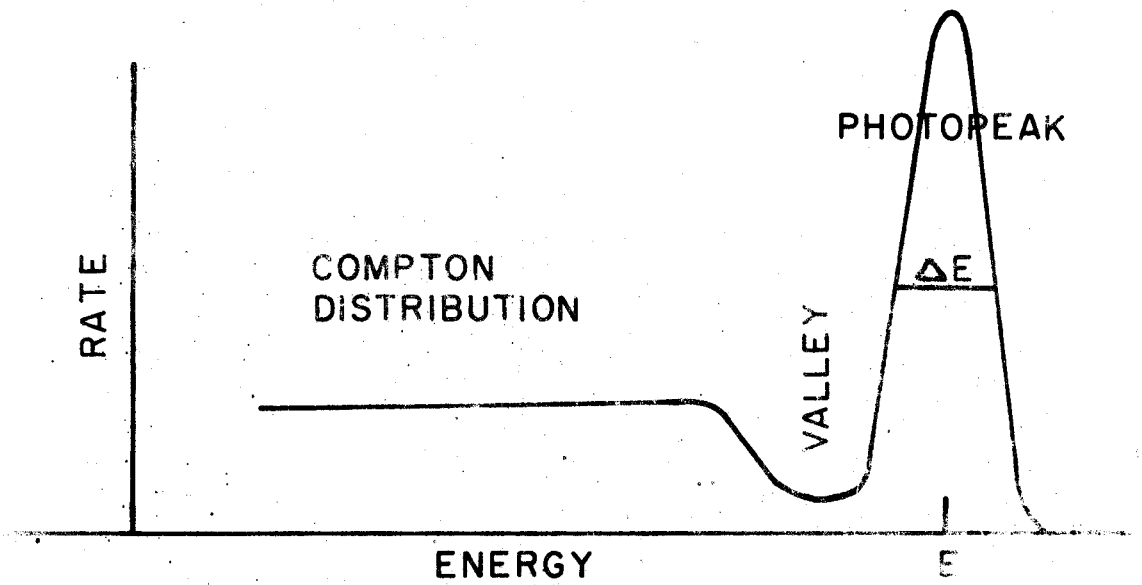

FIG 3

The broadness of the photopeak is due to a statistical fluctuation in the number of electrons produced at the photocathode of the photomultiplier. A measurement of the broadness of the peak at half height, ΔE, compared to the energy of the peak, E, is the resolution of the crystal, $R = \Delta E/E$. Since this is a function of the energy ($R = a + b/\sqrt{E}$ where a is very much smaller than b), the resolution or figure of merit of a crystal is given in terms of the Cs^{137} 661-kev line.

Gamma rays of sufficient energy ($E \geq 1.02$ Mev) can cause pair production. The spectrum of such a gamma ray is complicated by the presence of two escape peaks 0.51 and 1.02 Mev below the main peak. These arise when one or both of the annihilation gamma rays, produced in the destruction of the positron, escape from the crystal, and are quite weak for gamma rays below 2 Mev.

In the work described in this thesis, 5.0 cm. x 3.7 cm. NaI(Tl) crystals integrally mounted to Phillips 56 A.V.P. photomultipliers were used as gamma ray detectors. Several crystals were employed and the best had a resolution of 8%. A highly regulated power supply provided a high voltage sufficiently stable that no drift in the position of the photopeaks caused by a voltage change could be detected in either the Tracerlab single channel analyser or Nuclear Data multichannel analyser used to record the spectra. A schematic diagram of a scintillation spectrometer can be seen in Figure 4A.

Directional Correlation Experiment

The direction which a radiation takes from a nucleus is correlated with the direction of the nuclear spin. One of the methods of detecting this relationship is through a directional correlation experiment (Chapter I). Brady and Deutsch (1947) were the first to successfully use this technique to measure the spins of excited states. Since then the measurement of the directional correlation of successive gamma rays has become a valuable tool in determining the properties of excited states.

The correlation experiment requires the observation of two gamma rays and the detection of a coincidence between them. Figure 4A is the schematic diagram of the gamma-gamma coincidence apparatus used in this work. The two crystals are supported on a metal table in such a way that they face the source in its holder at the centre of the table. One crystal is fixed in position while the second is free to rotate in a semi-circle about the source as shown in Figure 5. This arrangement makes possible the measurement of a directional correlation pattern.

Before a directional correlation experiment can be performed, several circumstances must be taken into consideration:

(1) The physical nature of the source must be such that there is no interaction of the intermediate state with its surroundings. This condition is satisfied if the lifetime of the intermediate state is sufficiently short ($\lesssim 10^{-10}$ secs.). For one of the states of

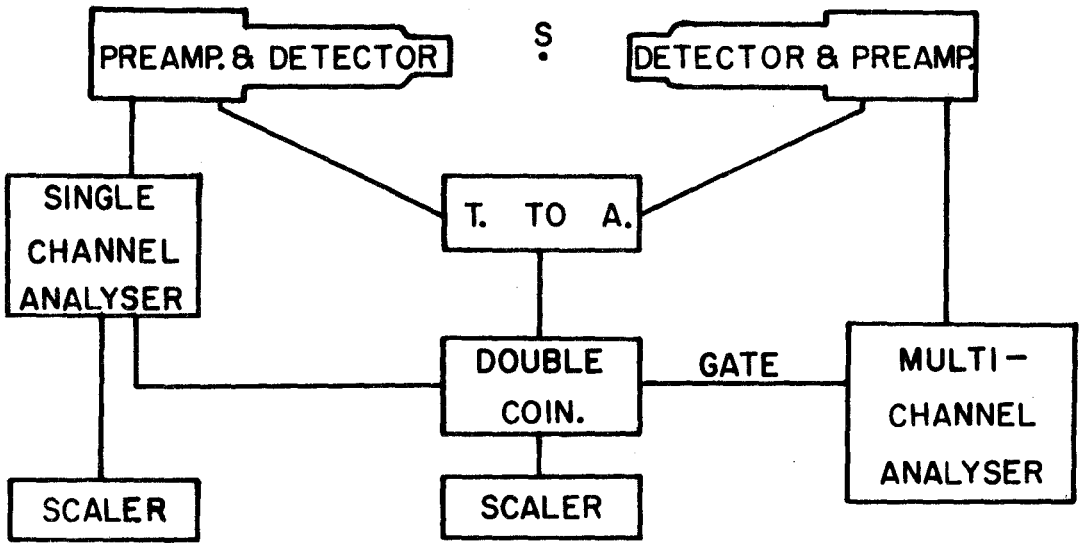
PREAMP. & DETECTOR
S
DETECTOR & PREAMP.
SINGLE CHANNEL ANALYSER
T. TO A.
DOUBLE COIN.
GATE
MULTI-CHANNEL ANALYSER
SCALER
SCALER

FIG 4(A)

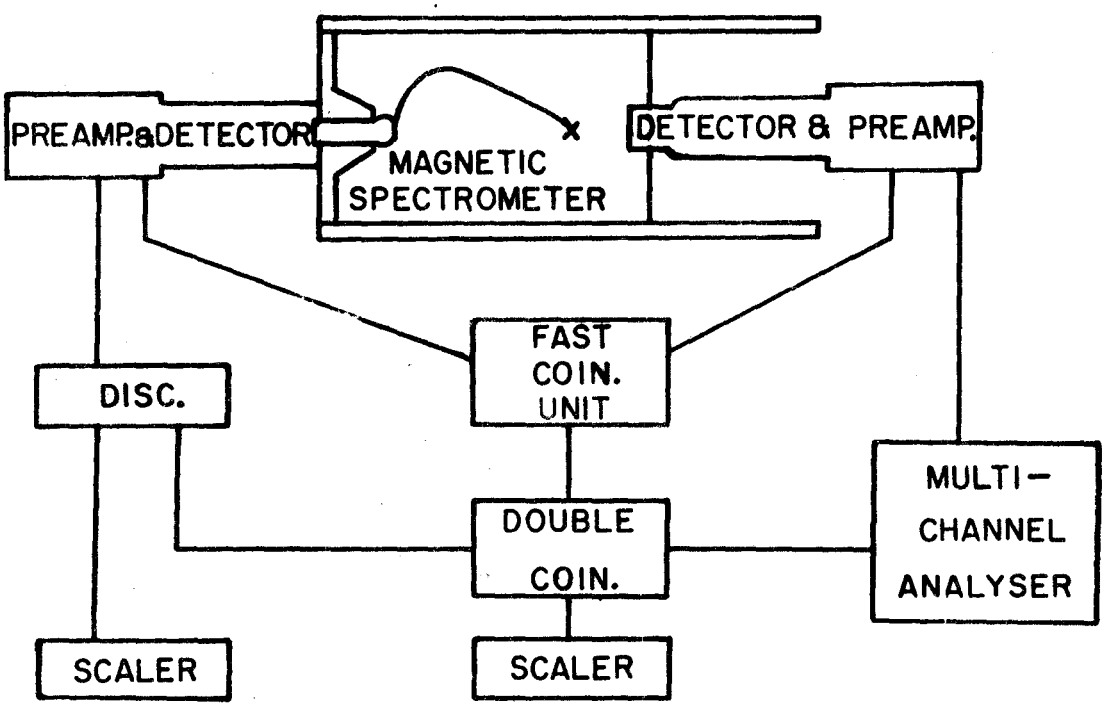
PREAMP.&DETECTOR
MAGNETIC SPECTROMETER
DETECTOR & PREAMP.
FAST COIN. UNIT
DISC.
DOUBLE COIN.
MULTI-CHANNEL ANALYSER
SCALER
SCALER

FIG 4(B)

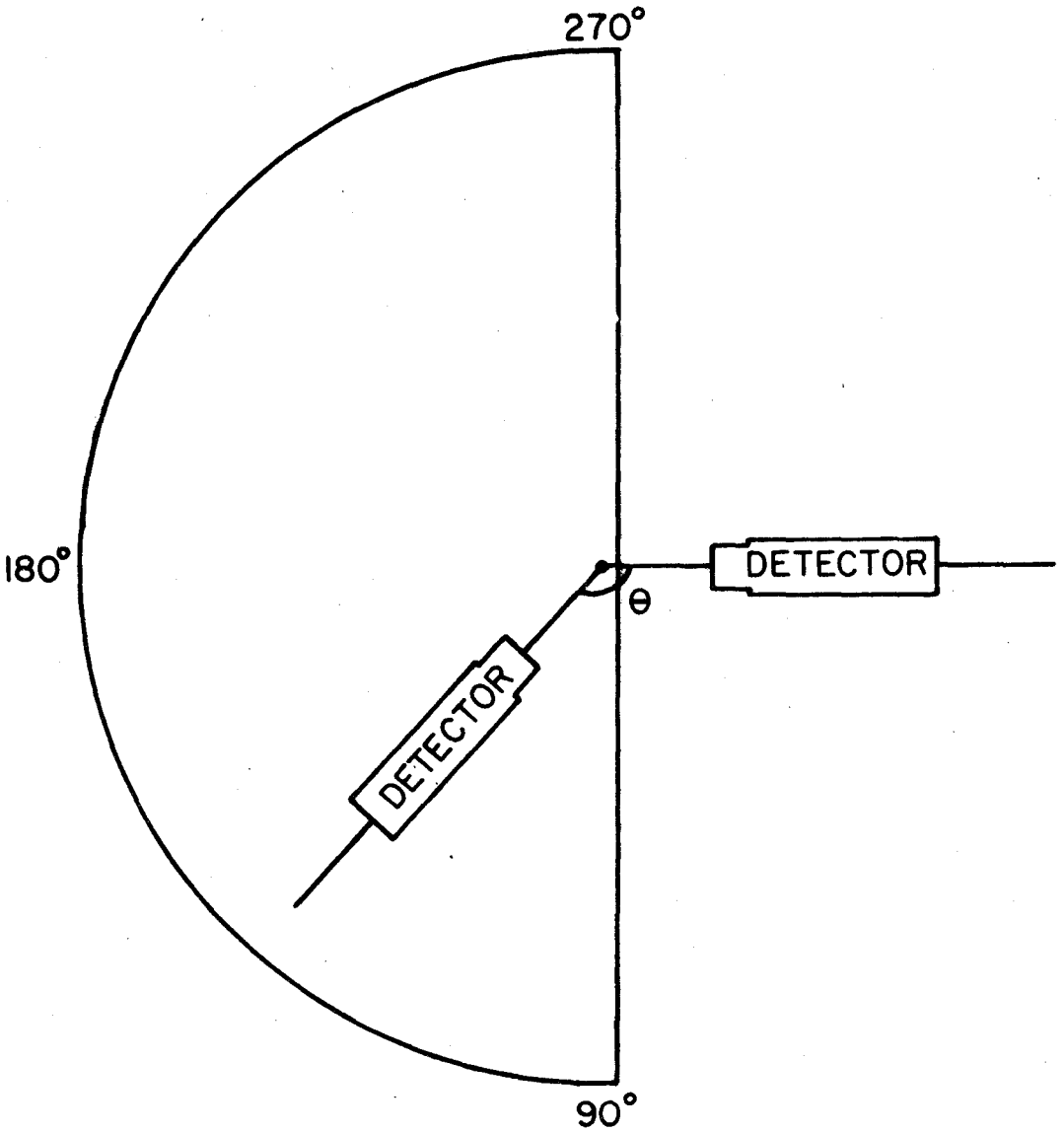

DIRECTIONAL CORRELATION TABLE

FIG 5

interest in this work, this is known to be the case - 328-kev, Ir^{194} (McGowan and Stelson (1957)). For the other states, this can be assumed to be the case because the transition from the level in question has the same multipolarity and about the same energy. Therefore, no influence on the orientation of the intermediate state exists even if a solid source is used.

(2) The source volume should be as small as possible because the finite extension of the source influences the correlation pattern observed. In the experiments described here, samples of iridium weighing about a tenth of a milligram were sealed in small quartz tubes and irradiated. The small amount of material and the narrow tube made the source appear as a point to the detectors so that no correction was applied for the size of the source.

(3) The experimental conditions must be such that the source is aligned on the horizontal axes of the two detectors and is positioned at the centre of the circle on which the movable counter moves. In these experiments, the source was situated on the axes by visual observation with the aid of a straight edge, and at the centre of the circle by the observation of the singles counting rate in the movable counter at several angles between 90° and 270°. The latter was performed carefully since no record of the singles rate was made during the course of the experiment and so no first order correction could be made by obtaining the coincidence rates per gamma ray observed at each angle. This deficiency was partially overcome by measuring the

correlation pattern in two quadrants and averaging the results.

The directional correlation was obtained by measuring the coincidence rate at nine angles in the angular range 90° to 270°. If the rates at the complementary positions were the same, the results were averaged and a least squares fit in one quadrant was made by Rose's method (1953). This fit is of the form

$$W(\theta) = (a_o \pm \sigma a_o) + (a_2 \pm \sigma a_2)\, P_2(\cos\theta) + (a_4 \pm \sigma a_4)\, P_4(\cos\theta)$$

and never contained higher Legendre polynomials because the second transition in the cascade was always a quadrupole radiation.

The coefficients in this expansion had to be corrected for the finite size of the detectors because the latter tends to obliterate the correlation pattern. This correction was made through the use of solid angle correction factors which were determined experimentally as outlined in Appendix II. It is also convenient to normalize the correction so that the first term is one. When these two operations are performed the correction function becomes

$$W(\theta) = 1 + (A_2 \pm \sigma A_2)\, P_2(\cos\theta) + (A_4 \pm \sigma A_4)\, P_4(\cos\theta).$$

The two coefficients, A_2 and A_4, are then used to determine the spin sequence and the mixing ratio of the first transition in the cascade.

A convenient method for determining the possible spin sequences when the second cascade is $2 \rightarrow 0$, is a set of graphs due to Arns and Wiedenbeck (1958) on which A_4 is plotted against A_2 for several cascades

that can arise in even-even nuclei. A much more complete tabulation from which graphs can be prepared for other cascades has been made by Taylor and McPherson (1960, 1961). The sequences presented involve a 2→0 transition as the second member of the cascade and so can be used for the cascades discussed in this thesis. When the rectangle formed by the possible values of the coefficients is plotted on this graph, the spin sequences that are allowed by those coefficients are immediately obvious because the rectangle intersects the curves of those spin sequences.

When it is recalled that the coefficients A_2 and A_4 are products of factors which depend only on the separate transitions, i.e. $A_2 = A_2^1 A_2^2$ and $A_4 = A_4^1 A_4^2$, the mixing ratio for the first transition can be obtained in the following way (Lide and Wiedenbeck (1959)). The factors for the first transition A_2^1 and A_4^1 are determined from A_2 and A_4 by dividing by the known factors of the 2→0 transition - $A_2^2 = -0.598$ and $A_4^2 = -1.069$. The deduced factors with their errors are then plotted on a graph (e.g. 11b) which depicts the values of A_2^1 and A_4^1 as a function of the fraction, Q, of the higher multipole radiation in the transition. Each factor permits a range of Q - values and the region where these overlap is considered as the range of Q - values consistent with the experimental data. Since Q is related to the mixing ratio, δ, by $Q = \frac{\delta^2}{1 + \delta^2}$ the range of δ may be deduced. Its sign also may be deduced from an examination of the same diagram.

Double Lens Magnetic Spectrometer

A magnetic field is a very convenient device for measuring the momentum and thereby the energy of an electron. In it, electrons move in curved paths whose trajectories are determined by the strength of the field. When a fixed path between the source and the detector is defined by geometrical means, the momentum of the focussed electrons is linearly related to the magnetic field.

Mono-energetic electrons will appear as a momentum distribution of finite width, i.e. a peak, because of the finite size of the geometrical openings and because of the imperfect focussing properties of the instrument. The resolution of such an instrument is defined as the ratio of the momentum width for the peak at half height, Δp, to the mean momentum of the peak, p ($R = \Delta p/p$). It is determined by the instrument, and is not a function of the energy of the radiation.

In addition to the construction of the instrument, the physical nature of the source can affect the resolution because the electrons produced in a source of finite thickness may lose some of their energy in passing to the surface of the material and escaping. A peak may, therefore, be asymmetric having a gentler slope on the low than on the high energy side. This phenomenon is called source broadening and is especially troublesome for low energy electrons.

The double lens magnetic spectrometer of the Gerholm type (1955) consists of two thick lens spectrometers viewing a common

source. With such a configuration, this instrument is ideally suited for coincidence experiments between conversion electrons in one end and conversion electrons or beta rays in the other. Its design is described in detail by Habib (1961) and the construction of one end is depicted in Figure 6. Of primary importance for the operation of this instrument are:

(1) the centre iron pole piece which reduces the magnetic field to zero at the source and therefore prevents any interference between the two magnetic fields;

(2) the outside pole piece protruding into the spectrometer along the axis which helps to create the trapezoidal field shape necessary for the desired electron trajectories;

and (3) the outer baffles at the position where the electrons are brought to a ring focus and which partially determine the resolution and transmission of the spectrometer. For small sources 2mm. in diameter, the instrument yields 1½% resolution with 2½% transmission.

If the baffle system from one end is removed and replaced by a NaI(Tl) gamma ray detector, this spectrometer is ideal for coincidence experiments between gamma rays and conversion electrons or beta rays. A schematic diagram for this experimental arrangement is presented in Figure 4B.

Coincidence Circuitry

Many radioactive nuclei are found to emit a large number of

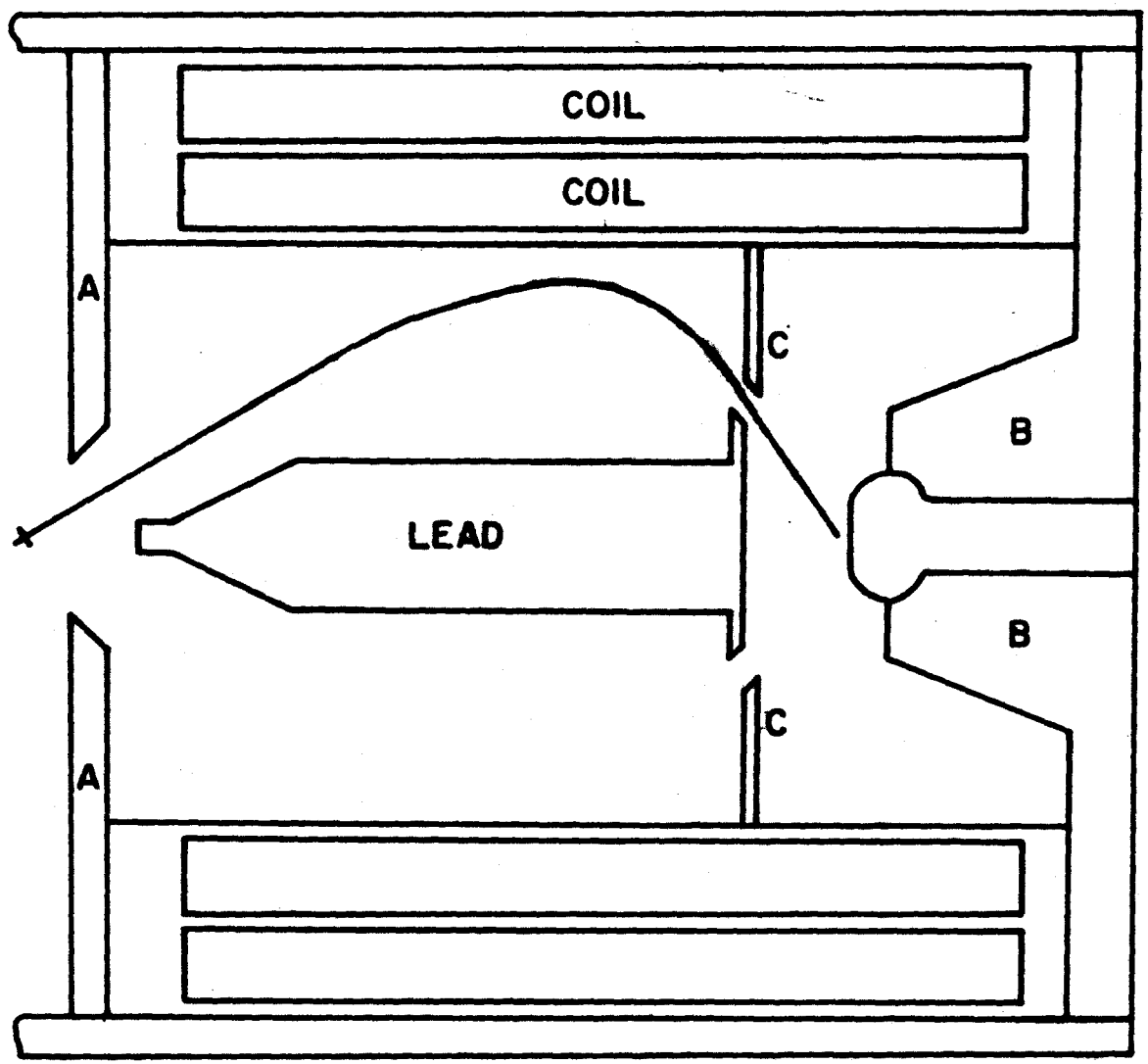

A INNER POLE PIECE B PROTRUDING POLE PIECE C BAFFLES

FIG 6

gamma rays. When this is the case, a measurement of the energy for each transition may leave the details of the decay scheme in doubt. Then the observation of a time relationship, i.e. a coincidence between two radiations, is very useful and, indeed, when all of the coincidences in a disintegration are known, the decay scheme can be constructed with confidence. The observation of a coincidence event is also important in determining other properties of the decay scheme, e.g. spins through a directional correlation experiment.

The detection of a coincidence event is accomplished by an electronic circuit which requires two input signals to give one output signal. The circuit's primary duty is to distinguish between two events which are related in time and two events which are not. Its ability to do so is governed by the resolving time of the circuit. It is therefore desirable to reduce this to a length of time as short as possible. Many parameters are involved in determining this resolving time, and for the two circuits described below, those primarily responsible will be indicated.

In addition to the detection of a coincidence event it is desirable to know the energy of the related events. This may be accomplised in two ways. In one method, the energy of the radiations is measured and then the coincidence relationship is determined. It is obvious that this method is employed in the electron-electron and electron-beta experiments because the magnetic spectrometers select the energy of the radiations before the radiation is detected. However, in experiments involving gamma rays, electronic sorting performs

the energy selection before the coincidence is determined. These complete circuits are then of the slow-fast variety. The second method involves an immediate detection of the related events in a fast coincidence circuit. Then from these coincidences, only those with the proper energy requirements, as determined by auxiliary equipment, are selected by means of another coincidence circuit of long resolving time. This fast-slow coincidence circuit is usually the type of circuit used in gamma-gamma coincidence experiments. It is inherently faster because the slow-fast circuit includes the time jitter of the energy sorting process in the resolving time of the coincidence circuit.

The earliest circuits (Rossi (1930)) had a resolving time of the order of 10^{-7} seconds which was quite adequate for use with geiger counters whose pulse rise time is long. The photomultipliers used in conjunction with scintillators produce pulses which have a fast rise time so that faster coincidence circuits are more desirable. These are several types of circuits, two of which were used in this work.

The double lens magnetic spectrometer employed a standard Bell-Graham-Petch (1952) coincidence circuit. In this circuit, pulses each of duration, τ, and of standard size serve as the input pulses to a diode discriminator which conducts only if two pulses occur together. The exact manner in which this is accomplished is outlined below and in Figure 7A.

The pulses from the anode of each photomultiplier are limited in size by a 404A pentode and sent from opposite ends along a common delay cable. At some point a short side cable - the stubbing cable - is placed. When a pulse reaches this junction, it travels down the stubbing cable. At the shorted end, it is reflected with a change in polarity and returns to the junction with the main cable. From there it travels to the end of the main cable and is absorbed in the terminating resistors. However, at the junction, a pulse appears whose duration, τ, is the length of time it takes for the pulse to travel along the stubbing cable and back. A diode leading from this point is biased in such a manner that it will not conduct unless two pulses from the opposite ends of the main delay cable overlap in the shorted cable.

This coincidence circuit is adjusted for operation in the following manner. The bias on the diode is raised until the singles pulses from either limiter are eliminated at the output. Then the effective position of the junction of the stubbing cable and the diode with the main cable is changed by inserting or removing lengths of cable in either section of the main cable between one limiter and the junction. For each length of cable, the counting rate is determined, and a plot of the coincidence rate against time delay produced by the cable is made. This delay curve is flat-topped when the circuit is performing at 100% efficiency and the time difference corresponding to the width of the delay curve at half height is the

resolving time of the circuit. If the diode bias has been raised just sufficiently to exclude singles pulses, the resolving time is twice the pulse duration determined by the stubbing cable (2 τ). For 100% efficiency in this circuit therefore, the parameter fixing the resolving time is the length of the stubbing cable, or equivalently, the pulse duration. However, it should not be concluded that the resolving time can be made as short as it is wished by the use of very short stubbing cables because the diode fails to discriminate properly. This occurs since the higher frequencies, present to a much greater amount in the short pulses, pass through the diode as though it were a capacitor.

In the gamma-gamma coincidence apparatus, a time-to-amplitude circuit (Kane et al. (1960)) employing a dual control pentode is used in place of the fast coincidence unit described above. The limited pulses from the two detectors are applied to the two grids of the 6BN6 coincidence tube (Figure 7B) after they have been "clipped" in duration by a shorted cable. This feat prevents ragged trailing edges on the pulses and improves the performance of the circuit. The size of the pulse on the anode of the 6BN6 is a measure of the time for which both grids were activated and hence the amount of overlap of the coincident pulses. It is also a measure of the time relationship of the two events. In order to make the size of the anode pulses a strongly varying function of this time relationship between the pulses, an artificial delay of about 4 nanoseconds is introduced into the second input.

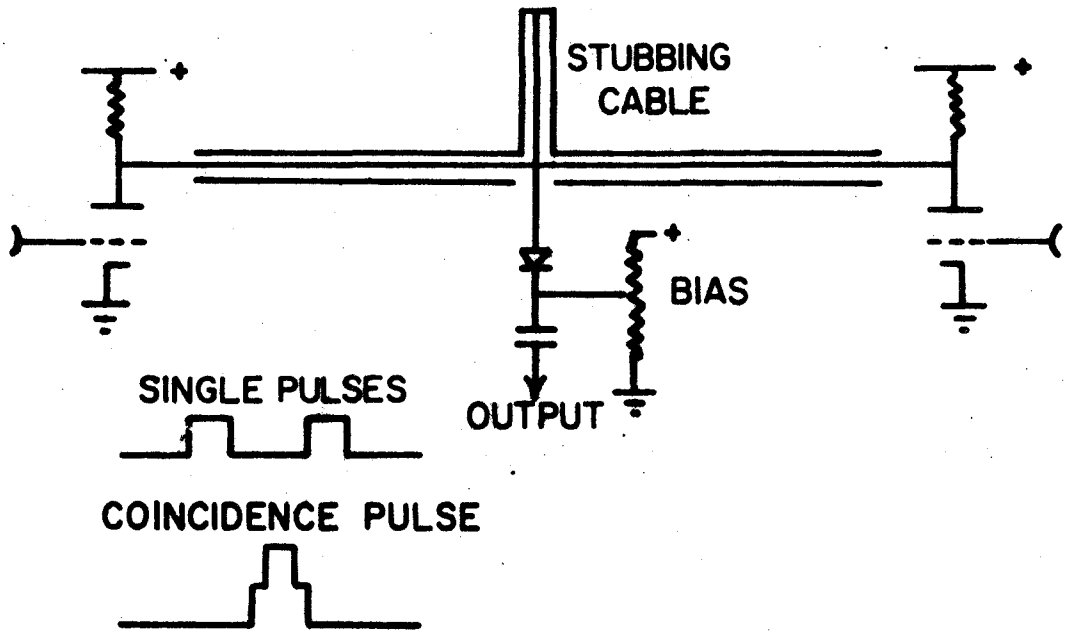

FIG 7(A) FAST COINCIDENCE UNIT FOR DOUBLE LENS SPECTROMETER

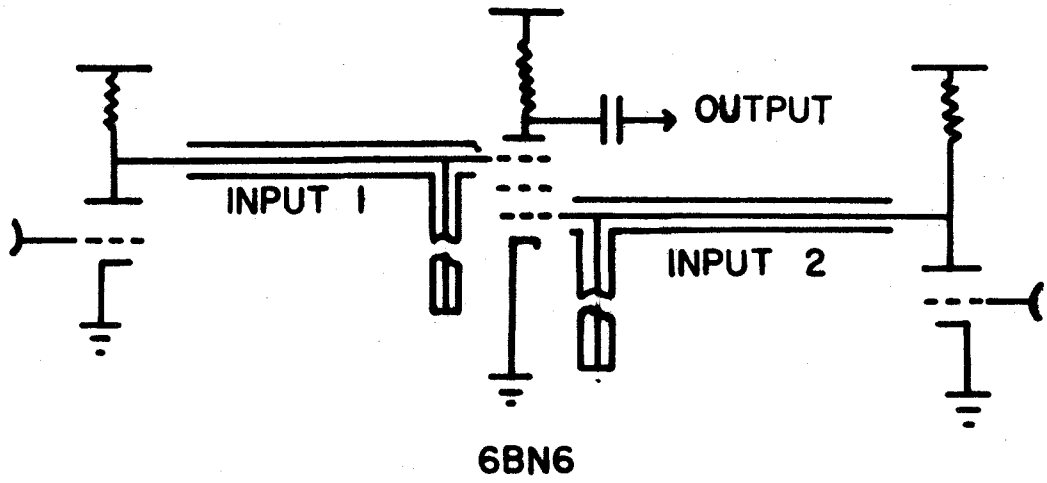

FIG 7(B) TIME TO AMPLITUDE CONVERTER FOR GAMMA-GAMMA SPECTROMETER

When the height of the anode pulses is analysed, the pulses from coincident events are found to cluster in a narrow band giving a peak in the pulse height spectrum. The width at half the peak height is defined as the resolving time of this circuit. However, if lower coincidence efficiency is tolerable, experiments with resolving times of about 1/10 of the value are possible by accepting only those pulses in a narrow window of the pulse spectrum.

As pointed out above, the size of the pulses from the 6BN6 is a measure of the time relationship between the two pulses. The broadness of the peak in the pulse spectrum is caused by the fluctuation in the time of arrival of the two pulses at the coincidence tube. This fluctuation is produced by an inherent property of a scintillation detector (Post and Schiff (1950)) and therefore this latter limitation determines the resolving time of this type of circuit.

Both these fast coincidents indicate only that a pair of coincidence events have occurred. From the total number of coincidences, specific pairs of events with the correct energy are selected by a slow triple coincidence unit in which pulses from the fast unit and from two energy selecting devices are needed for a recordable count. If one of these latter units is a multichannel analyser, a slow double coincidence is formed and used to trigger the multichannel unit (Figure 7A or 7B). In this way, all the gamma rays in coincidence with a photon or electron of specific energy can be recorded.

Theory of Coincidence Counting

In addition to the simple detection of coincidences, the coincidence method can be used to measure the intensities of beta groups and electromagnetic transitions. The expressions for these quantities, which may be quite complex, will be needed for an understanding of the experimental work in this thesis and hence the basic ones will be outlined here.

For a simple spectrum of a single beta group, the counting rate at any momentum p, is $N\Delta p$ where Δp is the momentum spread accepted by the spectrometer and N is the number of electrons of momentum p reaching the detector. The counting rate per unit momentum interval is then

$$N(p) = \frac{N\Delta p}{p} = NR \qquad \text{(III.1)}$$

where R is the resolution - a constant independent of p. But $N = N_o \omega \phi(p)$ where N_o is the source strength, ω is the transmission and $\phi(p)$ is the probability that a beta particle will be emitted with a momentum p. The total counting rate summed over the whole beta group is then

$$\int NRdp = N_o \omega R \int \phi(p)dp$$

$$= N_o \omega R \qquad \text{(III.2)}$$

where $\int \phi(p) = 1$ by definition of the probability function.

The simplest case when a coincidence experiment is useful arises from a decay scheme as shown in Figure 8A. The counting rate per unit momentum interval for the beta group, β_1, of intensity, δ_1, is

$$N_o \; R \; \omega \; \phi_1(p) \; \delta_1 . \qquad \text{(III.3)}$$

Of these electrons,

$$N_{\beta\gamma}(p) = N_o \; R \; \omega \; \delta_1 \phi_1(p) \; (\omega\epsilon)_A \frac{N_\gamma}{N_T} \qquad \text{(III.4)}$$

will be detected in coincidence with gamma ray A where $(\omega\epsilon)_A$ is the product of the solid angle and the photopeak detection efficiency for the gamma ray, and N_γ and N_T are the number of gamma ray transitions and the total number of transitions from the level being depopulated. N_γ/N_T may also be written $1/(1 + \alpha_A)$ where α_A is the total internal conversion coefficient for the transition. The total coincidence rate, i.e. the rate summed over the entire coincidence spectrum, is then

$$\int N_{\beta\gamma}(p)dp = N_o \; R \; \omega \; \delta_1 (\omega\epsilon)_A \frac{1}{1 + \alpha_A} . \qquad \text{(III.5)}$$

The singles counting rate for the beta particles at the momentum p is

$$N(p) = N_o \omega R \left[\delta_1 \; \phi_1(p) + \delta_o \phi_o(p)\right] \qquad \text{(III.6)}$$

from which the total rate is

$$\int N_\beta(p)dp = N_o \; \omega R \; (\delta_1 + \delta_o). \qquad \text{(III.7)}$$

But $\delta_1 + \delta_0 = 1$ because all the beta particles must be in one group or the other. When equations (III.5) and (III.7) are combined, the following expression results

$$\int N_{\beta\gamma}\, dp / \int N_\beta\, dp = \delta_1 \left[(\omega\epsilon)_A \frac{1}{1 + \alpha_A} \right]. \qquad \text{(III.8)}$$

For the decay scheme shown, the value of δ_1 can not be found unless the part of the expression for the gamma ray, $\left[(\omega\epsilon)_A \frac{1}{1 + \alpha_A} \right]$, is known from other information.

In an electron-beta experiment on the same decay scheme, the gamma ray part is replaced by one depending on the particular conversion line used in the experiment. If the K - line of the transition is used, the expression is $(\omega\alpha_{KA})/(1 + \alpha_A)$ where α_{KA} is the K - shell internal conversion coefficient. Because the transmission of the magnetic spectrometer has been calibrated when the baffles are wide open (Habib (1961)), a measurement of the K - line peak height or area at the spectrometer setting used in the experiment and with the baffles wide open gives the transmission, ω, directly. In addition quite accurate values of the internal conversion coefficients for transitions of a known multipole nature are available (Rose (1958), Sliv and Band (1958)) so that $(\omega\alpha_{KA})/(1 + \alpha_A)$ is known and δ_1 can be deduced.

When the decay scheme is complicated by the addition of a transition to the first excited state as shown in Figure 8B, a coincidence experiment between gamma ray A and a conversion line of B is

useful. The counting rate for the K conversion line of transition B is

$$N_{eB} = N_o \omega \alpha_{KB} \delta_B / 1 + \alpha_B \qquad \text{(III.9)}$$

The coincidence rate between γ_A and e_B can be measured by choosing positions on the peak and off the peak and then taking the difference between the two rates. By this method, the coincidence rate is

$$N_{e\gamma} = N \omega \alpha_{KB} \frac{(\omega \epsilon)_A}{1 + \alpha_A} \delta_B \qquad \text{(III.10)}$$

from which the ratio $N_{e\gamma}/N_{eB} = (\omega \epsilon)_A/(1 + \alpha_A)$ can be deduced. When this is combined with expression (III.8), the intensity of δ_1 follows. It should be noted that this determination does not require the evaluation of any solid angle or efficiency factor, but depends only on the ratios of counting rates and the areas under the total and partial beta spectra.

Many situations arise in which more than one gamma ray depopulates a level. The coincidence rate for a beta-gamma experiment is then reduced by a factor which accounts for the presence of the other gamma rays. From the decay scheme shown in Figure 8C, the coincidence rate between β_2 and γ_B is

$$N_o \omega R \delta_{\beta 2} \frac{(\omega \epsilon)B}{1 + \alpha_B} b_{B-C} \qquad \text{(III.11)}$$

where b_{B-C} is the branching ratio of B from the level 2. Its presence requires additional information to be known before a value of

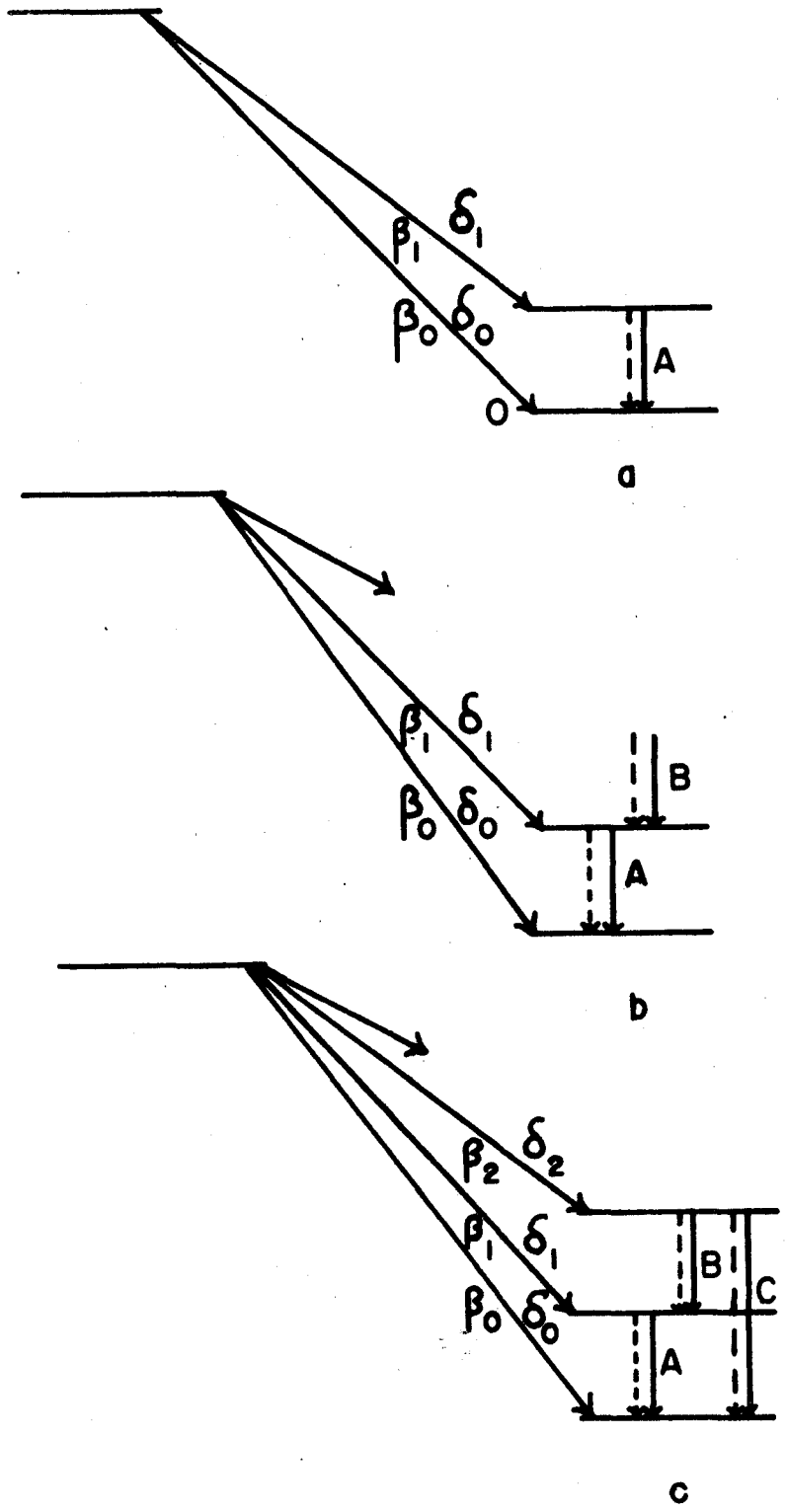

FIG 8

δ_{B2} can be deduced.

The coincidence rate for gamma-gamma experiments can be stated in a similar manner. From the last figure, the observed rate between gamma rays A and B would be

$$N_{AB} = N_o (\omega \epsilon)_A \frac{1}{1 + \alpha_A} (\omega \epsilon)_B \frac{1}{1 + \alpha_B} \delta_B \qquad \text{(III.12)}$$

in which the meaning of all the quantities has been explained. The intensity measurements are more difficult in gamma-gamma experiments because the two detectors must be calibrated for $(\omega\epsilon)$ at all energies of interest. This is a tedious and a less certain process than the solid angle calibrations for beta experiments.

All these types of experiments will be applied in the study of Ir^{192} and Ir^{194}. In their decay schemes, more complex situations will arise than have been illustrated here; however, they will require only an extension of the ideas presented in this section.

Chance

A coincidence circuit is analogous to two switches operated together by two related events. However, if the switches are operated individually a great many times in a random fashion, it is possible to have an event recorded which is due to the operation of the two switches by unrelated pulses. The two detectors in a coincidence experiment count events at the rate N_1 and N_2, and these, applied to the coincidence unit, act as random pulses. From a knowledge of these rates and the resolving time, the chance rate can be determined

because

$$N_{CH} = 2\tau N_1 N_2 .$$

(It should be pointed out that this is only half of the chance rate when using the time-to-amplitude converter because, although one pulse is designed to arrive at the coincidence unit ahead of the other for a true coincidence, either pulse may arrive first for a chance coincidence.) Conversely, from a measurement of the chance and the singles counting rate in channels one and two, the resolving time can be determined. For the experiments described in this thesis, this measurement was made by inserting a long delay cable into one side of either coincidence unit in order to destroy the time relationship of the true coincidence pulses. The random coincidences, by their vary nature, are not affected by this cable. This method was found to give the same chance rate as the "double-source" procedure in which each detector is placed in front of its own source and the random rate measured with no delay inserted into the coincidence circuit. The agreement between the two methods indicates that there is no serious pulse attenuation introduced by the extra delay cable.

In the experiments discussed in this thesis, a calculation of the resolving time was made from the chance rate and compared with that determined from the delay curve or pulse height analyser. If these numbers agreed, the circuit was assumed to be operating as designed. In addition, the measurement of the chance rate once or

twice during the course of the experiment was used to calculate the chance rate for all the data. It was felt that this method was adequate because in no experiment did the chance rate influence the final result to more than 7%. It is true that in some coincidence experiments involving beta rays, the chance rate exceeded the true rate near the end of the coincidence beta spectrum. However, little weight is ever ascribed to this data.

When the multichannel analyser was used, it was not convenient to measure the singles rate N_1 in it. Therefore the quantity $(N_{CH}/N_2)_t = 2\tau N_1$ (where N_2 is the counting rate in the gating channel), was formed from the chance rate at the time, t. This rate was then decay corrected with the half life of the source material to the time, T, when a measurement of the chance was required and multiplied by the counting rate in the gating channel at this time. The calculated chance was then

$$N_{CH} = (N_{CH}/N_2)_t \left[\exp - \lambda (T - t)\right] N_2(T) .$$

CHAPTER IV

Co^{58}

Introduction

The technique of nuclear alinement (Blin-Stoyle, Grace and Halban (1955)) offers a method of observing the spin change in a beta transition and also the character of that transition. Unfortunately, only some of the elements can be alined with the experimental methods presently available. One of these elements is cobalt.

The nucleus Co^{58} has been alined by Dagley et al. (1958) and Chapman et al. (1961) in order to study the main beta transition. In its decay, Figure P1, Co^{58} emits a strong 810 kev gamma ray whose anisotropy as a function of temperature has been used to investigate the nature of the beta decay preceding it. However, the presence of a weak gamma ray of about the same energy distorts the anisotropy expected for the single transition . Since some of the uncertainty in the results of the alinement experiment is due to inadequate knowledge about the decay of Co^{58}, the work presented in this chapter was performed to reduce some of the uncertainties in the decay scheme. This work has been accepted for publication in Nuclear Physics in the form given below. My share in this effort was the determination of

the angular correlation function of the 865-810 kev cascade and the identification of the Co^{60} contamination.

From the more accurate information on the decay scheme, the uncertainty in the character of the beta transition can be reduced. An interpretation of this transition is then given in the discussion which has been added to this chapter.

The Paper

THE DECAY OF Co^{58}

D. MacArthur*, R. Goodman, A. Artna** and M. W. Johns
McMaster University, Hamilton, Ontario

ABSTRACT

Magnetic spectrometer measurements and gamma-gamma coincidence experiments have been carried out to show that the energies of the gamma rays following the decay of Co^{58} are 810.48 $\pm$ 0.10, 865 $\pm$ 1, and 1673 $\pm$ 10 kev with intensities 100%, 1.20 $\pm$ 0.06% and 0.66 $\pm$ 0.05%, respectively. The γ-γ angular correlation pattern for the 810-865 kev cascade leads to the interpretation of the 865 kev transition as M1 + E2 with δ = +1.5 $\pm$ 0.4. The improved value of the branching ratio for the 865 kev transition, when applied to the Oxford data on the alinement of Co^{58}, leads to a value of 0.8% $\pm$ 0.4% for the Fermi admixture in the beta transition to the 810 kev state of Fe^{58}.

* Holder of a National Research Council Studentship.

**Now at National Academy of Sciences, Nuclear Data Project, National Research Council, Washington, D.C., U.S.A.

THE DECAY OF Co^{58}

Introduction

The current decay scheme[1] of Co^{58} is shown in Fig. P1. By coincidence experiments, Frauenfelder et al.[2] showed that γ_2 has an M1 + E2 mixture with $\delta = 2.2 \pm 0.3$ and an intensity of $1.6 \pm 0.5\%$. They were unable to obtain its energy but deduced that $\left| E_{\gamma_2} - E_{\gamma_1} \right| \leq$ 10 kev from the shape of the γ-γ coincidence peak in their NaI(Tl) coincidence spectrometer. Nuclear alinement experiments carried out by Chapman et al.[3] showed that the strong beta transition to the 810 kev level of Fe^{58} is predominantly G.T. in character and set an upper limit of 2% on the Fermi admixture present in the decay. The limit on this Fermi admixture was set by uncertainties in the intensity and mixing ratio of γ_2. The present experiments, carried out to improve the available data concerning γ_2 and the Fermi admixture in the dominant beta transition, involve both γ-γ coincidence measurements similar to Frauenfelder's and magnetic spectrometer determinations of gamma energies.

Coincidence Measurements

The gamma-gamma coincidence measurements were carried out with 2" x 1½" NaI(Tl) detectors integrally mounted on 56 AVP photomultipliers. These were coupled to a fast-slow coincidence circuit of conventional design with a resolving time of 5 nanoseconds (Fig. 4). The fast coincidence circuit employed 404 A tubes as limiters to feed a 6BN6 time-to-amplitude converter[4].

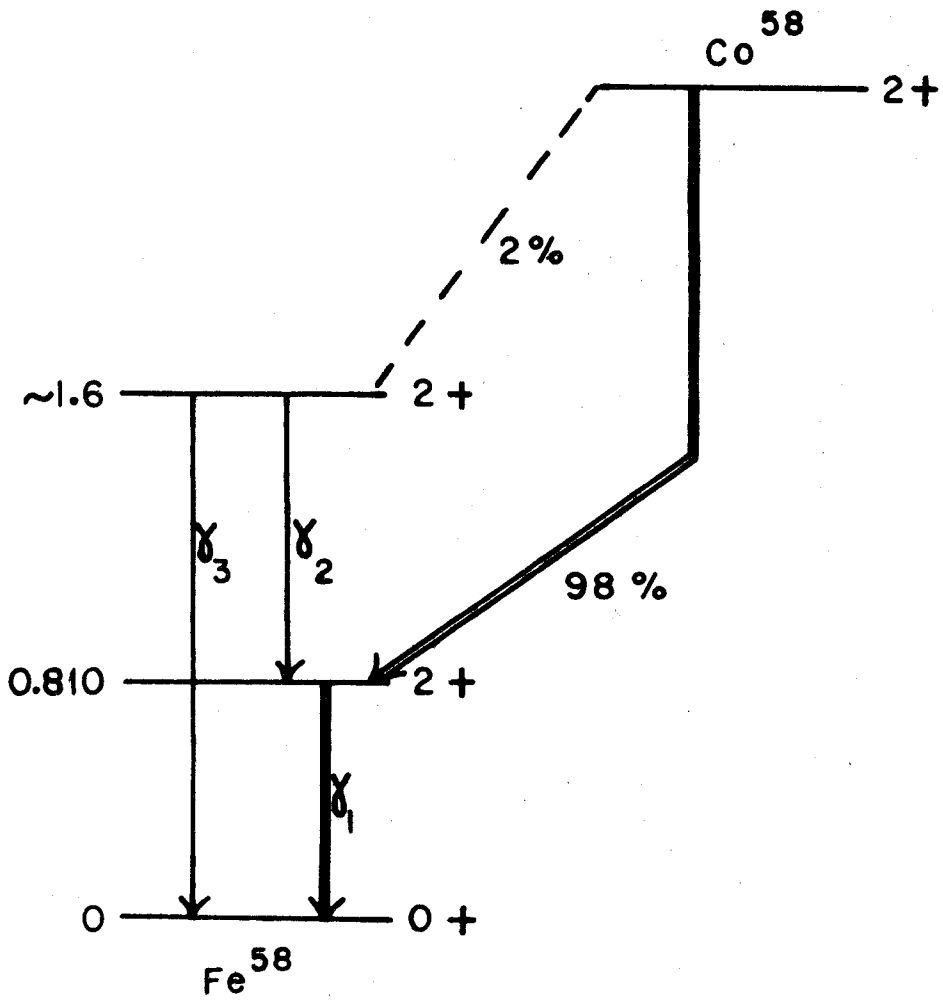

FIG P1

The time sorting was then achieved by analysing the output of the time-to-amplitude converter with a single channel analyser. The coincidence pulses from this analyser and the energy selected pulses from channel A were fed into a 1 μsec coincidence circuit whose output gated a Nuclear Data Model 120 analyser, fed directly from channel B. The stability of the photomultiplier plus the analysing equipment was such that the position of the strong 810 kev peak in channel 170 did not change by more than one channel over the period of two months during which most of these experiments were carried out.

The sources used for coincidence work ranged in strength from one to twenty micro-curies. Figure P2 presents typical gamma ray spectra. Curve A-C is a composite spectrum, the portion from 400 kev to 1000 kev being obtained at the same time as the coincidence spectrum of curve B and the high energy portion being recorded six months later when the Co^{60} contamination present in the original material had grown in more strongly. For purposes of presentation, the two curves have been normalized to give the same counting rate on the 810 kev peak. It is clear from the shift between the coincidence and single channel peaks that the weak gamma ray, γ_2, in coincidence with γ_1 has an energy considerably above 810 kev. From this shift, the energy separation of the doublet was found to be 55 $\pm$ 5 kev. The peak-to-valley ratio for the 810-865 kev coincidence peak is much smaller than for either the 810 kev peak or the 810-511 kev coincidence peak. The observed reduction in this ratio is due to the doublet character of

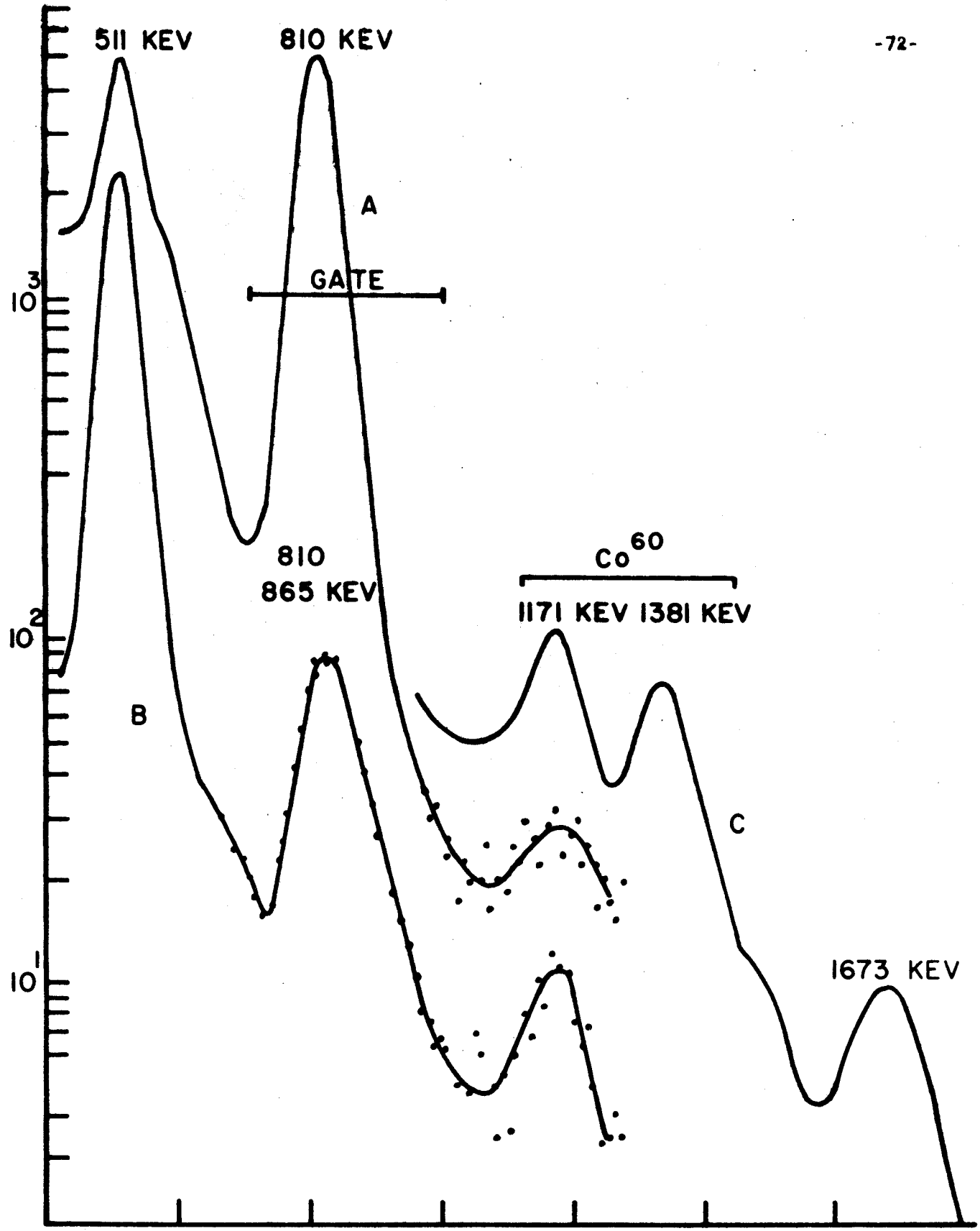
511 KEV
810 KEV
A
GATE
10^3
10^2
10^1
810
865 KEV
Co^{60}
1171 KEV 1381 KEV
B
C
1673 KEV
600
800
1000
1200
1400
1600
ENERGY (KEV)

FIG P2

the peak and to the Co^{60} coincidences present. By gating channel A on the 1171 and 1331 kev regions, it was shown clearly that this distribution possessed the spectrum characteristic of the Co^{60} Compton distribution in the 700-1000 kev region.

Angular Correlation Function for γ_1 and γ_2

The angular correlation function for the $\gamma_1 - \gamma_2$ cascade was determined with the counters 7 cm from a point source. This distance was chosen because the corrections to the correlation coefficients for the finite solid angles subtended by the detectors had been experimentally determined for this distance. Coincidences were recorded for 24 hours at each of ten angles between 90° and 270° and the data displayed in the manner of Figure P2 for each position. The counting rate as a function of angle was then determined from an analysis of these graphs. The single channel rates, monitored at frequent intervals during the period, showed no significant variation except for that expected from decay. The rates, after correction for chance and the underlying background of Co^{60}, were analysed using the method described by Rose[5]. The least squares fit to the data, presented in Figure P3, leads to values of A_2 and A_4 (corrected for solid angle) of 0.39 ± 0.07 and 0.23 ± 0.10, respectively. These values are consistent with a 0-2-2 cascade in which the second transition is a M1 + E2 mixture with $\delta = 1.5 \begin{smallmatrix} + 0.4 \\ - 0.5 \end{smallmatrix}$.

The large error on the 180° point reflects the experimental difficulties associated with this measurement. In this position, the fast coincidence rate is increased many-fold by annihilation photons and

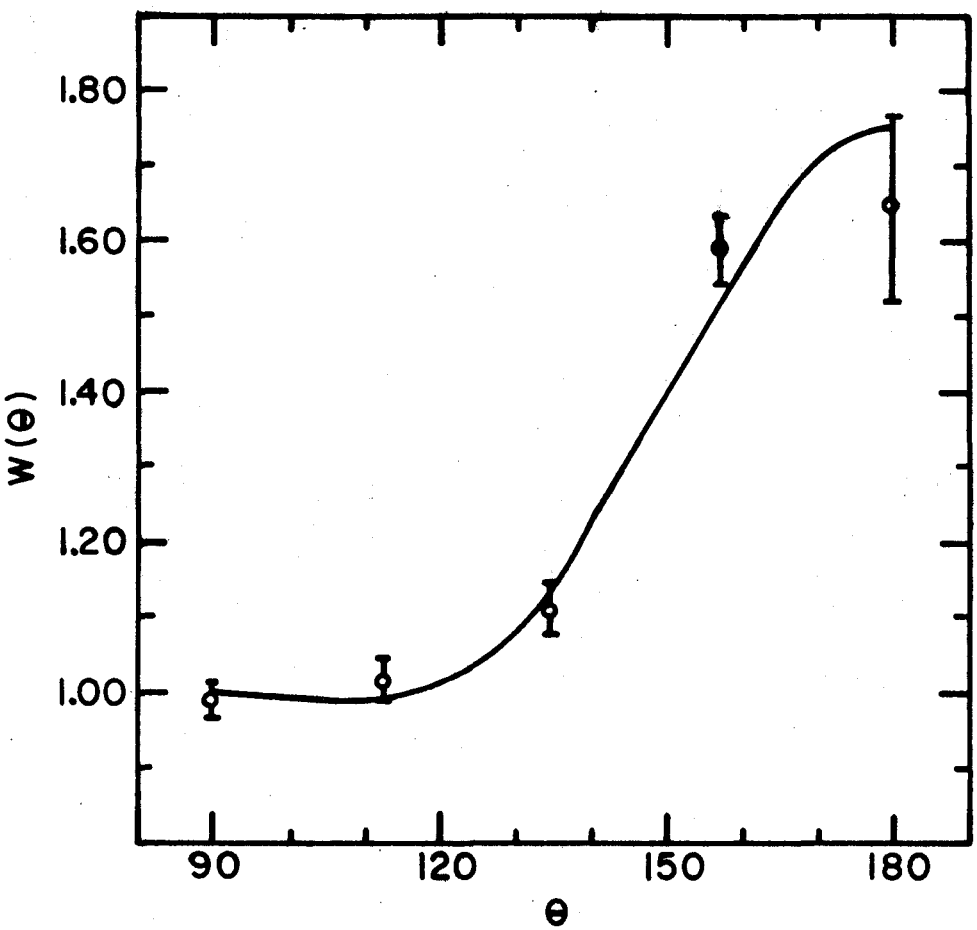

FIG P3

the process for detection of 511-810 kev coincidences is altered radically by the presence of a second 511 kev photon which will simultaneously be accepted in the detector gated on the 810 kev photopeak. Thus the pulse distribution associated with the detection of an 810 kev gamma ray in coincidence with a 511 kev transition is a broad spectrum which is fairly flat out to $\sim$1300 kev. Both of these effects increase the opportunity for pile-up pulses to be recorded as spurious γ_1 - γ_2 coincidences. To guard against this, the 180° position was compared with the 90° position, using a much weaker source than that used for the other measurements. The errors shown in Figure P4 reflect the errors in both the 180° and 90° measurement used in obtaining the ratio.

Intensity of γ_2 from the Coincidence Measurements

If f_0, f_1, f_2 and ϵ_0, ϵ_1, ϵ_2 represent the intensitites and photopeak detection efficiencies for the annihilation (γ_0) and gamma radiations (γ_1, γ_2), and if ϵ_{ij} represents the efficiency of the circuit when recording coincidences between γ_i and γ_j, it can be readily shown that

$$f_2/f_1 = (\epsilon_1/2\,\epsilon_2\,\epsilon_{12}) \times (1 + f_2\,\epsilon_2/f_1\,\epsilon_1)^2 \times (N_{12}/N_{1a}) \times (f_1 N/N_{1b}) \quad (1)$$

$$f_2/f_1 = (\epsilon_1\,\epsilon_{10}/2\,\epsilon_2\,\epsilon_{12})\,(1 + f_2\,\epsilon_2/f_1\,\epsilon_1) \times (N_{12}/N_{01}) \times (N_{0a}/N_{1a}) \quad (2)$$

where N_{12}, N_{01} are coincidence counting rates and N_{1a}, N_{1b}, N_{0a} are single channel counting rates in the photopeaks of γ_0 and γ_1 in detectors a and b. In the decay of Co^{58}, f_1 is very close to unity.

Equation (1) gives the branching ratio in terms of the coincidence counting rate, single channel rates and the source strength, while equation (2) involves only relative coincidence and single channel rates without the necessity of knowing any absolute source strength. The ratio $\epsilon_1/\epsilon_2 = 1.08$ for the crystals used.[6]

Using a standard Co^{60} source, the coincidence efficiency of the circuit was measured to be unity within a statistical error of 5% when the fixed channel was gated on the 1.33 Mev photopeak. By gating on various portions of the Compton distribution and showing that there was no observable change in shape of the coincidence spectrum for energies above 250 kev, it was concluded that the coincidence efficiency was essentially unity for photon energies above this value.

The strength of the Co^{58} source used was determined by comparing it with a standard source of Mn^{54} (Abbott Laboratories, Oak Ridge) whose single gamma ray has an energy (840 kev) very close to that of the strong 810 kev transition in Co^{58} and by making the appropriate small corrections for the change in detection efficiency with energy.

Finally, it was necessary to correct the measured efficiencies for the angular anisotropy in the $\gamma_1 - \gamma_2$ cascade. Most of the measurements were taken at an angle of 135° between the detectors since in this position the corrections for this effect were less than 3% and hence quite insensitive to the solid angles subtended by the detectors at the source. It should perhaps be pointed out that

equation (2) is not valid for the 180° position for reasons discussed earlier.

Intensity and Energy of Cross-Over Gamma Ray

Since the energies reported for γ_3 in the literature are not consistent with its interpretation as a cross-over in the light of the present measurements of the energies γ_1 and γ_2, the energy and intensity of γ_3 were re-examined, using the scintillation spectrometer and a Co^{58} source which had decayed through five half-lives. At this time, the 1331 kev peak due to the Co^{60} contaminant had acquired an intensity of roughly five times that of γ_3 and therefore provided an excellent internal calibration peak (see Fig. 2). In preliminary experiments, sources of Sc^{46}, Co^{60} and Na^{24} were used to establish the linearity of output pulse height with input gamma energy over the region of interest and at the same time to determine the detection efficiency of the spectrometer as a function of energy. The experimental response curve agreed very well with the theoretical predictions (6). The energy of 1673 ± 10 kev obtained by extrapolation from the Co^{60} peak is in excellent agreement with that expected for a cross-over transition, but in considerable disagreement with earlier measurements.

Magnetic Spectrometer Measurements

A beta source of carrier-free Co^{58} was deposited on a gold-coated mylar backing and the internal conversion spectrum in the 800 kev region was examined with a 50-cm Siegbahn-type spectrometer (7). The K and L conversion lines of the 810 kev peak are shown in curve B

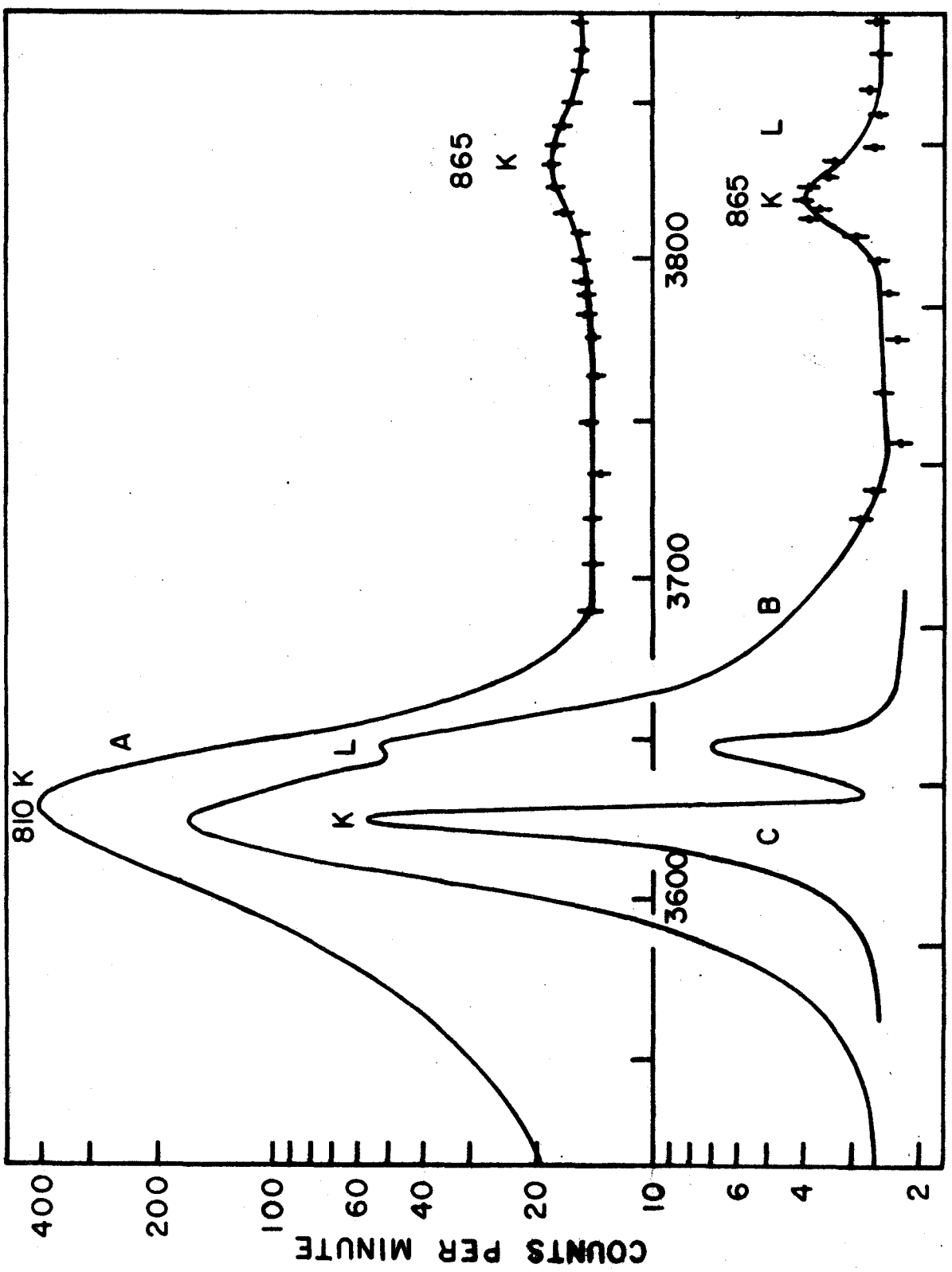
COUNTS PER MINUTE
400
200
100
60
40
20
10
6
4
2
4000
4100
4200
Bρ — GAUSS-CM.
3600
3700
3800
810 K
A
K
L
B
C
865
K
L
865
K

FIG P4

of Figure P4 (incompletely resolved). This experiment was performed before the coincidence experiments had shown that γ_2 was ~55 kev above the strong 810 kev peak. In a search for it close to the main peak, the source was taken to Chalk River where the large $\pi\sqrt{2}$ iron-free spectrometer (8) was used to examine the spectrum. This spectrum, which is shown in curve C of Figure P4, gave an accurate energy measurement for the 810 kev transition, but the search was not extended far enough to find the weak peak. After the coincidence experiments had located its position, the weak peak was found by means of the 50-cm spectrometer, using an anthracene crystal coupled to an EMI photomultiplier as the detecting unit. With the discriminator bias in the pulse amplifier set to give 100% detection efficiency when set on the strong K peak of the 810 kev transition, the counter background was 2.4 counts per minute and the 865 kev K peak 1.5 counts per minute high on this background.

By covering the beta source with a 9.3 mg/cm^2 uranium radiator, the peaks of the two gamma rays appeared in external conversion, as shown in curve A of Figure P4.

While it was impossible, by their decay rates, to rule out the possibility that the weak peaks of Figure P4 were due to some other cobalt isotope, the fact that they have the energy and intensity expected from the results of the coincidence experiments leaves no doubt that they are due to a transition of energy 865 kev in the decay of Co^{58}.

Experimental Results

The results of all the above experiments are summarized in Table PI.

The K/L ratio for γ_1 is in agreement with the well-known E2 character of this transition but does not add any support to this assignment since this ratio is quite insensitive to multipolarity. The internal conversion coefficient of γ_2 was found by comparing the internal and external conversion peaks due to γ_1 and γ_2, and then using the theoretical α_{K+L} value of 3.20×10^{-4} for an 810 kev (E2) transition.

The internal conversion coefficient of γ_2 is characteristic of an M1 + E2 mixture but the internal conversion coefficient is relatively insensitive to the mixing ratio. The angular correlation pattern provides a somewhat more sensitive test of the intensity of the E2 component in the transition; within the limits of error both of the results quoted in Table PI agree with each other and with Frauenfelder's value of 83%.

The two measurements of the intensity of γ_2 also show satisfactory agreement. The mean intensity of $1.20 \pm 0.06\%$ agrees with the measurement of Frauenfelder et al. within their rather wide limits of errors. The measured energy of γ_2 is in radical disagreement with the earlier workers.

The energy of γ_3 is consistent with its interpretation as a cross-over transition.

The Fermi Admixture in the Decay of Co^{58}

Extensive work on the alinement of Co^{58} carried out at Oxford by Dagley et al. (9) and Chapman et al. (3) has shown that the main decay mode is consistent with a spin sequence $2 \xrightarrow{\beta} 2 \xrightarrow{\gamma} 0$ in which the beta transition is almost pure Gamow Teller in character. The angular distribution is sensitive to the degree of Fermi admixture, λ, in the decay and to the intensity, f, and mixing ratio, δ, of the 865 kev transition. This gamma ray was unresolved from the 810 kev peak in the Oxford experimental arrangement. The theoretical angular distribution to be expected for small values of f and λ under the conditions of the experiment is

$$W(\theta) = 1 - B_2P_2[0.2988 + 0.299\lambda - 0.87\ f] + B_4P_4[0.712 - 1.78\lambda - 1.17\ f]$$

where the coefficients are products of the usual U and F functions. The coefficients of f are moderately insensitive to δ in the M1 + E2 mixture, a change of less than 1% being created in these coefficients by a change in δ from +2.2 (Frauenfelder's value) to +1.5 (present work). The anisotropy depends on temperature through the coefficients B_2 and B_4; P_2 and P_4 are the usual Legendre polynomials.

As the temperature is reduced W(0) decreases and $W(\pi/2)$ increases until W(0) reaches a saturation value independent of $W(\pi/2)$ for values of the latter quantity above 1.15. The saturation value of W(0) is a linear function of both λ and f and for f = 1.2%

has value of 0.830 and 0.824 for $\lambda = 0$ and $\lambda = 0.01$, respectively.

The Oxford measurements include twelve determinations of the saturation value of W(0), using three different crystals. Six of these were direct measurements of this saturation value associated with values of $W(\pi/2)$ greater than 1.15. The remaining six, associated with values of $W(\pi/2)$ between 1.10 and 1.15, could be reliably corrected for their small lack of saturation by using the theoretical curve. The saturation value of W(0) obtained in this way is 0.825 ± 0.001. (Each individual determination had a standard deviation of 0.003.) Uncertainties in f introduce an uncertainty into the theoretical values of $\pm$ 0.001, so that these experiments indicate that the Fermi admixture in the beta decay of Co^{58} is 0.008 ± 0.004. This result, which is consistent with the value of 0.01 ± 0.01 given by Chapman et al. (3), indicates that a small Fermi component actually exists in the decay.

TABLE PI

Transitions in Fe^{58}

E_γ in kev	I_γ (relative)	$\alpha_{K+L} \times 10^4$	Comment
810.48 ± 0.1	100	3.20 (theoretical)	Chalk River $\pi\sqrt{2}$ Spectrometer K/L = 11.8
864.8 ± 1.0	1.13 ± 0.15 } Mean 1.20 ± 0.06 1.24 ± 0.07 }	2.64 ± 0.4	Internal conversion and external conversion in U Coincidence measurements
1673 ± 10	0.66 ± 0.05)		Scintillation spectrometer

E2 admixture in 864.8 kev transition $82^{+18}_{-50\%}$ from internal conversion

$68^{+10}_{-18\%}$ with δ positive from angular correlation

REFERENCES

1. Nuclear Data Sheets published by Nuclear Data Project, National Academy of Sciences, National Research Council, Washington, D.C.

2. H. Frauenfelder, N. Levine, A. Rossi, S. Singer, Phys. Rev. 103 (1956) 352.

3. G. J. S. Chapman, J. M. Gregory, R. W. Hill and M. W. Johns, Proc. Roy. Soc. A 262 (1961) 541.

4. J. V. Kane, R. E. Pixley, R. B. Schwartz and A. Schwarzchild, Phys. Rev. 120 (1960) 162.

5. M. E. Rose, Phys. Rev. 91 (1953) 610.

6. W. F. Miller, J. Reynolds and W. J. Snow: Argonne National Laboratory Report (1958) 5902.

7. M. W. Johns, D. MacAskill and C. D. Cox, Can. J. Phys. 31 (1953) 225.

8. R. L. Graham, G. T. Ewan and J. S. Geiger, Nuclear Instr. and Methods 9 (1960) 245.

9. P. Dagley, M. A. Grace, J. S. Hill and C. V. Sowter, Phil. Mag. 3 (1958) 489.

ACKNOWLEDGMENTS

The authors wish to thank the beta-ray spectroscopy group at the Chalk River Laboratories of Atomic Energy of Canada for permitting them to use their large $\pi\sqrt{2}$ beta-ray spectrometer. In particular, they would like to acknowledge the assistance of Dr. J. S. Geiger in planning and carrying out the measurements with this instrument.

This work was supported by the National Research Council of Canada.

Discussion

An explanation of the observed character of the beta transition and a description of the nuclear structures of the parent and daughter nuclei are interdependent. The latter structures arise from proton and neutron configurations that are not far removed from closed shell structures. Therefore, a description of these configurations, from a shell model viewpoint, should not be too unrealistic. This last statement is not contradicted by the nature of the first excited state of Fe^{58} which is believed to be a collective excitation like the first excited states of nuclei nearby (Kisslinger and Sorensen (1960)). In fact, since it has a collective motion, its intrinsic structure will be the same as that of the ground state. Therefore, although the main beta decay of Co^{58} goes to this first excited state, the transition is between states describable in terms of shell model configurations.

The most likely configurations for these nuclei are presented in Table II. (The proton closed shells up to 20 and the neutron closed shells up to 28 have been omitted.)

TABLE II

Ground State Configurations of Co^{58} and Fe^{58}

	Protons	Neutrons		
Co^{58}	$(1f_{7/2})^{-1}$	$(2p_{3/2})^3$,	$(2p_{3/2})^2\ 1f_{5/2}$,	$(1f_{5/2})^3$
Fe^{58}	$(1f_{7/2})^{-2}$	$(2p_{3/2})^4$,	$(2p_{3/2})^2 (1f_{5/2})^2$,	$(1f_{5/2})^4$

Since Co^{58} decays by positron emission and electron capture, the

proton configuration of the parent is the most important feature in the beta transition. This configuration is one nucleon less than a closed shell, $(1f_{7/2})^{-1}$, and requires that the spin of the protons be 7/2-. This situation is substantiated by the observed ground state spins of the odd cobalt isotopes, Co^{57} and Co^{59}. In addition, the configuration is expected to be quite pure because the levels next in energy are relatively far removed.

Since the ground state spin of Co^{58} is known to be 2 +, a $(2p_{3/2})^3$ neutron configuration is suggested. However, configuration mixing is possible because the $1f_{5/2}$ level is nearby and is likely to be present to some extent. The neutron configuration of Co^{58} is therefore probably not pure but is composed of at least the configurations listed in Table II.

With these assumptions about the nucleon arrangements of the parent, it is not difficult to construct the corresponding configurations of the daughter in which one proton has been removed from the level, $1f_{7/2}$, and a neutron has been added to the suggested states of the parent.

The experimental observation that the beta transition has predominantly an allowed Gamow-Teller character means that the proton transforming to a neutron changes its angular momentum from $\ell + \frac{1}{2}$ to $\ell - \frac{1}{2}$, i.e. suffers a "spin-flip". Such a beta transition is possible between the proton $1f_{7/2}$ level and the neutron $1f_{5/2}$ level present in the configurations of Co^{58} and Fe^{58}. However, this is the only

transition permitted. Since the log ft value of the beta transition is higher than normal for an allowed transition (Goeppert-Mayer (1953)), the neutron configuration of the daughter is probably not pure $(1f_{5/2})^4$. This is also suggested by the fact that the observed spin of Fe^{55} is 3/2-.

In allowed Fermi transitions, there is no spin-flip and therefore the nucleon must not change any of its shell model quantum numbers in transforming from one nucleon species to the other. A Fermi admixture in the beta decay of Co^{58} is therefore difficult to understand because the neutron $1f_{7/2}$ level is completely filled. The least objectionable hypothesis permitting this type of transition is the destruction of the pure proton configuration of the parent and the addition of the configurations $(1f_{7/2})^{-2}$ $(1f_{5/2})$ and/or $(1f_{7/2})^{-2}$ $(2p_{3/2})$. These configurations will permit an allowed Fermi transition to some of the neutron configurations of the daughter. When it is recalled that the energy separation of the levels $1f_{5/2}$ and $2p_{3/2}$ from the level $1f_{7/2}$ is relatively large, the smallness of the admixture is reasonable.

CHAPTER V

Pt^{192}

Introduction

The platinum metals have nuclei whose nucleon configurations are sufficiently far removed from closed shells that they are not rigidly spherical, but not so far removed that they are strongly deformed. Among these transition nuclei are the even-even nuclei Pt^{192} and Pt^{194} which can be studied through the beta decay of the odd-odd iridium nuclei of the same masses. By means of the spectrometers described in Chapter III, several features of these two decays have been investigated. In this chapter the experiments on Pt^{192} will be discussed while the next chapter will be devoted to Pt^{194}.

Because of its long half life and ease of production from Ir^{191} whose neutron capture cross section is quite high, Ir^{192} has been the object of many careful investigations. As a result of those involving the gamma rays, a decay scheme has been constructed which has five well established excited states and several other states of a less secure nature. In addition, the spins of the first four excited states have been determined from several directional correlation experiments. All of this information is summarized in the Nuclear Data Tables (1959) and reference to the original papers

will be made when needed.

Knowledge of the beta rays of Ir^{192} is much more sparse. Studies of them have been confined mainly to a measurement of the end point of the highest energy group (Nuclear Data Tables (1959)) although Bashilov, Anton'eva and Dzhelepov (1952) did resolve the continuum into three groups. In addition, two beta-gamma correlation experiments have been performed (Shiel, Wyly and Braden (1958), Deutsch, Doumont and Macq (1958) and the results of these investigations will be included in the discussion of the beta experiments conducted in this chapter.

The experimental work described in this chapter is based on the accepted decay scheme whose features of importance in this work are presented in Figure 9. In this figure, a number of weak gamma rays have been omitted in the interest of clarity of presentation. Since the experiments are of two types, this chapter has been divided into two parts. In Part A, the directional correlations of the two weak cascades through the first excited state are described. These were performed to measure the spins of the 1381-kev and 1201-kev levels. In Part B, several beta-gamma coincidence experiments are reported. Of primary interest was the shape of the first inner beta group. This was measured through a coincidence experiment involving the 600-kev gamma rays. In addition, the beta-gamma experiments provide a new approach to the analysis of the several beta groups. These experiments have the following advantages:

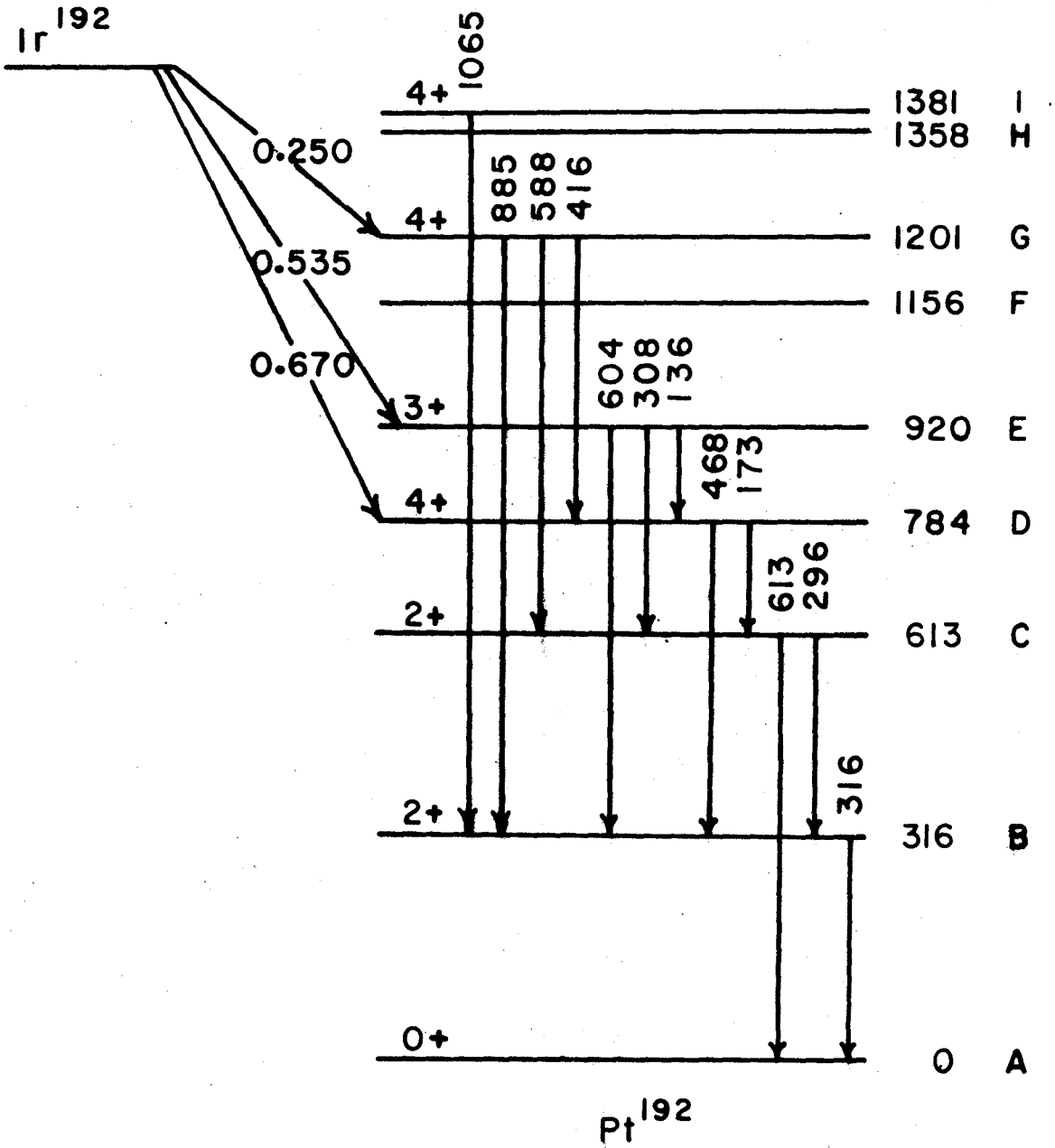
Ir 192
1065
4+
1381 I
1358 H
0.250
885
588
416
4+
1201 G
0.535
1156 F
0.670
604
308
136
3+
920 E
468
173
4+
784 D
613
296
2+
613 C
316
2+
316 B
0+
0 A
Pt 192

FIG 9

(1) they extend the region of the beta spectrum that is free of conversion lines

and (2) they mix the beta groups in different proportions from that present in a singles spectrum, and therefore their intensities can be obtained in several independent ways.

A. DIRECTIONAL CORRELATION

Introduction The spins of the first four excited states of Pt^{192} have been determined in several directional correlation experiments (Taylor and Pringle (1955), Baggerly et al. (1955), Mraz (1957), Shiel, Wyly and Braden (1957), Kawamura, Aoki and Hayashi (1958)). In some instances, the internal conversion coefficients of the relevant transitions have been used to remove an ambiguity (Baggerly et al. (1955)). Pt^{192} is an even-even nucleus and therefore has a ground state spin of 0. Its first excited state (level B) has a spin of 2, and these two facts form the basis of the interpretation of the measured correlation functions.

The spin of the level D is found to be 4 from a measurement of the 468-316 kev cascade. This cascade is easy to interpret because it involves only two gamma rays.

The spins of states C and E have been determined from a 300-300 kev coincidence experiment. Since the different 300-kev gamma rays cannot be separated in NaI(Tl) detectors, this experiment measures the combined correlation of four cascades through the first and second excited states. Although the spin of the level C is deduced

to be 2 from this experiment, an ambiguity exists for the spin of the state E. Fortunately this can be removed by a 600-300 kev correlation experiment which, although complex, established the value of this level as 3.

In addition, the conversion coefficients and the mixing ratios are consistent only with transitions arising from states of the same parity as the ground state; therefore, the first four levels have even parity.

One other cascade involving the 1201-kev level (level G) has been investigated. In that experiment, the correlation of the 588- and 613-kev gamma rays was measured. This experiment is difficult to perform because of the interference from the simultaneous detection of the 296- and 316-kev gamma rays in one counter instead of a single 613-kev gamma ray. Nevertheless, the spin of this 1201-kev level was determined to be 3 or 4.

The directional correlations described in this chapter were designed to clarify the last assignment and to measure the spins of the 1381-kev level. After this work was complete, a paper by Simons, Spring and Wendt (1962) appeared which, besides confirming the experiments of the earlier workers, reported the results of experiments similar to those described here. A discussion of their conclusions will be postponed until after the present work has been described.

Experimental Method Ir^{192} can be obtained free of all interfering radioactivity by irradiating natural iridium and waiting several

weeks for the Ir^{194} to decay. Figure 10 shows the gamma ray spectrum in coincidence with the 300-kev peak. This spectrum closely resembles that of a simple singles spectrum, and is illustrated to show the high energy lines at 885-kev and 1065-kev which are difficult to see above background in a singles spectrum. It is these gamma rays which were used in the correlation experiments and the arrows indicate the range of pulse heights included in each photopeak.

As pointed out earlier, the correlation pattern must be corrected for the finite solid angle of the detectors. In order to reduce this, the crystal can be moved a long way from the source. However, this decreases the solid angle and therefore the counting rate. As a compromise a source-to-detector distance of seven centimeters was chosen and all of the experiments were performed in this arrangement. In addition, the experiments to determine the solid angle correction factors were performed at this distance (Appendix II).

Besides the precautions outlined in Chapter III for any directional correlation experiment, several additional precautions peculiar to this experiment which lasted several weeks were observed.

(1) Although the experimental equipment had been tested for drifts in energy and found to be quite stable, the spectrum in the gating channel was observed before and after the count at each angle was taken to check that neither a drift nor a sudden change in gain had occurred. In addition, the window in the energy spectrum of this

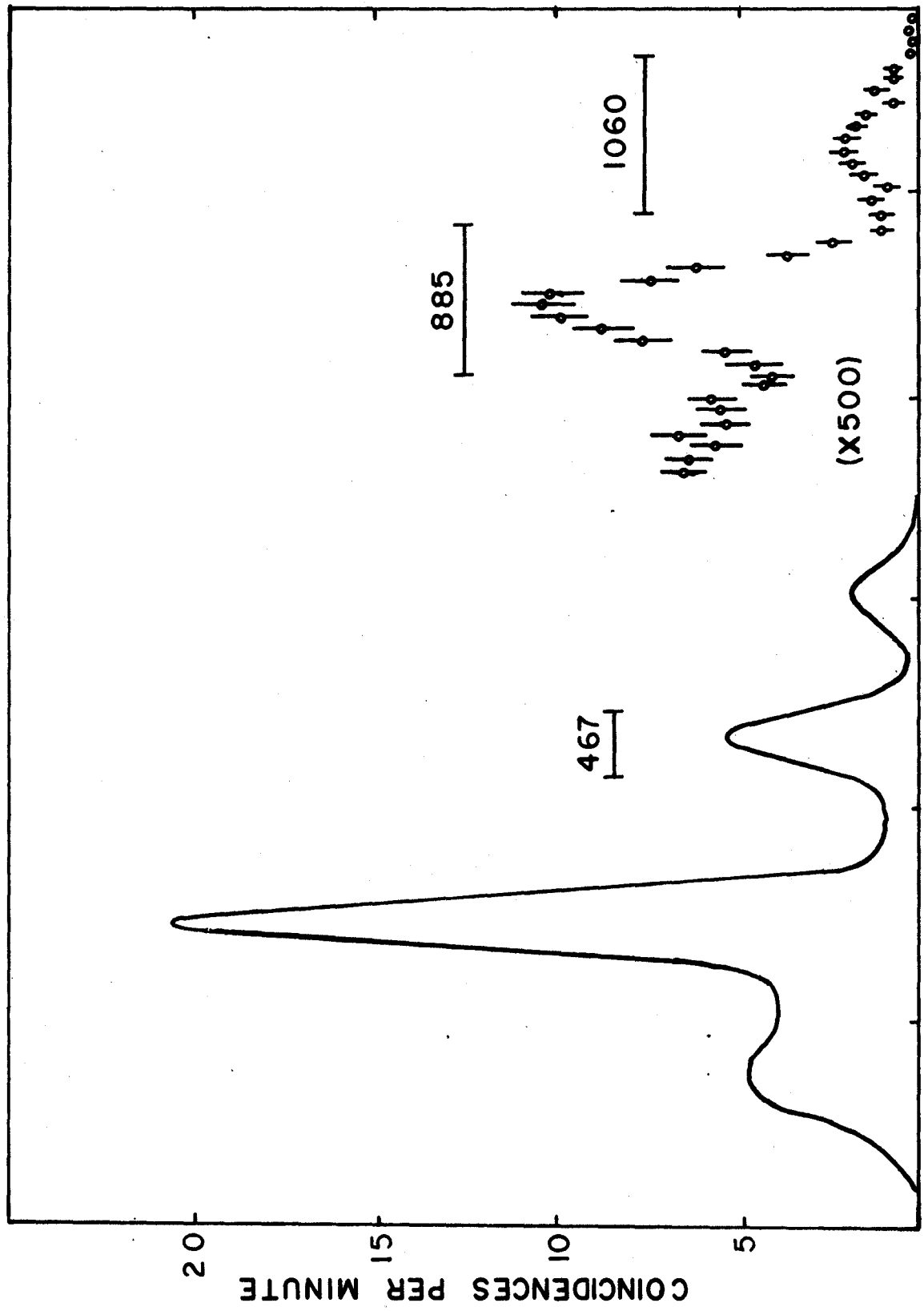
COINCIDENCES PER MINUTE
20
15
10
5
0
200
400
600
800
1000
ENERGY (KEV)
467
885
1060
(X500)

FIG 10

channel was made quite wide in order that any small drift might not affect the coincidence rate greatly. For the multichannel analyser the accumulated spectrum was available and a visible observation could be made of the position of each gamma ray peak. Throughout the course of the experiment, these positions were observed to wander slightly (less than 2%). A correction for this was made by shifting the region assigned to the various gamma rays, the few channels indicated.

(2) From previous experience, the performance of the fast coincidence unit was known to be such that the coincidence efficiency was quite constant. However, as a further check, the correlation pattern was not obtained by placing the movable counter at the predetermined angles in a sequential manner from 90° to 270°, but by selecting the predetermined angles in a random fashion. In this way, changes in efficiency would be evident in coincidence rates that would not follow a smooth curve.

(3) The chance for a pile-up pulse in the region of the gamma rays of interest was reduced by a factor of five by inserting 1.8 gm./cm.^{2} of lead in front of the counter recording the high energy spectrum. This amount of lead was chosen because it does not attenuate the high energy gamma rays by more than 25%, but strongly attenuates the 300-kev trio and the 468-kev transition.

The coincidence spectrum at each angle was observed twice for at least seven hundred minutes each time and the counts in the channels containing the photopeak of interest were added. A

correction for chance, which was not more than 7% in any cascade, was made in the manner outlined in Chapter III and then the totals were corrected for the decay of the source. After a comparison of the rates for the different runs at the complementary angles had shown that the variations between them were within statistics, the results were averaged and combined to give the coincidence rates at the five angular positions 90°, 112.5°, 135°, 157.5° and 180°. Before a least squares fit to the data was performed (Rose (1953)), any contribution from the compton distribution of a higher energy transition was subtracted in a manner to be outlined. The actual fit was then to experimental data involving only one cascade.

On the graphs depicting the results of the correlation experiment, these fits are displayed as dotted lines. Also appearing on the figures are solid curves which represent the pattern when a correction for the finite size of the detectors has been applied. Since any addition treatment of the data involves the corrected coefficients, these are shown in the upper right corner of each figure.

Results

(1) The 1065-316 kev Cascade The 1065-kev transition is the most energetic gamma ray in coincidence with the 316-kev gamma ray. Therefore, no correction for the compton distribution of higher transitions was needed. From a total of about three hundred counts per position, the correlation pattern shown in Figure 11a was obtained. Since the

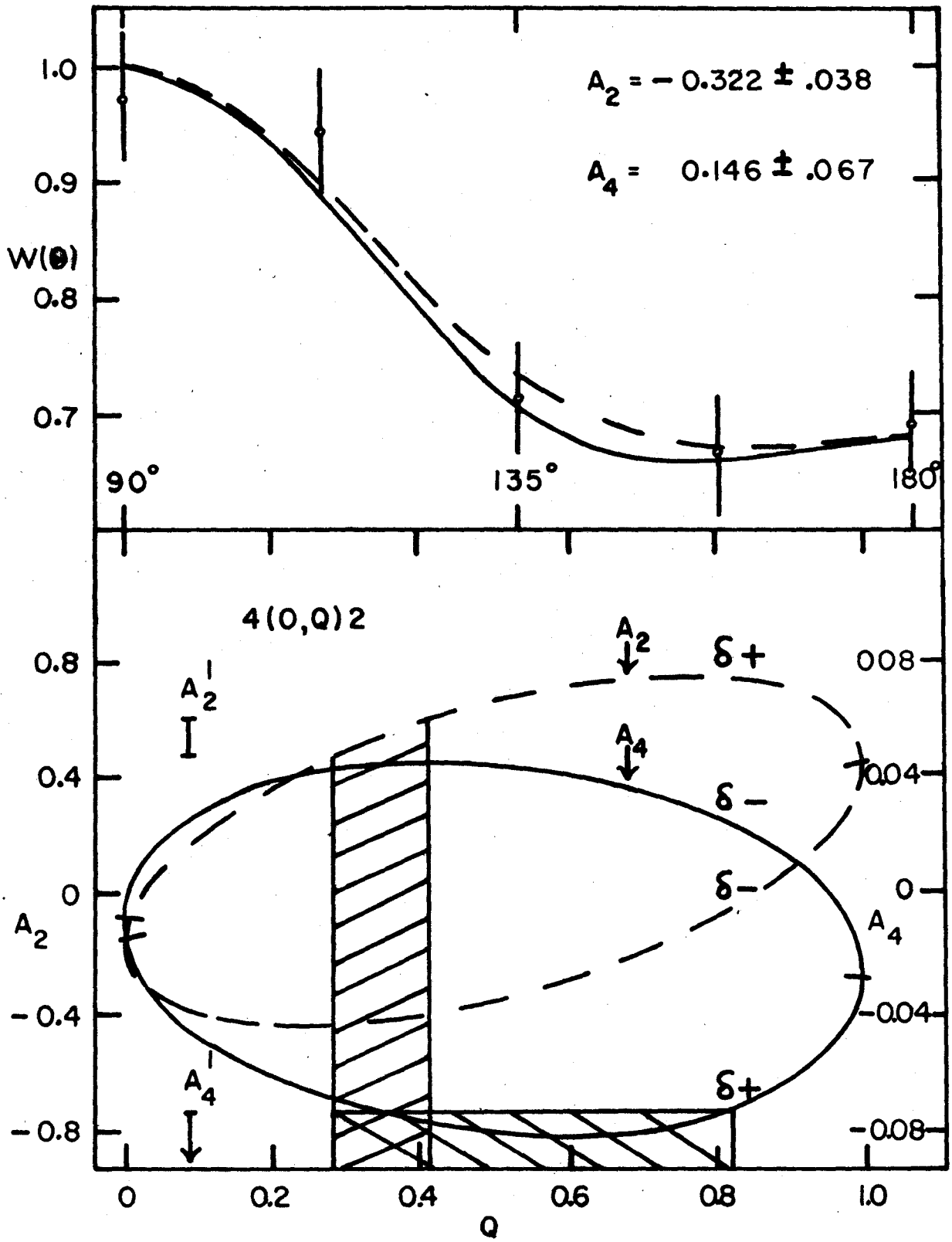
$A_2 = -0.322 \pm .038$
$A_4 = 0.146 \pm .067$
W(θ)
1.0
0.9
0.8
0.7
90°
135°
180°
4(0,Q)2
A_2'
A_4'
A_2
A_4
δ+
δ−
δ−
δ+
0.8
0.4
0
−0.4
−0.8
0.08
0.04
0
−0.04
−0.08
0
0.2
0.4
0.6
0.8
1.0
Q

FIG 11a & 11b

316-kev transition is known to have a pure E2 character, the coefficients, $A_2 = -0.322 \pm .038$ and $A_4 = 0.146 \pm .067$ determine the possible spin sequences as 2-2-0 or 4-2-0 in a manner shown in Figure 13. The former sequence can be rejected because a spin of 2 for the 1381-kev level would allow a ground state transition to occur. Moreover, it is hard to see any mechanism for exciting the 1381-kev level unless there is a beta group feeding it. If this state has spin 2 and a beta group feeding it, there should be intense beta groups feeding levels B and C. Since these are not observed, the 1381-kev level can hardly have such a low spin.

The 4-2-0 cascade can be considered more closely. The coefficients are distinctly different from those of a pure quadrupole-quadrupole sequence. In fact the A_2^1 and A_4^1 factors, $0.54 \pm .08$ and $0.14 \pm .07$ respectivley, indicate that this transition is a quadrupole-octupole mixture. The situation is presented in Figure 11b. From the figure, one deduces that $Q = 0.4 \pm .08$. This leads to a value of $0.83 \pm .03$ for δ.

(2) The 885-316 kev Cascade The coincidence spectrum of the 885-kev peak in coincidence with the 316-kev peak is distorted by the underlying compton of the 1065-kev transition. Instead of estimating the contribution from the compton to the total rate in the 885-kev region, a comparison of the compton rate in this region to the photopeak rate of the 1170-kev line of Co^{60} was made. The line shape of the 1170-kev gamma ray was determined by a coincidence

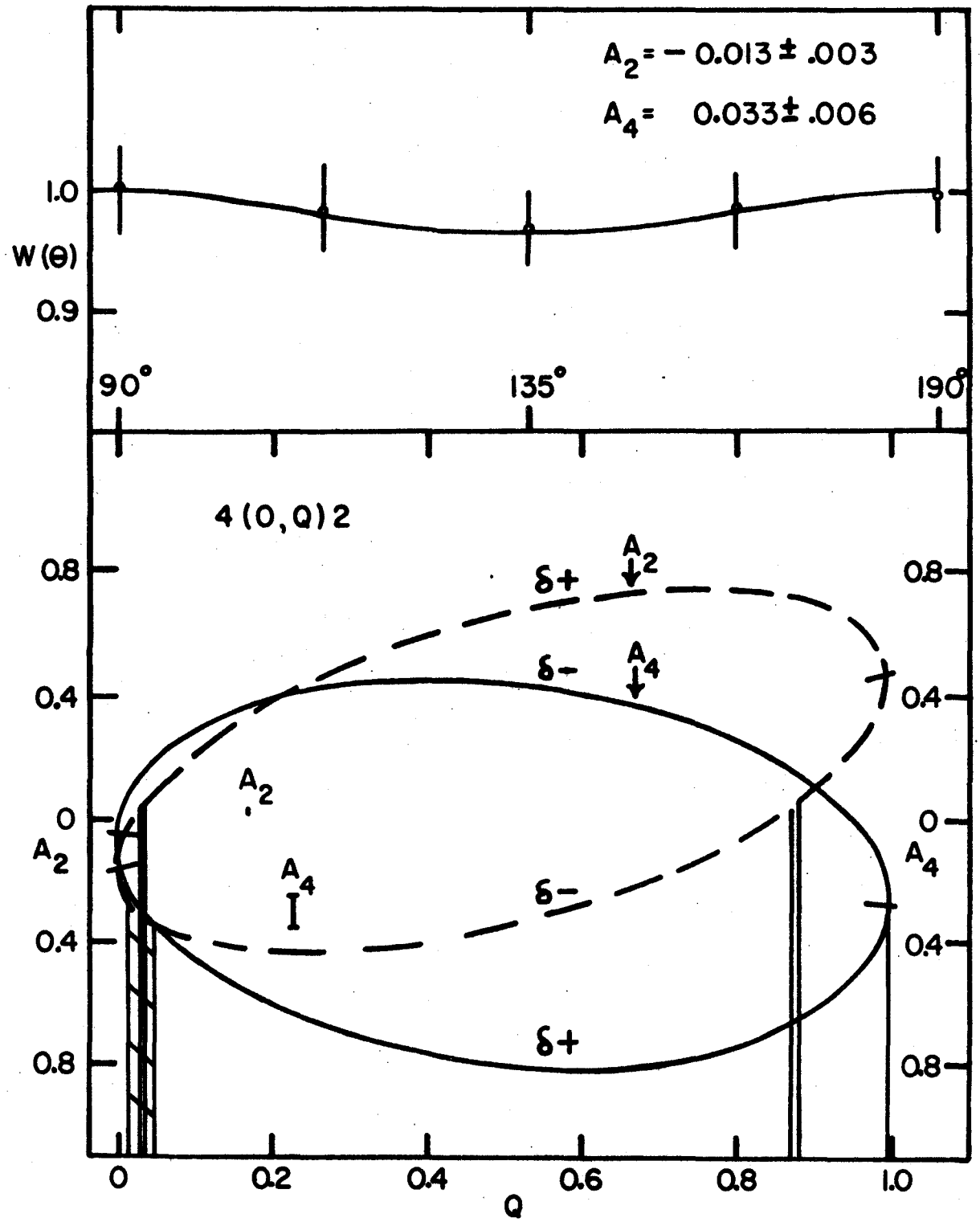
A2 = − 0.013 ± .003
A4 = 0.033 ± .006
1.0
W(θ)
0.9
90°
135°
190°
4(0,Q)2
0.8
0.4
0
A2
0.4
0.8
δ+
A2
δ−
A4
A2
A4
δ−
δ+
0.8
0.4
0
A4
0.4
0.8
0
0.2
0.4
0.6
0.8
1.0
Q

FIG 12a & 12b

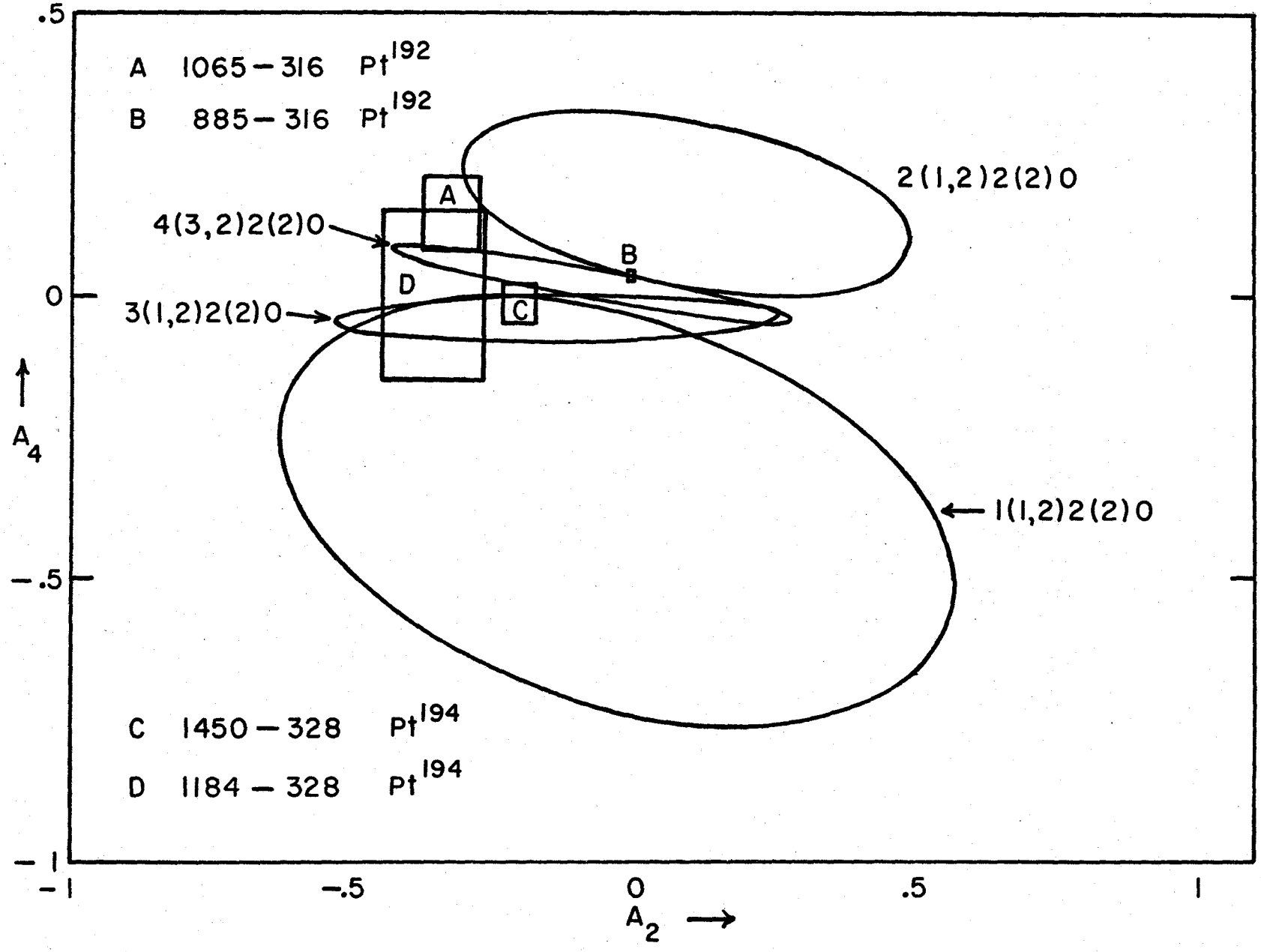
.5
0
−.5
−1
−1
−.5
0
.5
1
A_4
A_2
A 1065 − 316 Pt^{192}
B 885 − 316 Pt^{192}
C 1450 − 328 Pt^{194}
D 1184 − 328 Pt^{194}
A
B
C
D
4(3,2)2(2)0
3(1,2)2(2)0
2(1,2)2(2)0
1(1,2)2(2)0

FIG 13

experiment in which the gating pulses correspond to an energy of 1330 kev. The factor from this comparison was found to be 0.7. This factor and the counting rate of the 1065-316 kev cascade were then used to correct the 885-316 kev cascade for each angle individually. Although there is a difference in the energy between the cobalt line and the iridium 1065-kev line, the comparison was thought to be justified because the compton distribution does not change quickly with energy. In addition, the 885-316 correlation data is insensitive to the size of this correction within rather wide limits.

From the net rate for the 885-316 kev cascade of about two thousand counts per position, the correlation pattern shown in Figure 12a was deduced. The coefficients $A_2 = -0.013 \pm .003$ and $A_4 = 0.033 \pm .006$ indicate from Figure 13 that the sequences 2-2-0 and 4-2-0 are permitted. The former may be rejected by arguments similar to those used for the 1065-316 kev cascade. The latter cascade has been analyzed for the mixing ratio of the octupole to quadrupole radiation as shown in Figure 12b. The result is $\delta = 0.18 \pm .01$.

(3) The 478-316 kev Cascade As has been pointed out, this cascade has been well studied and is known to be a 4-2-0 cascade of two E2 transitions. Since the experimental method allowed this cascade to be observed simultaneously with the cascades involving the higher energy transitions, the results for this cascade served as a check on the reliability of the entire group of experiments.

Since the 468-kev photopeak sits on the compton distribution of several transitions grouped at 600 kev, a careful analysis of the compton profile of these transitions under the 468-kev peak was made by constructing a composite 600-kev peak from the known relative intensities of the gamma rays and the measured spectral shape of the Cs^{137} gamma ray. The factor for the ratio of the compton distribution under the 468-kev region to the photopeak of the 600-kev line was found to be 0.2. From the net rates of the 468-316 kev cascade, the coefficients are found to be $A_2 = 0.099 \pm .019$ and $A_4 = -0.005 \pm .026$ and these agree well with the theoretical values for a 4-2-0 cascade of two pure quadrupole radiations and with the results of other workers.

Discussion

(1) The 1201-kev Level The spin of this level has been investigated through the 588-613 kev cascade as discussed earlier and is thought to be 3 or 4. The present work indicates that the spin is 4 and that the 885-kev gamma ray is predominantly an E2 transition with an admixture of 3% octupole radiation. Simons, Spring and Wendt (1962) agree with the spin assignment, but require only an admixture of 0.5% in the 885-kev transition because their correlation pattern is much closer to that of a pure 4-2-0 cascade.

(2) The 1381-kev Level The present experiments suggest that this level has a spin of 4 with a 40% octupole admixture in the 1065-kev transition. The correlation pattern found by Simons, Spring and

Wendt for this cascade is much less anisotropic than the one presented here. Although their pattern permits four possible interpretations, they consider only the following three:

3-2-0	98% quadrupole
3-2-0	100% dipole
4-2-0	94% octupole

Of these, they prefer the second because it produces a 3-, 1381-kev state in analogy to a similar state found in Os^{190}.

Because of the large positive A_4 coefficient, a spin sequence of 3-2-0 is definitely excluded by the correlation pattern obtained in this work. Since a large octupole admixture in a gamma ray transition is unusual, the experimental coincidence rates producing the observed correlation pattern were closely scrutinized for systematic errors. Errors which would increase the counting rate at 90° and 112.5° or decrease it at 135°, 157.5° and 180° could cause the large anisotropy observed, but all attempts to find sources for such errors were fruitless. It is much easier to discover effects that will reduce an anisotropy than effects which will increase it. Moreover, the fact that the 468-316, 885-316 and 1065-316 kev cascades were recorded simultaneously and that the first two of these are in reasonable agreement with other workers, makes it difficult to imagine a mechanism which could uniquely distort one correlation function.

The effects of possible pile-up have also been considered. It is easy to imagine a mechanism for pile-up in the 885-316 kev

cascade, but almost impossible to conceive of a mechanism for pile-up in the 1065-316 kev cascade.

In conclusion, the present work forces one to believe that the 1381-kev level has a spin of 4 and that there is a large amount of octupole radiation in the 1065-kev transition.

B. BETA-GAMMA COINCIDENCES

Introduction Since the beta continuum of Ir^{192} has strong conversion lines throughout its length, a singles spectrum offers little hope for reliable analysis. However, from an observation of the decay scheme, it can be seen that the beta groups in coincidence with some gamma rays should not be difficult to analyse and therefore the information from these experiments should be relatively reliable.

Experimental Method When beta spectra are examined in the low energy region, source thickness is a great problem. In order to produce thin sources, the sputtering technique described in Appendix I was developed. It is believed that this aim was achieved sufficiently that significance could be attached to data for beta rays with energies as low as 100-kev because

(1) several beta spectra (Ir^{194}) which are believed to be free of conversion lines in the region of interest were found to be linear to this energy,

and (2) conversion lines of Pt^{192} at approximately 130 kev showed no source broadening.

The deposited layers of iridium were irradiated for ten hours. After the Ir^{194} had died away, Ir^{192} sources of a few tens of microcuries were available for experimentation. The gamma rays in coincidence with beta rays of different momentum were observed in the double lens magnetic spectrometer in which one baffle system has been replaced by a NaI(Tl) crystal (Figure 4B).

The fast coincidence unit was adjusted for operation as described in Chapter III and had a resolving time of sixteen nanoseconds for most of the experiments. Since the experiments described here were performed over considerably shorter lengths of time than the directional correlation experiments, the elaborate precautions taken for those experiments were not necessary although periodic checks of the same general nature were made. In the operation of the magnetic spectrometer, the momentum settings were known to be reproducible to better than one part in a thousand.

The beta-gamma experiments were performed by using the magnetic spectrometer to choose momentum settings that avoided conversion lines. In the most extensive experiments, fourteen measurements in the momentum range 1,000 to 3,600 gauss-cm. were used to define the beta groups. At each momentum setting, the beta singles rate, $N\beta$, and the gamma spectrum in coincidence with these electrons were taken for a period of thirty minutes. These momentum settings were repeated a number of times to provide statistical accuracy and checks of reproducibility.

A typical gamma coincidence spectrum can be imagined from Figure 10. The 467-kev peak contains one gamma ray, while the 300- and 600-kev peaks are composed of several gamma rays whose relative contributions to the coincidence rate change with the momentum setting. The beta-gamma coincidence rate associated with each photopeak was determined from the number of counts in the peak as collected by the multichannel analyser. Since these rates were very small near the end point of the beta spectrum, it was necessary to choose the number of channels associated with the peak from the spectrum recorded for a momentum setting near the maximum of the beta spectrum.

These rates were immediately corrected for chance by the method outlined in Chapter III. The singles rate, N_β, for the beta continuum at the momentum settings employed in the experiment was used for N(T) in the chance expression.

For the 600-kev coincidence rate, a Fermi analysis could be performed without further corrections because no compton distribution from the higher energy gamma rays is included in this peak. At each momentum setting the rates for the two lower energy peaks were corrected for the underlying compton distribution in the following way. The spectrum of a single gamma ray of about the same energy as that producing the underlying compton (661 kev for the 600-kev peak and 411 kev for the 461-kev peak) was taken, and the ratio of the compton distribution in the region of interest to the photopeak of the gamma ray was measured. This ratio was then used in conjunction

with the photopeak counting rate of the interfering gamma ray to make the appropriate correction.

From the Fermi analysis performed on the net rates thus obtained, the product of an intensity and a gamma detection efficiency factor ($\omega\epsilon$) was deduced. This factor for the 316-kev gamma ray was determined by a coincidence experiment between the gamma ray and the K-shell conversion line of the 467-kev transition in the manner outlined in Chapter III. Also a Cs^{137} source of known strength was available and was used to calibrate the gamma detector at 661-kev. With these two experimentally determined efficiencies as standards, the theoretical curves of Miller, Reynolds and Snow (1958) were used to obtain the 467-kev efficiency factor by interpolation.

Results

(1) Coincidences Between the 467-kev Gamma Rays and Beta Rays The 467-kev peak sits on the compton distribution of the 600-kev lines. In order to correct for this, 30% of the 600-kev coincidence peak was subtracted from the 467-kev rate. (This does not imply that the correction is a fixed percentage of the true 467-kev-beta rate). The net rate for the 467-kev peak was then used to construct the Fermi plot shown in Figure 14. An examination of this plot reveals that the beta transition in coincidence with the 467-kev gamma ray has an end point of $0.670 \pm .005$ Mev, and that it is represented by a straight line, at least down to 160 kev. Points below 120 kev (not shown on the figure) reveal some departure from the straight line and may indicate the presence of a weak low energy group with an end point of <200 kev feeding this 467-kev line indirectly.

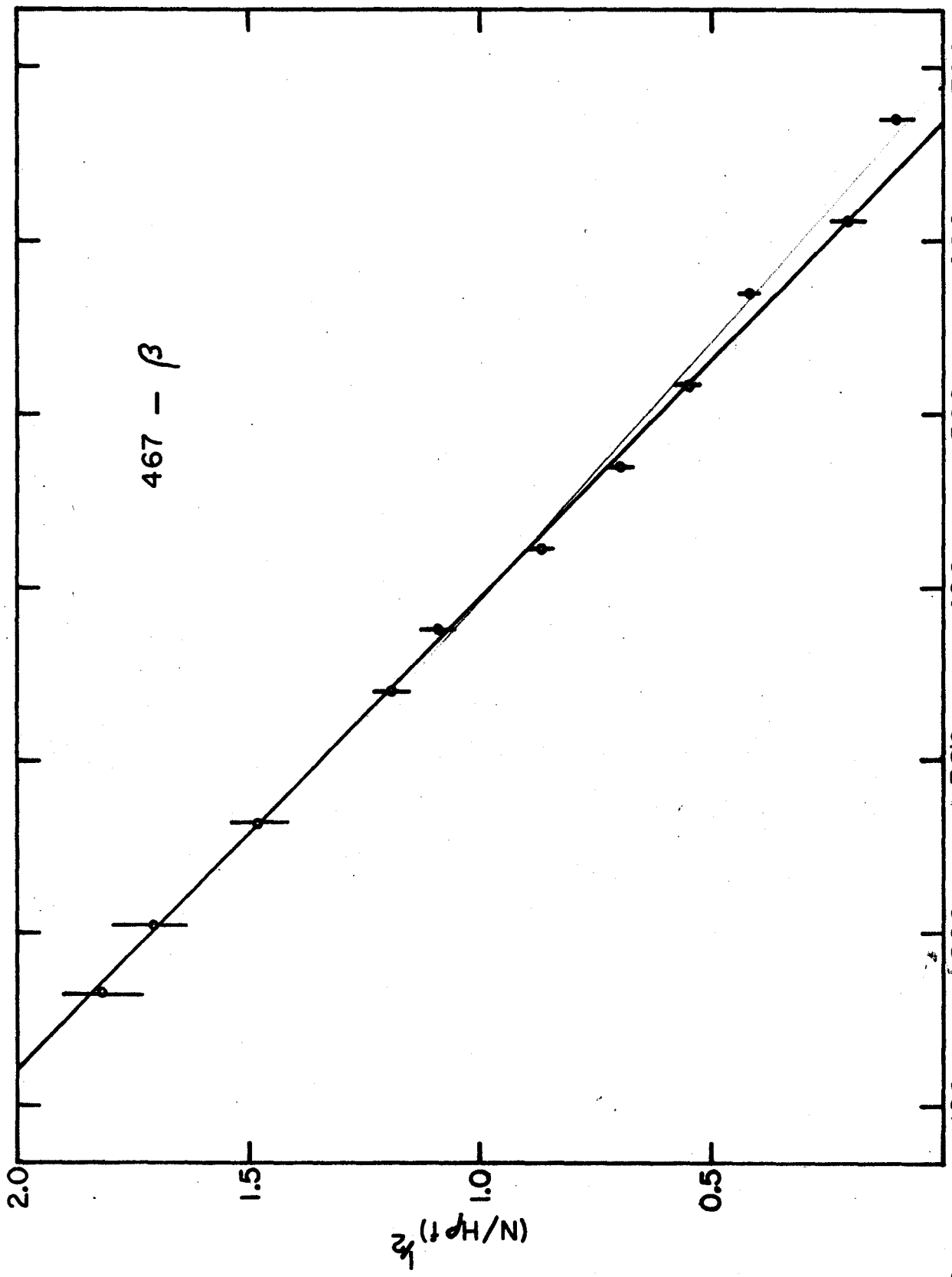

FIG 14

(2) Coincidences Between the 600-kev Gamma Rays and Beta Rays This experiment was performed to study the nature of the fist inner beta group. From an analysis of the decay scheme (Figure 9) and the intensities of the gamma rays (Table III), it can be seen that this experiment offers the best chance of observing the first inner beta group free of the higher energy group.

The 600-kev coincidence peak has no contribution from higher energy gamma rays so that the rates can be used directly in a Fermi analysis. The latter is shown in Figure 15. L_1 represents the contribution of the high energy group and was constructed in such a manner that the end point was 670-kev. It is not possible to define this line very precisely but its position has little influence on the analysis of the 535-kev group. The circles of Figure 15 represent the data after the high energy group has been subtracted. Although a straight line can be drawn through this data so that it intersects the flags representing the errors on each circle, a curve offers a better representation of the trend of these circles. Moreover, the straight line would intersect the energy axis above 550 kev at much too high an energy for the expected 0.535-Mev beta group. If the data is treated as being associated with a first forbidden unique transition and the corresponding approximation $a_1 = p^2 + q^2$ is applied, the circles transform into the crosses. The resulting straight line is a good representation of the trend of these points and intersects the energy axis at 533 ± 7 kev very close to the expected energy.

A third group is left after the subtraction of this first forbidden unique transition. It has an end point of $0.250 \pm .025$ Mev.

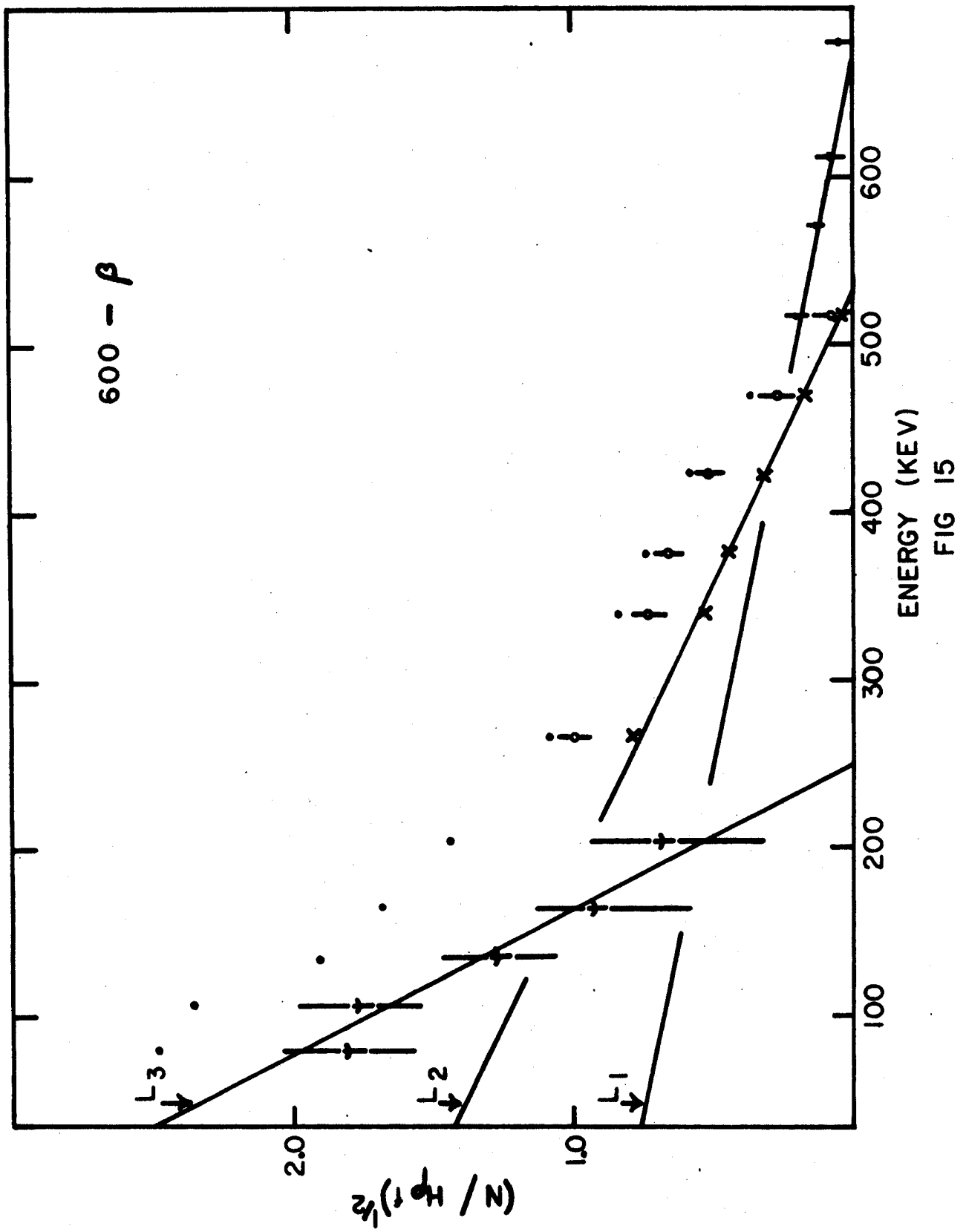

FIG 15

(3) Coincidences Between the 300-kev Gamma Rays and Beta Rays The 300-kev peak is the prominent peak in the gamma spectrum. It is a composite peak of at least three gamma rays; 296-kev, 308-kev and 316-kev. An examination of the decay scheme will show that these are in coincidence with all of the beta groups. This composite peak sits on the compton distribution of the 467-kev and 600-kev gamma rays. The corrections for these contributions were respectively 20% and 30% of the net rate for the photopeaks of the latter transitions. The corrected rates were then used to construct the Fermi plot shown in Figure 16.

Again the high energy group is difficult to determine because there are few momentum settings available at which conversion lines are not a serious problem. However, with a knowledge of the end point of this group from the previous work, a quite definite straight line can be drawn. When this group is subtracted, the remaining data appears as the circles on the Fermi analysis. It is not apparent that a curved line is needed to represent this data; however, a straight line representation again intersects the energy axis above 550 kev. When the shape for the unique transitions is applied, the crosses result. A straight line through these depicts them well and also gives an end point of 538 $\pm$ 10 kev for this beta group.

Again a third group with an end point of 0.270 $\pm$ .040 Mev appears when the two high energy beta transitions have been subtracted.

(4) Intensities of the Beta Groups The intensities of the beta groups

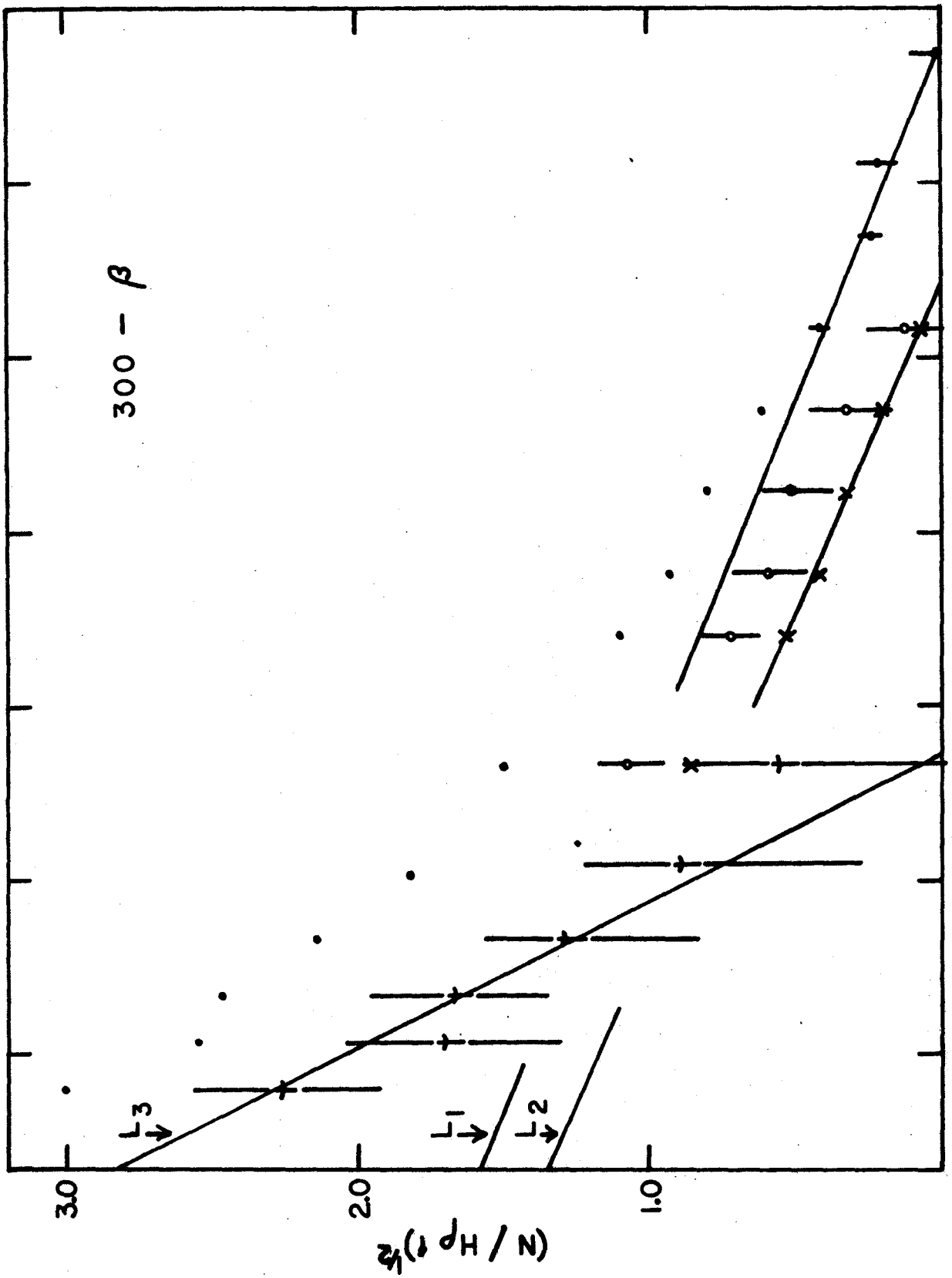

FIG 16

can be determined in the manner outlined in Chapter III. In those expressions, the coincidence rate was governed in a simple manner by the intensity of the beta group of interest. Because of the complexity of the Ir^{192} decay scheme, the particular beta group in coincidence with the gamma rays may be detected through several cascades. Therefore a probability-of-detection factor P must be introduced to relate the measured intensties to the true beta intensities. If the notation developed in Chapter III is used, the following expressions result:

In the 467-kev-beta experiment, the probability-of-detection of the 0.670-Mev group is

$$P_{0.670} = b_{467 - 173}$$

In the 600-kev-beta experiment,

$$P_{0.670} = b_{173 - 467}\, b_{613 - 296}$$

$$P_{0.535} = b_{604 - (308 - 136)} + b_{308 - (604 - 136)}\, b_{613 - 296}$$

$$P_{0.250} = b_{588 - (885 - 417)} + b_{588 - (885 - 417)}\, b_{613 - 296}$$

In the 300-kev-beta experiment,

$$P_{0.670} = b_{468 - 173} + 2b_{173 - 468}\, b_{296 - 613}$$

$$P_{0.535} = b_{308 - (604 - 136)} + 2b_{308 - (604 - 136)}\, b_{296 - 613} + b_{604 - (308 - 136)} + b_{136 - (604 - 308)}$$

$$P_{0.250} = 2b_{588 - (885 - 416)}\, b_{296 - 613} + b_{885 - (588 - 416)} + b_{416 - (588 - 885)}$$

Because the numerical values of these factors depend on the intensities of the gamma rays in Pt^{192}, a set of these as measured by Baggerly et al. (1955) is included in Table III for the convenience of the reader.

TABLE III

Intensties of Relevant Gamma Rays in Pt^{192}

Gamma Ray (kev)	Relative Intensity
136	0.2
173	1.0 (Johns and Nablo)
296	36
308	35
316	100
417	1.6
467	64
588	7.1
604	14
613	8.4
885	0.5

The numerical values deduced for these factors given in Table IV are insensitive to the particular set of intensities used, and essentially the same ratios would have resulted had the values of Johns and Nablo (1954) been employed.

Table IV presents a summary of the experimental data and probability-of-detection factors for the beta-gamma coincidence experiments performed with Ir^{192}. The resultant intensities are also set

TABLE IV

Experimental Results

Beta Group	0.670-Mev		0.535-Mev		0.250-Mev		Units
Experiment	1	2	1	2	1	2	
467-kev-β							
$N_{\beta\gamma}$	$12.8 \pm .8$	$15.4 \pm .9$					c/m
$N_\circ \omega R$	77 ± 4	90 ± 5					10^2 c/m
$(\omega\epsilon)/1 + \alpha_T$	42 ± 5						10^{-4}
P	0.98						
δ	41 ± 9	42 ± 9					%
300-kev-β							
$N_{\beta\gamma}$ (U)	20 ± 2	30 ± 5	21 ± 3	22 ± 5	33 ± 9		c/m
$N_{\beta\gamma}$ (N-U)	20 ± 2	30 ± 5	31 ± 5	26 ± 7	27 ± 10		c/m
$N_\circ \omega R$	77 ± 4	90 ± 5	77 ± 4	90 ± 5	90 ± 5		10^2 c/m
$(\omega\epsilon)/1 + \alpha_T$	73 ± 5*		75 ± 5#		75 ± 5#		10^{-4}
P	1.00		2.16		1.76		
δ (U)	35 ± 8	45 ± 12	17 ± 4	15 ± 5	27 ± 11		%
δ (N-U)			25 ± 7	18 ± 7	23 ± 11		%
600-kev-β			Combined				
$N_{\beta\gamma}$ (U)	$1.0 \pm .3$		$4.8 \pm .5$		4.1 ± 1.0		c/m
$N_{\beta\gamma}$ (N-U)	$1.0 \pm .3$		$5.3 \pm .8$		3.2 ± 1.0		c/m
$N_\circ \omega R$	167 ± 9		167 ± 9		167 ± 9		10^2 c/m
$(\omega\epsilon)/1 + \alpha_T$	32 ± 4		32 ± 4		32 ± 4		10^{-4}
P	$0.20b_{173\text{-}468}$		0.420		0.920		
δ (U)	$0.670b_{173\text{-}468}$		22 ± 6		8 ± 3		%
δ (N-U)	$= .10 \pm .05$		24 ± 8		6.5 ± 3		%

U - value when shape is unique
N-U - value when shape is allowed
\# - mean efficiency of 293-308-316 kev triplet
* - efficiency of 316-kev gamma ray alone

forth in this table.

In the calculation of the intensity of the 0.670-Mev beta group, a minor difficulty arises because the intensity of the 173-kev transition relative to the 467-kev gamma ray is not very well known. The data available from the 467-kev-beta and 600-kev-beta coincidence experiments suggests that $b_{468-173} = 0.8$ and that the intensity of the 173-kev transition is therefore 13 in violent disagreement with the figure of 1 - 2 observed by Johns and Nablo. The cause of this discrepancy is pile-up pulses in the NaI(Tl) detector which enhance the high energy group in the 600-kev-beta experiment. The occurrence of pile-up pulses is very probable because the 670-kev-beta group is in coincidence with the strong 468-316 kev gamma ray cascade. The ratio of the probability for detecting solid angle pile-up of these gamma rays to that for detecting a single 600-kev photon is approximately 10^{-2}. When this number is combined with the relative intensities of the beta groups, it is possible to account for about 80% of the observed 0.670-Mev beta, 600-kev gamma coincidence rate. The remaining part of $\int_{0.670} b_{173-468} = 0.02$ may be readily reconciled with a 2% intensity for the 173-kev transition. It should be pointed out that the other beta-gamma experiments are much less sensitive to pile-up than this one. In fact it can be shown that pile-up contributions to the other experiments should be negligible.

Since further reference to the intensities of the various beta groups will be made, a summary of these is presented in Table V. The values quoted there are those obtained by averaging the results of the various experiments when a unique shape is assumed for the 0.535-Mev beta group. These values are only slightly different from those obtained when the 0.535-Mev group is assumed to have the allowed shape.

Discussion The shape characteristics of the high energy beta group and the first inner group in combination with the known spins of the 784- and 921-kev levels are sufficient to determine the spin of Ir^{192} as 5-. This agrees with the conclusion of Deutsch et al. (1958) who measured the beta-gamma anisotropy to be $0.016 \pm .013$. In their experiment they used gamma rays of energy greater than 100 kev and beta rays of energy greater than 470 kev.

The variation of the anisotropy with the energy of the electrons cannot cause the observed shape of the beta spectrum for the following reasons. In the expression for the directional correlation function between a beta and gamma ray - $1 + f(p,W_o)\ A_2\ P_2(\cos\Theta)$, (Alder, Stech and Winther (1957)) - the coefficient A_2 must be very small to give the small anisotropy observed by Deutsch et al. In the magnetic spectrometer, the focussed electrons are emitted at an angle of about $150^o \pm 8^o$ with the respect to the photons detected by the gamma counter. The value of P_2 for this angle (0.125) is small enough that the value of A_2P_2 would be essentially zero and no anisotropy could be observed.

TABLE V

Beta Intensities

Beta Group (Mev)	Intensity (%)	Comment	
0.670	41 ± 4	Beta-Gamma Experiments	MacArthur
	50 ± 10	Singles Analysis	MacArthur
	44	Singles Analysis	Bashilov *et al.*
	50	Intensity Balance	Johns and Nablo
0.535	19 ± 3	Beta-Gamma Experiments	MacArthur
	22 ± 8	Singles Analysis	MacArthur
	40	Singles Analysis	Bashilov *et al.*
	35	Intensity Balance	Johns and Nablo
0.250	8 ± 3	600-kev-beta Experiment	MacArthur
	27 ± 11	300-kev-beta Experiment	MacArthur
	28 ± 10	Singles Analysis	MacArthur
	16	Singles Analysis	Bashilov *et al.*
	15	Intensity Balance	Johns and Nablo

The spin assignment of 5- is more reasonable than that given in the Nuclear Data Tables from an argument advanced by Baggerly et al. They point out that the beta transitions to the first and second excited states of Pt^{192} would be only first forbidden unique if the spin of Ir^{192} is 4- and therefore should not be much slower than those to the 784- and 921-kev levels. In fact, Bashilov et al. (1952) put an upper limit for the intensity of the transition to the 613-kev level of 0.4% From this value a lower limit of 10.9 for the log ft value of the transition can be deduced. This is considerably higher than that for a first forbidden unique transition. Baggerly et al. would prefer a spin of 6- for Ir^{192} but this seems to be excluded because the transition to the 921-kev level would then be third forbidden.

A comparison of the intensities of the beta groups as measured in these experiments, those of Bashilov et al. and those deduced from gamma intensities shows that there is general agreement with regard to the intensity of the highest energy group, and some disagreement in the intensities of the lower energy groups as measured by the various methods.

The agreement of intensities for the 0.670-Mev beta group suggests that there is no systematic error in the measurement of the other intensities. Furthermore, it is hard to believe that there is some systematic error in the values of the NaI(Tl) detector efficiencies since it will be recalled that the latter were deduced from the

shape of a theoretical curve which was adequately followed by two efficiencies measured in different types of experiments.

In addition, in the experiment involving the 600-kev gamma rays, the first inner beta group is emphasized to such an extent that uncertainty in the intensity of the higher energy group does not affect the intensity of the 0.535-Mev beta group. This intensity is in good agreement with the intensity measured when the 300-kev gamma rays are required for a coincidence.

The results are also dependent on the probability-of-detection factors. If the decay scheme is assumed to be correct, the values of these factors are well defined and do not change significantly when the intensity measurements of the different published works are used. Therefore, these are not influencing greatly the intensity measurements obtained here unless the decay scheme is wrong.

Therefore it is felt that the present values are quite reliable, based as they are on absolute measurements of intensity rather than on the subjective values obtained from a Fermi analysis of a large number of groups. It should be noted that there is no attempt in these intensity measurements to force the sum of the beta intensities to be 100% as each measurement of a β is independent of the others. The fact that the observed β's do not add to 100% suggests either that other levels are being strongly fed or that the decay scheme is incorrect.

When the intensities of the beta groups are applied to an

energy balance for gamma intensities into and out of the different levels (Table VI), a disagreement of a different nature appears.

TABLE VI

Intensity Balance for the Levels of Pt^{192}

	Johns and Nablo (Intensities (%))		Baggerly et al. (Intensities (%))	
Level	In	Out	In	Out
1201	$\delta_{0.250}$	7	$\delta_{0.250}$	8
920	19 + 1	41	19 + 1	45
784	42 + 3	57	42 + 2	59
613	35	34	39	40
316	104	77	105	92
0	85	0	100	0

It is obvious that the beta groups do not supply the right intensity at the right places. Quite distinct from this fact is the observation that the 316-kev level appears to be a sink for gamma rays. This is intimately tied up with the intensity of the 467-kev gamma ray which essentially depopulates the 784-kev level. However the approximate 20% limits of error on this intensity measurement are sufficient to remove this discrepancy. In addition, if the intensity of this gamma ray is reduced by 20%, the intensity balance at the 784-kev level is quite good.

A second problem which arises at the 920-kev level is

less easily removed because most of the intensity out of this level is taken by the 308-kev gamma ray whose intensity is quite well known from a comparison with the intensities of the 316- and 296-kev gamma rays. These intensities can be expected to be very good because these lines are close together and because the 316-kev gamma feeds the ground state in almost 100% of the decays. Yet a beta intensity of 40% into this level is certainly not observed in any of the present measurements.

A third problem occurs with the beta group of 0.250 Mev because it seems to supply too much intensity to the highly excited states. It is interesting to note that the two coincidence measurements of its intensity are not in agreement; when measured in coincidence with a 300-kev gamma ray the intensity is much larger than when measured in coincidence with the 600-kev radiation. This suggests that a 300-kev gamma ray originates from a level that could be supplied by a beta group with an end point of about 250 kev. Such a situation would aid in resolving the difficulty at the 921-kev level also because this 300-kev gamma ray could be feeding into this level. Should the 308-kev line in fact be a doublet with intensities in the ratio of 1 to 2 with the weaker member feeding the 921-kev level from above, most of the discrepancies in this intensity balance system could be resolved. The intensities of the beta groups as measured would change because the probability-of-detection factors would be different. The value of $\alpha_{0.535}$ would

now become approximately 20% and the intensity of the beta energy group feeding the 1201-kev level would become 8%. It is now necessary to postulate a level at 1229 kev fed by a beta group of end point about 200 kev and intensity of 22%. The final beta group intensities would be

$$\delta_{0.670} = 43\%$$
$$\delta_{0.535} = 20\%$$
$$\delta_{0.220} = 22\%$$
$$\delta_{0.250} = 8\%.$$

It is difficult to accept this splitting of the 308-kev gamma ray because it has been measured with a crystal spectrometer (Baggerly et al.). Because this type of instrument has a very high resolution, the two transitions must be separated in energy by less than 1-kev. Such close doublets are scarce but have been found (Geiger (1962)). No experiments to test this postulate have been performed.

Conclusions

The results of the directional correlation experiments indicate that the spins of the 1201-kev and 1381-kev levels in Pt^{192} are both 4. The large octupole component in the 1065-kev transition is a necessary part of the spin assignment to the 1381-kev level.

The shape of the 0.535-Mev beta group has been determined in a beta-gamma experiment to be that of a first forbidden unique transition, and therefore the spin of Ir^{192} is 5-.

The beta-gamma coincidence experiments have also determined the absolute intensities of the 0.670-Mev beta group to be 42% and of the 0.535-Mev beta group to be 19%. The latter intensity is in disagreement with that deduced from the gamma ray intensities in the accepted decay scheme. This disagreement has not been resolved although a suggestion has been made for explaining it. The intensity of the 0.250-Mev group feeding the 1201-kev level has an intensity of 8%, while the 0.250 beta group in coincidence with the 300-kev gamma rays has a larger intensity (approximately 30%) suggesting that it feeds at least two levels in the 1200-kev region.

CHAPTER VI

Pt^{194}

Introduction

In contrast to Pt^{192}, Pt^{194} has a level structure which is less well established. This is partially due to the fact that the nuclei decaying to this nucleus, Ir^{194} and Au^{194}, have short half lives and cannot be formed free of competing radioactive nuclei. Also the large number of gamma rays present in both decays makes the interpretation of the experimental data difficult.

Au^{194} has been studied by Backstrom et al. (1960) with a double focussing magnetic spectrometer and found to emit over one hundred gamma rays. They also performed many electron-electron coincidence experiments which enabled them to propose a level structure for Pt^{194}. Nearly all of the transitions which they found could be fitted into this structure.

The energies and intensities of the gamma rays accompanying the decay of Ir^{194} have been studied by Johns and Nablo (1954) and by Kern and Backstrom (1960). The latter workers used iridium metal enriched in Ir^{193} and found many lines not seen by Johns and Nablo. Nevertheless, very few transitions were revealed which could not be fitted into the level structure of Pt^{194} proposed by Backstrom et al.

from the decay of Au^{194}. Previously, some coincidence experiments had been performed by Mandeville, Varma and Saraf (1955), but they were handicapped in the interpretation of their experiments by their lack of knowledge of the many transitions present in the decay of Ir^{194}.

Since it was the intention of this work to determine the spins of some of the excited states in Pt^{194} through directional correlation experiments, it was felt necessary to verify the decay scheme proposed by Kern and Backstrom as much as possible in order that the results of the correlation experiments could be interpreted properly. This examination took the form of beta-gamma and gamma-gamma coincidence measurements and will be described in Part A of this chapter. The second part is devoted to directional correlation experiments on several of the gamma-gamma cascades.

A. COINCIDENCE EXPERIMENTS ON THE DECAY SCHEME OF Ir^{194}

Introduction The decay scheme of Ir^{194} as proposed by Kern and Backstrom with the aid of the work on Au^{194} by Backstrom et al. is shown in Figure 17. A few of the weak lines from levels that had been very poorly established are omitted in the interest of clarity of presentation. Some evidence to support the level structure below 1300 kev has been given by the experiments of Mandeville, Varma and Saraf if some of their coincidence measurements are reinterpreted in the light of present information. They also supplied some information about the beta groups of Ir^{194} through beta-gamma coincidence

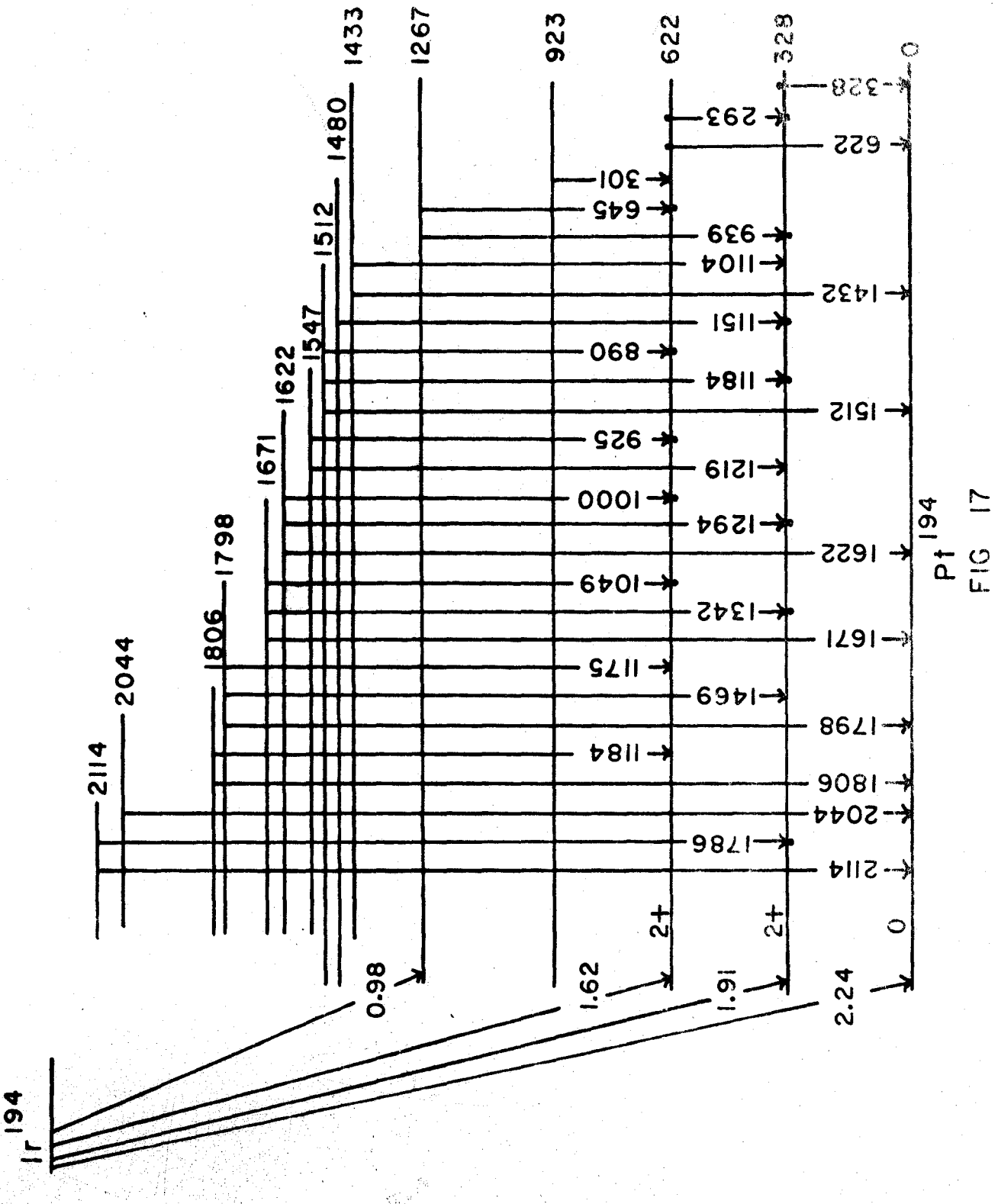
194 Ir
194 Pt
0.98
1.62
1.91
2.24
2+
2+
0
328
622
923
1267
1433
2293
622
301
645
939
1104
1432
1151
890
1184
1512
925
1219
1000
1294
1622
1049
1342
1671
1175
1469
1798
1184
1806
2044
1786
2114
1480
1512
1547
1622
1671
1798
1806
2044
2114

FIG 17

experiments employing scintillation crystals for beta detectors. Further knowledge of the beta groups is supplied by a Fermi analysis on a singles spectrum performed by Johns and Nablo. It is on this analysis that the absolute intensities of the gamma rays and beta groups as given by Kern and Backstrom are based.

Although the experiments described in this section tested many facets of the decay scheme of Ir^{194}, they were designed particularly to clarify the role of the 1186-kev transition in the decay scheme. The beta-gamma experiments were designed to provide more detail than had been available concerning the intensities of the beta groups to the various levels.

Experimental Methods For the gamma-gamma coincidence experiments, iridium metal enriched to 98.7% in the isotope Ir^{193} was irradiated for various lengths of time up to a maximum of 20 minutes in the pneumatic system of the McMaster reactor. The short irradiation period and highly enriched isotope allowed coincidence experiments to be performed without any interference from the Ir^{192} decay for a considerable period of time.

The coincidence measurements designed to test the decay scheme were performed with the experimental arrangement shown in Figure 4A. Different source-to-detector distances and angles between the detectors were employed in order that the interpretation of the coincidence data might not be confused by the effects of solid angle pile-up and directional correlation. The first effect is particularly likely

when examining coincidences with the 622-kev gamma ray. However, since (328 + 293)-kev pile-up merely increases the effective intensity of the 622-kev transition, it had no effect on the relative intensities of the gamma rays feeding the 622-kev level. A correction for the directional correlation was difficult to apply because the intensity measurements were made with the counters closer than the 7 cm. source-to-detector distance at which the actual correlation experiments had been performed. In fact since most of the experiments were performed at an angle of about 150^{o} where the effect of the correlation is small, no correction for this effect was applied.

Since the coincidence measurements were particularly sensitive to energy drifts in the detectors, the stability of the electronics was checked at frequent intervals and, where drifts of $>1\%$ occurred, the data was rejected. The linearity of the detection system was frequently tested by placing a Co^{60} source close to the detector and observing the photopeaks of the 1171- and 1331-kev transitions and the sum peak at 2502 kev. In the low energy region, the peaks in coincidence with the 328-kev transition are dominated by one gamma ray so that these could be used as internal calibration points.

From the singles spectrum shown in Figure 18, the gating channel selected pulses corresponding to windows A, B, C and D. The multichannel analyser was then used to record the gamma ray spectrum coincident with pulses in each window. Unfortunately,

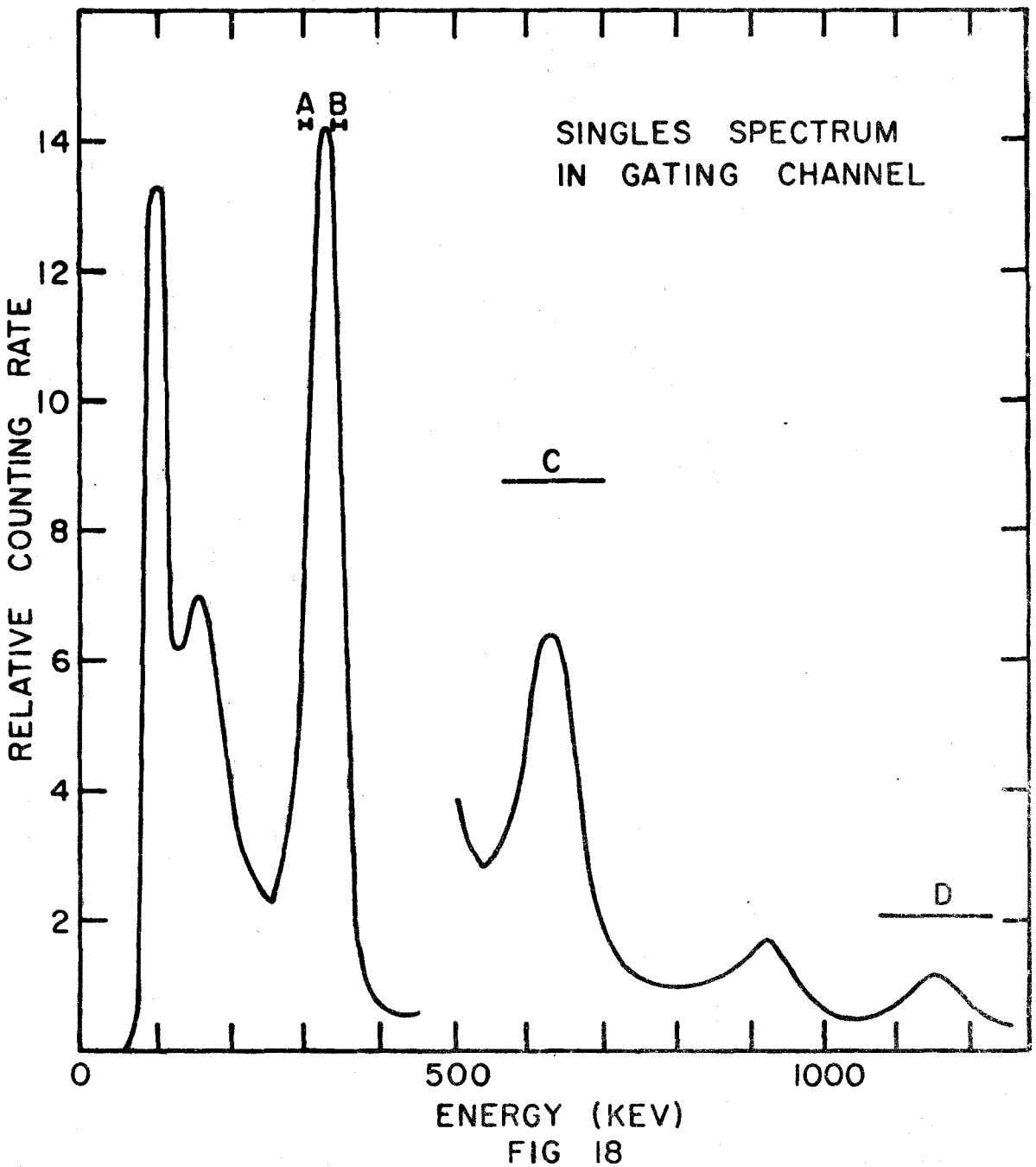
SINGLES SPECTRUM
IN GATING CHANNEL
A
B
C
D
RELATIVE COUNTING RATE
14
12
10
8
6
4
2
0
500
1000
ENERGY (KEV)

FIG 18

neither the windows nor the peaks in the coincident spectrum were due to a single gamma ray alone, so that the interpretation of the results was complicated. The two windows on the 300-kev peak were chosen in order that coincidences with the 328-kev transition and the 293-kev transition might be measured. Although window A contains some pulses from the 328-kev gamma ray, these contributed less than 20% to the total gating count. The spectrum in coincidence with window A can thus be considered to be due chiefly to the 293-kev transition. Window B on the other hand contains very few pulses from the 293-kev transition.

The intensity of the various coincidence relationships was determined through an analysis of the coincidence spectra obtained. This analysis entailed adding the counts in the channels corresponding to the various peaks, correcting for the underlying compton distributions through the use of standard line shapes of various energy, correcting for chance ($< 1\%$) and correcting for the difference in detection efficiency of the different gamma rays with the aid of the curve discussed in Appendix II.

A further correction was also made for the presence of lead absorbers in front of the counter feeding the multichannel analyser. These lead absorbers of known thickness up to 15 gm./cm.^{2} were used in order to reduce the number of low energy pulses (chiefly the 328-kev photons) and thus permit the use of stronger sources. The lead effectively eliminated the 300-kev peak in the coincidence spectrum

without seriously attenuating the rest of the spectrum. For the greatest thickness used, the variation in attenuation factor from 600 kev to 1750 kev was about 2.5. In all cases, it was possible to correct reliably for the absorption and thus to measure the intensities of the gamma rays in the coincidence spectra relative to the 645-kev transition.

The comparison of the intensities of the gamma rays to that of the 645-kev gamma ray has the additional advantage that in the spectra coincident with the 328- and 293-kev transitions, the 645-kev peak is due to a single transition.

Since the 293- and 328-kev gamma rays are not separated cleanly by windows A and B, the following method of analysis was used to discover the probability of a coincidence between a selected gamma ray and each of the 293- and 328-kev transitions alone.

Let X represent the probability that the gamma rays included in a given peak, P, of the coincidence spectrum be in direct coincidence with the 328-kev transition, and Y represent the probability that the gamma rays in the same peak be in direct coincidence with the 293-kev transition. Then, since the 293- and 328-kev transitions are in cascade, that part of the coincidence peak counting rate due to coincidences with the 328-kev pulses in window A will be

$$N_o \left[\frac{\omega\epsilon}{1+\alpha_T}\right]_P \left[\frac{\omega\epsilon}{1+\alpha_T}\right]_{328} F_A\,(X+Y)$$

where F_A is the fraction of the 328-kev photopeak contained in window

A. A similar expression exists for the 293-kev coincidences. The total coincidence rate in P associated with window A is then

$$N_{PA} = N_o \left[\frac{\omega\epsilon}{1+\alpha_T}\right]_P \left\{\left[\frac{\omega\epsilon}{1+\alpha_T}\right]_{328} F_A (X+Y) + \left[\frac{\omega\epsilon}{1+\alpha_T}\right]_{293} f_A Y\right\}$$

where f_A is the fraction of the 293-kev photopeak. This expression is of the form

$$N_{PA} = N_o (C_A X + k_A Y)$$

where C_A and k_A depend on F_A and f_A which can be found from a graphical analysis of the singles spectrum in the gate A and on solid angle factors which are known (Appendix II). Similarly for the window B we have

$$N_{PB} = N_o (C_B X + k_B Y).$$

Once N_{PA} and N_{PB} are measured, these two equations are sufficient to determine N_oX and N_oY - the intensities of the gamma rays in the peak, P, directly in coincidence with the 328- and 293-kev transitions respectively. This process was performed for all the peaks in the coincidence spectrum. Then since the experiments had not been performed with a source-to-detector distance of 7 cm., intensities relative to the 645-kev transition were obtained in order that a comparison might be made to the intensities as deduced by Kern and Backstrom.

This method of determining X and Y was tested by varying the fractions F and f in the two windows A and B. It was found that relative intensities deduced were quite constant even when these

parameters were varied over a wide range.

In addition, the method has an internal consistency check. Since it is well known that the 645-kev transition feeds the 622-kev level, the value of X for this case is expected to be zero. In fact, the measured values of X obtained for the 645-kev peak in different runs were found to be small and scattered randomly about the value zero. In a similar fashion, the pair of unresolved gamma rays at 1715 and 1786 kev, predicted by the decay scheme to be in direct coincidence with the 328-kev transition, led to values of Y which scattered about zero.

The intensities of some of the gamma rays were also measured through an electron-gamma experiment employing the double lens magnetic spectrometer. In this experiment, the method outline in Chapter III was used; the counting rate in coincidence with the 328-kev transition was measured by taking the difference in the coincidence rate on and off of the 328 K conversion line. The intensities of the various gamma rays relative to the 645-kev transition were then determined from a knowledge of the underlying compton distribution and the photopeak detection efficiencies. The intensities of the gamma rays in coincidence with the 293 K - line were more difficult to determine because there was interference from Ir^{192} (for financial reasons, the sputtered sources were not made from the enriched iridium), and because the coincidence rate when sitting on the K - line was only slightly greater than that when

sitting off the peak. Consequently no reliable intensities were obtained from this electron-gamma coincidence experiment.

Additional information about the decay scheme can also be garnered from the measurement of the beta rays in coincidence with the different gamma rays. These experiments were performed in a manner similar to the ones outlined in Chapter V for Ir^{192}. Again sputtered spots of iridium were irradiated for 10 hours to produce workable sources. However, since Ir^{194} has beta groups of much higher energy than Ir^{192}, the range of momentum used in these experiments was extended to 8,000 Hρ.

The beta-gamma coincidence rate for each peak was taken as the sum of the counts in the appropriate channels of the analyser after the correct compton distributions had been subtracted.

Unfortunately, the gamma ray detector used for the beta-gamma experiments was slightly larger than that used in the gamma-gamma experiments (5.0 x 5.0 $cm.^2$ rather than 4.0 x 5.0 $cm.^2$) and its photopeak detection efficiency and compton response were not as well known experimentally. Therefore the data of Miller, Reynolds and Snow (1958) and the behavior of the 4.0 x 5.0 $cm.^2$ crystal were used to make the corrections for detection efficiency and for compton distributions.

Results The presentation of the experimental results will be kept as independent as possible of previous work. However, on occasions, it will be necessary to refer to the decay scheme of Figure 17 for guidance in the interpretation of the coincidence spectra.

(1) Coincidence Relationships The coincidence spectra obtained with the windows A, B and C (hereafter referred to as spectra A, B and C respectively) are shown in Figure 19. From these, information concerning a large number of cascades can be obtained. Although the appearances of these spectra are very similar, there are significant differences which will be discussed in turn.

(a) The rather prominent peaks at 905 kev and 1490 kev which appear in spectrum C are either not present in spectrum B or are masked by the much stronger 940- and 1450-kev peaks. Also in spectrum A, the peaks at 900 and 1450 kev are very broad suggesting that many components are present. These two observations indicate that there are 905- and 1490-kev transitions feeding the 622-kev level. The 905-kev peak is probably an unresolved (890 + 925)-kev doublet (Figure 17).

(b) In spectrum C, a bump is evident on the upper side of the 905-kev peak. This bump has been accentuated in the insert by subtracting the compton distribution of the 1160-kev peak. From the decay scheme, it can be seen that 1000- and 1049-kev gamma rays are expected to be in coincidence with the 622-kev transition. Indeed, this bump can be resolved into two peaks of equal intensity at these energies without forcing the data. Therefore, there is strong evidence that these gamma rays do feed the 622-kev level.

(c) A gamma ray of 940 kev appears in spectrum B but not distinctly in any other spectrum. Therefore there is a 940-328 kev cascade.

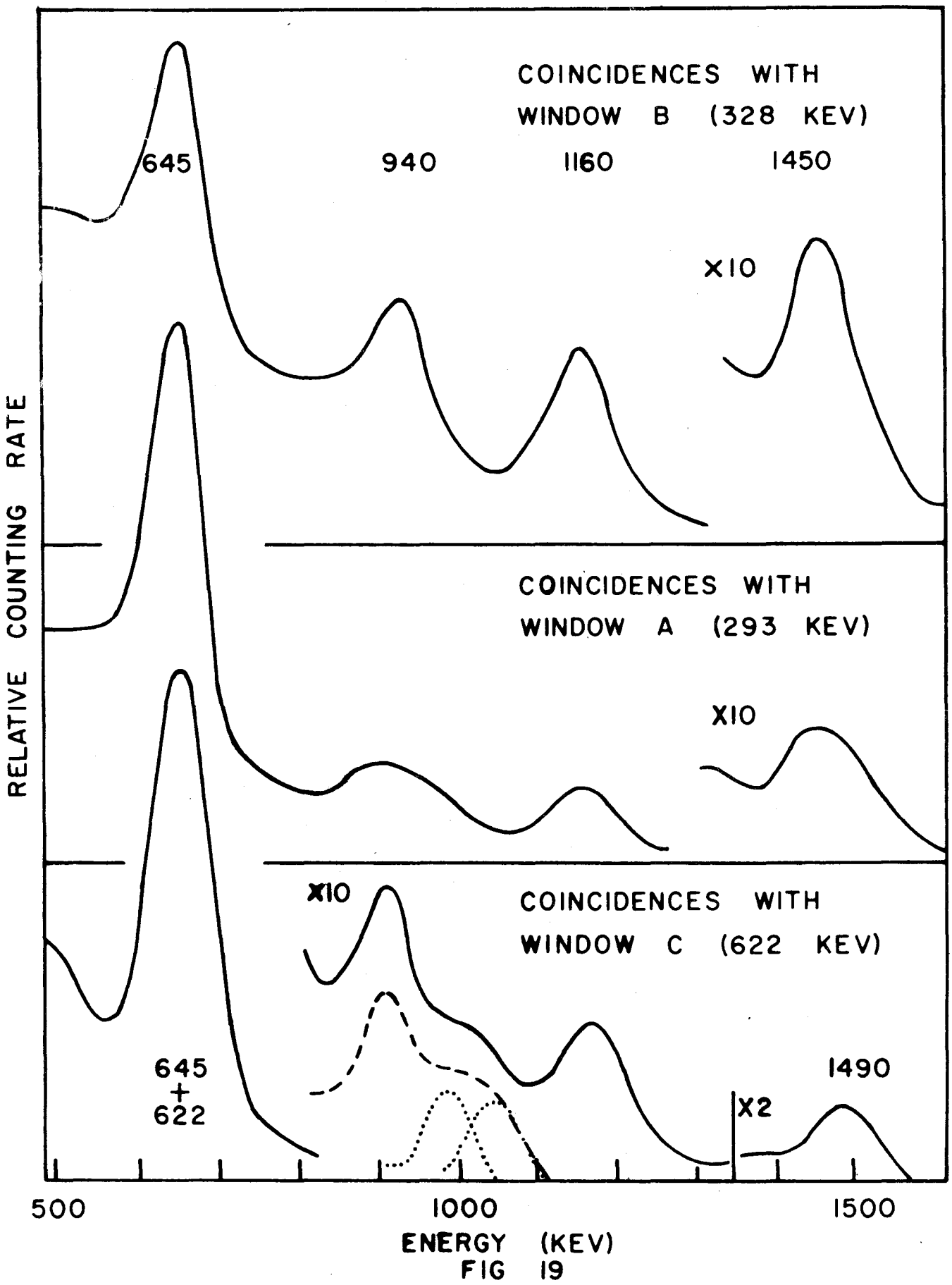
COINCIDENCES WITH
WINDOW B (328 KEV)
645
940
1160
1450
X10
COINCIDENCES WITH
WINDOW A (293 KEV)
X10
X10
COINCIDENCES WITH
WINDOW C (622 KEV)
645
+
622
1490
X2
RELATIVE COUNTING RATE
500
1000
1500
ENERGY (KEV)

FIG 19

(d) The peaks at 645 kev and 1160 kev are seen to be present in all three spectra. However, the height of the latter peak compared to that of the 645-kev peak is considerably reduced in the coincidence spectra associated with windows A and C. Therefore, although there is a transition of about 1160 kev (the decay scheme suggests that the gamma ray has an energy of 1184 kev or 1175 kev) feeding the 622-kev level, most of the intensity of the 1160-kev peak feeds the 328-kev level.

Figure 20 shows two regions of a spectrum taken in coincidence with a window that spanned the complete peak at 300 kev. The region of lower energy presents the spectrum between the 1160- and 1450-kev peaks. The data indicates that there is a gamma ray of about 1290 kev on the high energy side of the 1160-kev peak. When a compton distribution for the 1450-kev transition has been subtracted, the dashed curve of Figure 20 results. This curve accentuates the 1290-kev transition and suggests that a second still weaker transition of about 1340 kev is also present. Both of these transitions are present in the decay scheme.

The higher energy region shows the peak of highest energy in coincidence with the 300-kev gamma rays. This peak of 1750 kev is readily decomposed into two components with the aid of a line shape from a 1600-kev transition in La^{140}. The two transitions have energies of 1715 $\pm$ 10 and 1786 $\pm$ 10 kev respectively, and an intensity ratio of about 1 to 3.

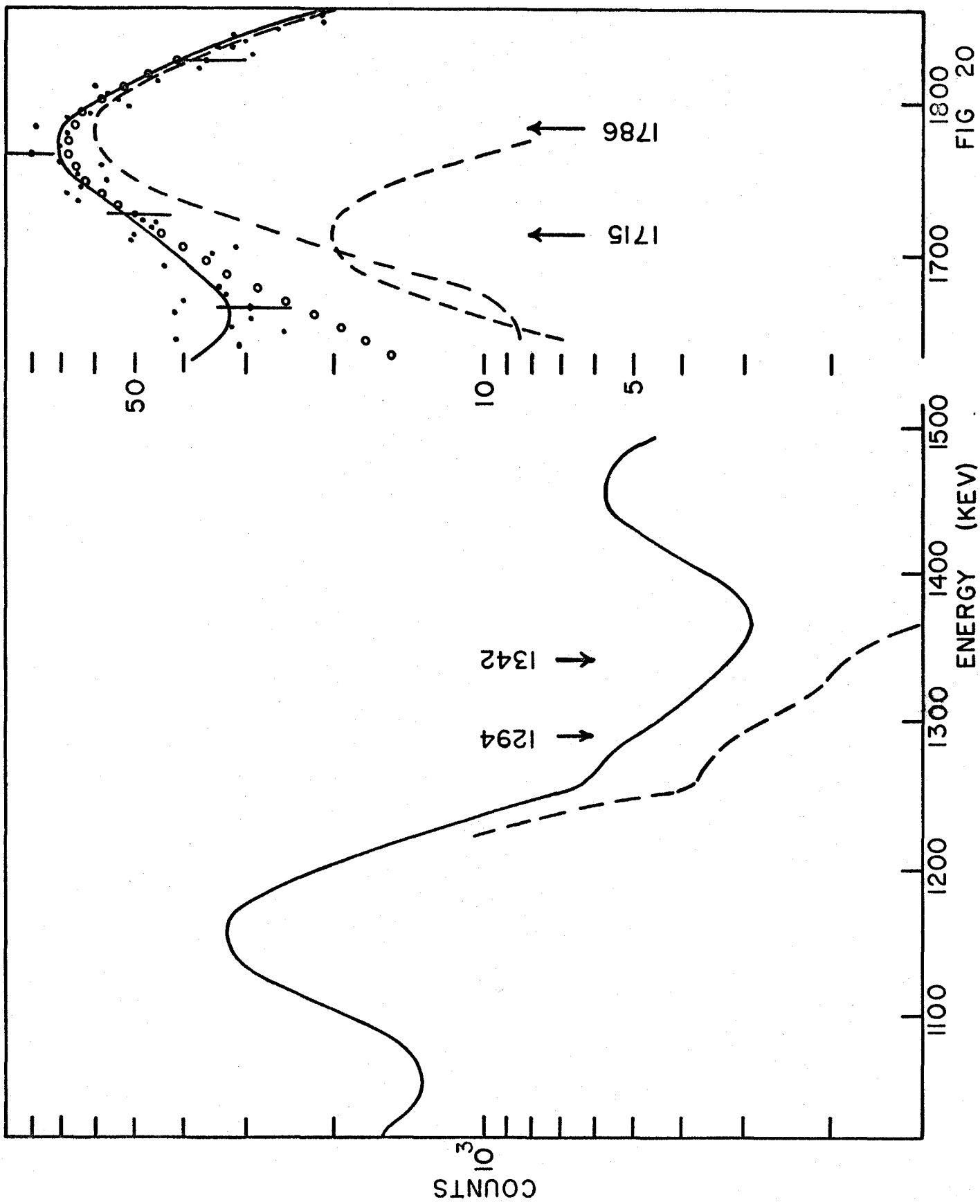
1786
1715
1342
1294
50
10
5
1800
1700
1500
1400
1300
1200
1100
ENERGY (KEV)
COUNTS
10^3

FIG 20

Coincidence experiments were also performed with window D and a window that extended from 1400 kev to the top of the spectrum. The results of the former experiment confirmed the fact that an 1160-kev gamma ray is in coincidence with both a 300-kev and a 600-kev gamma ray. The latter experiment showed that there were no prominent gamma rays between 150 and 275 kev.

The results of all of the coincidence experiments are summarized in Table VII. Instead of merely indicating that a coincidence has been observed, the entry in the matrix indicates the level from which the cascade originated. The energies of these levels have been taken from the work of Kern and Backstrom.

(2) Gamma Ray Intensity Measurements Before the results of the intensity measurements are presented, it is well to recall what has been measured by the technique employing windows A and B. In these experiments, the intensities of the gamma rays in direct coincidence with the 293-kev and the 328-kev transitions were obtained. However since the 293-kev transition depopulates a level from which another gamma ray radiates (622 kev), the intensities of the gamma rays measured in coincidence with the 293-kev transitions are smaller than the total intensities of these gamma rays. These total intensities can, however, be found if a correction for the branching ratio from the 622-kev level is applied. From Kern and Backstrom's intensity values for the transitions involved (293 kev and 622 kev) this ratio, $b_{293\text{ - }622}$, is 0.88. This is a small correction and any reasonable error in it does not seriously affect the results to be deduced. It

TABLE VII

Coincidence Cascades Observed

Energy of peak and components (kev)		Window A chiefly 293 kev	B 328 kev	C 645 + 622 kev	D 1160 kev	1400 kev
	293		622	1267	1806 and/or 1798	2114
	328	622		1267	1480 and 1512	yes
	622			1267	1798 and/or 1806	2114
	645	1267	1267	1267		
905	890	1512		1512		
	925	1547		1547		
	940		1267			
	1000			1622		
	1049			1671		
1160	1151		1480 and 1512			
	1186					
1160	1175 and/or 1186	1806 and/or 1798		1806 and/or 1798		
	1294		1622			
	1342		1671			
	1450		1778#			
	1490##	2114		2114		
1750	1715##		2044			
	1786		2114			

\# - Level not in the decay scheme of Kern and Backstrom
- New transition in Ir^{194}

might be pointed out that this factor is only necessary to obtain intensities relative to the 645-kev transition for the gamma rays directly feeding the 328-kev level.

These adjusted intensity ratios are presented in Table VIII. The first column lists the gamma rays for which results have been obtained. The second gives the relative intensities of these radiations as deduced from windows A and B. Each of these values is the mean of several determinations.

The third column presents the results when the 600-kev peak is used as the window. Because window C contains both members of the 622-645 kev doublet, the rate for the 645-kev peak will be doubled. This effect has been taken in account in calculating these ratios.

In the fourth column are the intensities of the gamma rays in coincidence with the 328 K conversion line from an electron-gamma experiment. As was pointed out earlier, the similar experiment with 293 K - line proved relatively fruitless. However, the coincidence rate obtained between this line and the 1160-kev gamma ray peak was compared to the same rate obtained with the 328 K - line. The result of this comparison, after a correction for the difference in the internal conversion coefficients of the two lines had been made, is also included in this column.

The fifth column contains the average of the columns 2, 3 and 4 renormalized at the intensity of the 645-kev transition to the scale of Kern and Backstom.

TABLE VIII

Intensities of Gamma Rays in Pt^{194}

Energy of Gamma Ray (kev)	Relative Intensities				
	From Windows A and B	From Window C	From e - γ	MacArthur	Kern and Backstrom
293	1.4		1.58	7.1 ± 1.5	11.8 ± 2
622					1.5 ± .3
645	1.00	1.00	1.00	4.9	4.9 ± .4
890	0.07	.11		0.4 ± .2	.19 ± .02
925					.16 ± .02
940	0.74		0.54	3.1 ± .8	2.7 ± .1
1000				.2 ± .1	0.15 ± .03
1049				.2 ± .1	0.13 ± .01
1151	1.05		0.88	4.7 ± 1.0	2.9 ± .1
1186					1.4 ± .1
1175 and/or 1186(293)	.06	.10	.06	.4 ± .2	0.3 ± .05
					1.4 ± .1
1294				.3 ± .15	.48 ± .05
1450	.13		.14	.66 ± .15	1.7 ± .1
1490	.04	.04		.18 ± .04	
1715	.04			.17 ± .04	
1786					.046 ± .015

Also included are the intensities for the 1000-, 1049- and 1294-kev transitions. The first two were obtained from a comparison of their peaks to that of the 1160-kev peak while the last was obtained from a comparison to the peak height of the 1450-kev transition.

The errors in all the measurements are very difficult to caluclate. The values shown were estimated from the constancy of all the intensity determinations and are quoted in the fifth column.

The last column lists the intensities of Kern and Backstrom for the gamma rays measured here.

(3) Beta-Gamma Coincidence Experiments The results of these experiments were obtained from the Fermi analyses shown in Figures 21 to 25 inclusive.

From the experiments which involved coincidences with the 300-kev gamma ray (Figure 21), beta groups of end-point energy $1.93 \pm .03$, $1.62 \pm .05$ and $0.97 \pm .07$ Mev were definitely found. Additional counting rate was left when these three groups had been subtracted, but because of the larger errors on the low energy data, it was impossible to draw any valid conclusions from them.

The experiment involving the 600-kev gamma rays (Figure 22) verified the existence of beta groups with end-point energies of $1.62 \pm .03$, $0.97 \pm .03$ and $0.48 \pm .06$ Mev. The low energy group was further identified by the coincidence experiment between gamma rays of 1450 kev and beta rays. In that study (Figure 25), this group appears alone and the energy of the end-point is found to

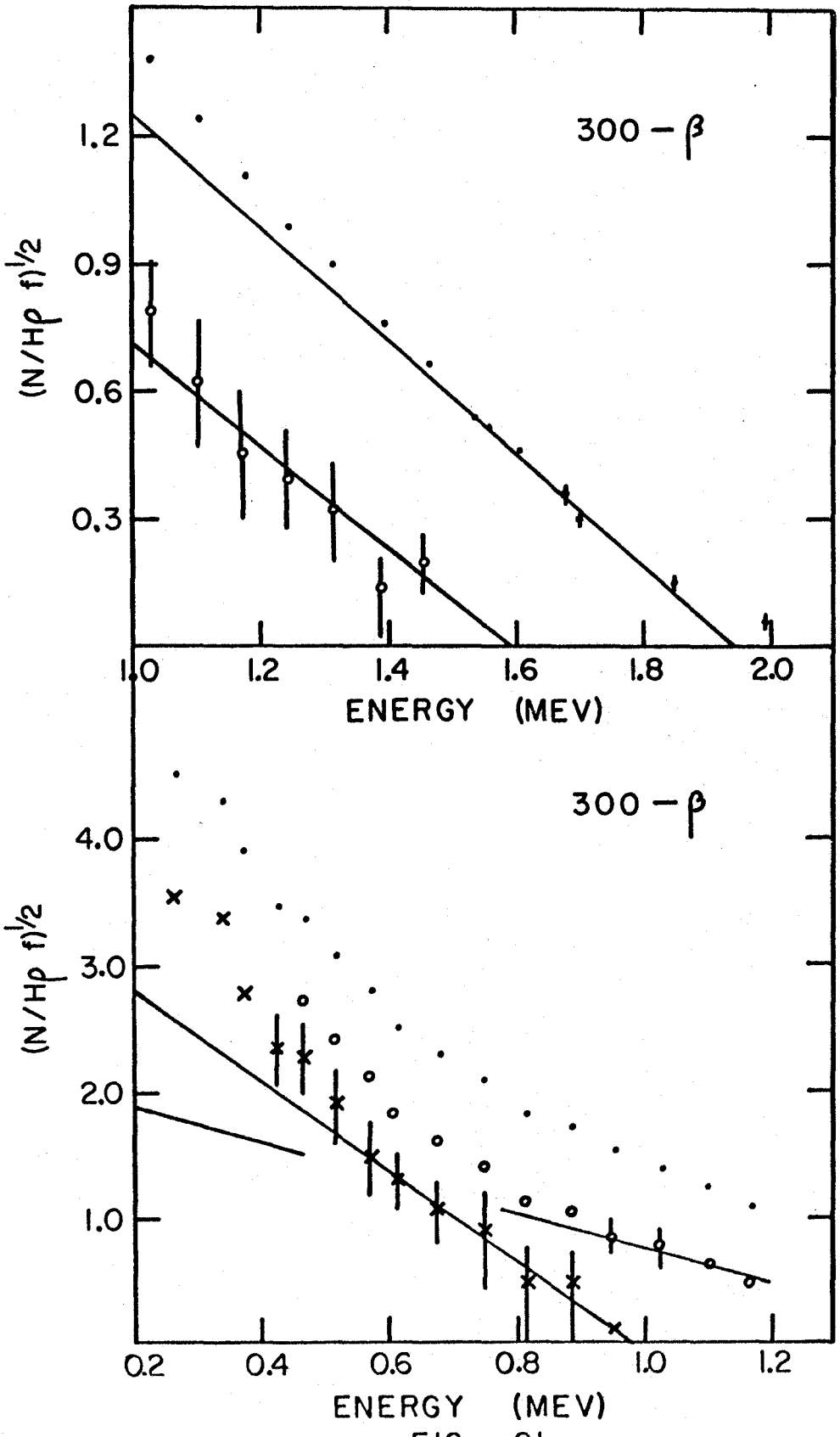
300 − β
(N/Hρ f)^1/2
1.2
0.9
0.6
0.3
1.0
1.2
1.4
1.6
1.8
2.0
ENERGY (MEV)
300 − β
(N/Hρ f)^1/2
4.0
3.0
2.0
1.0
0.2
0.4
0.6
0.8
1.0
1.2
ENERGY (MEV)

FIG 21

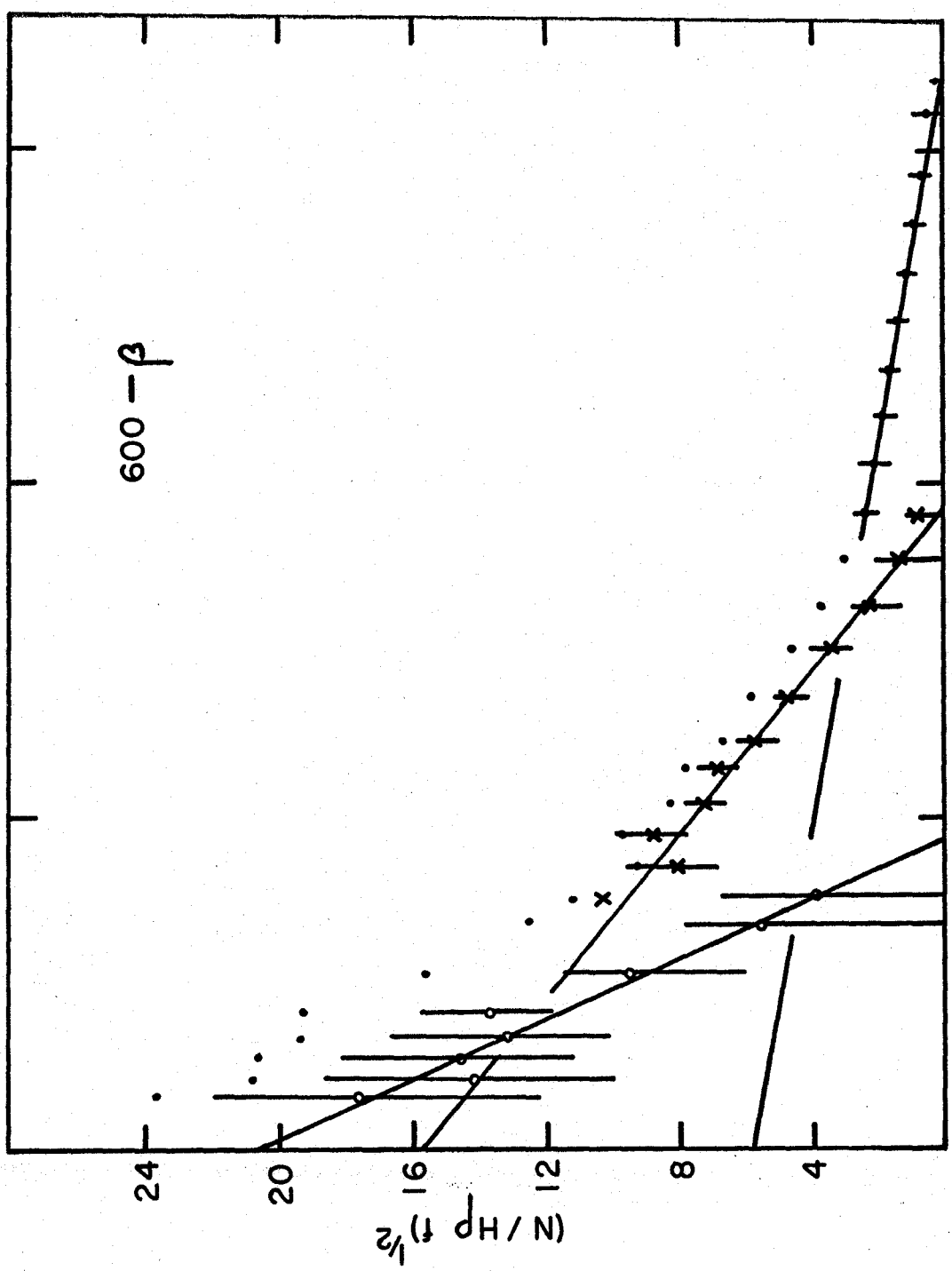

FIG 22

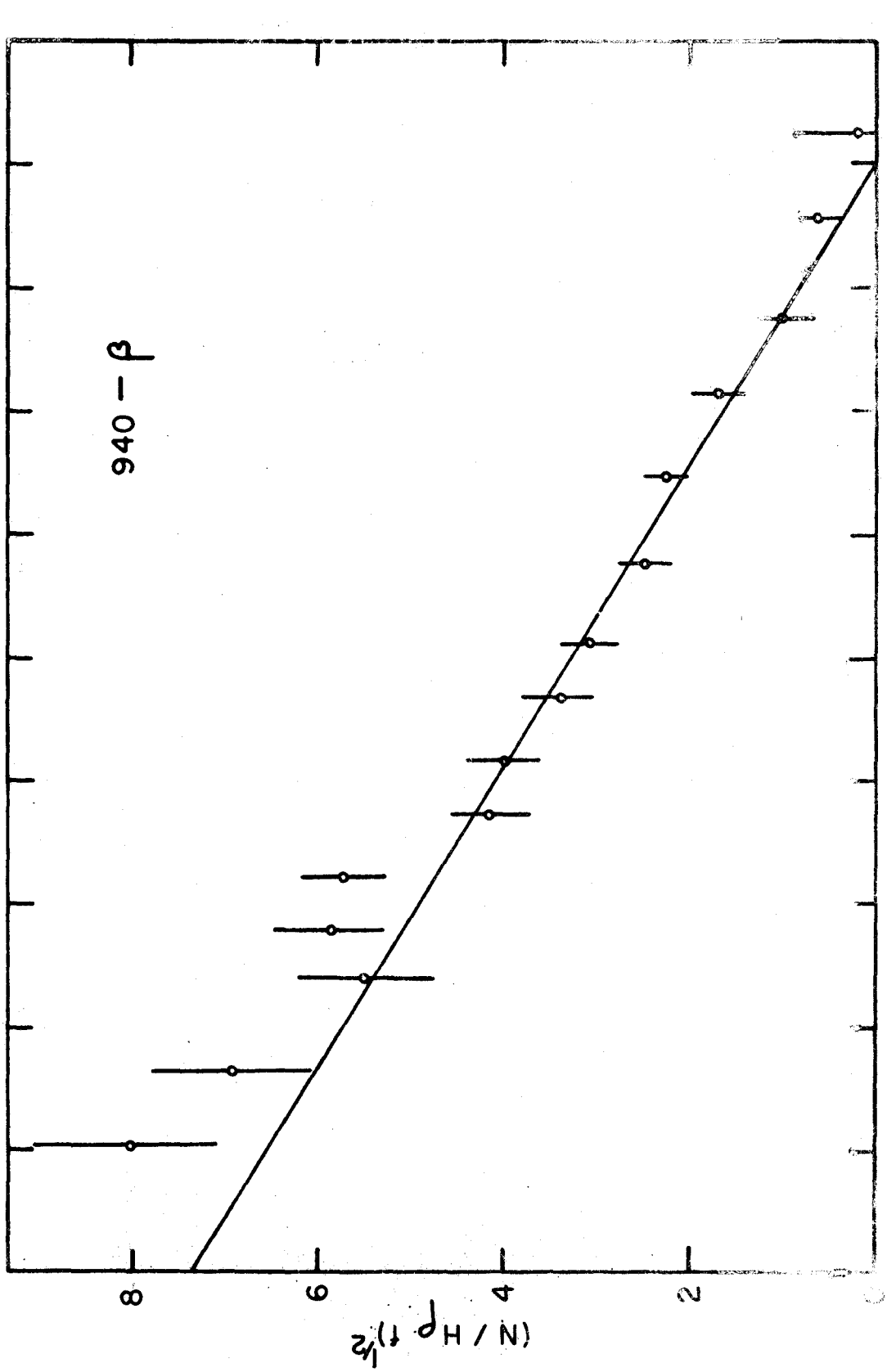
940 − β
(N / H ρ t)^1/2
8
6
4
2
100
200
300
400
500
600
700
800
900
1000
1100
ENERGY (KEV)

FIG 23

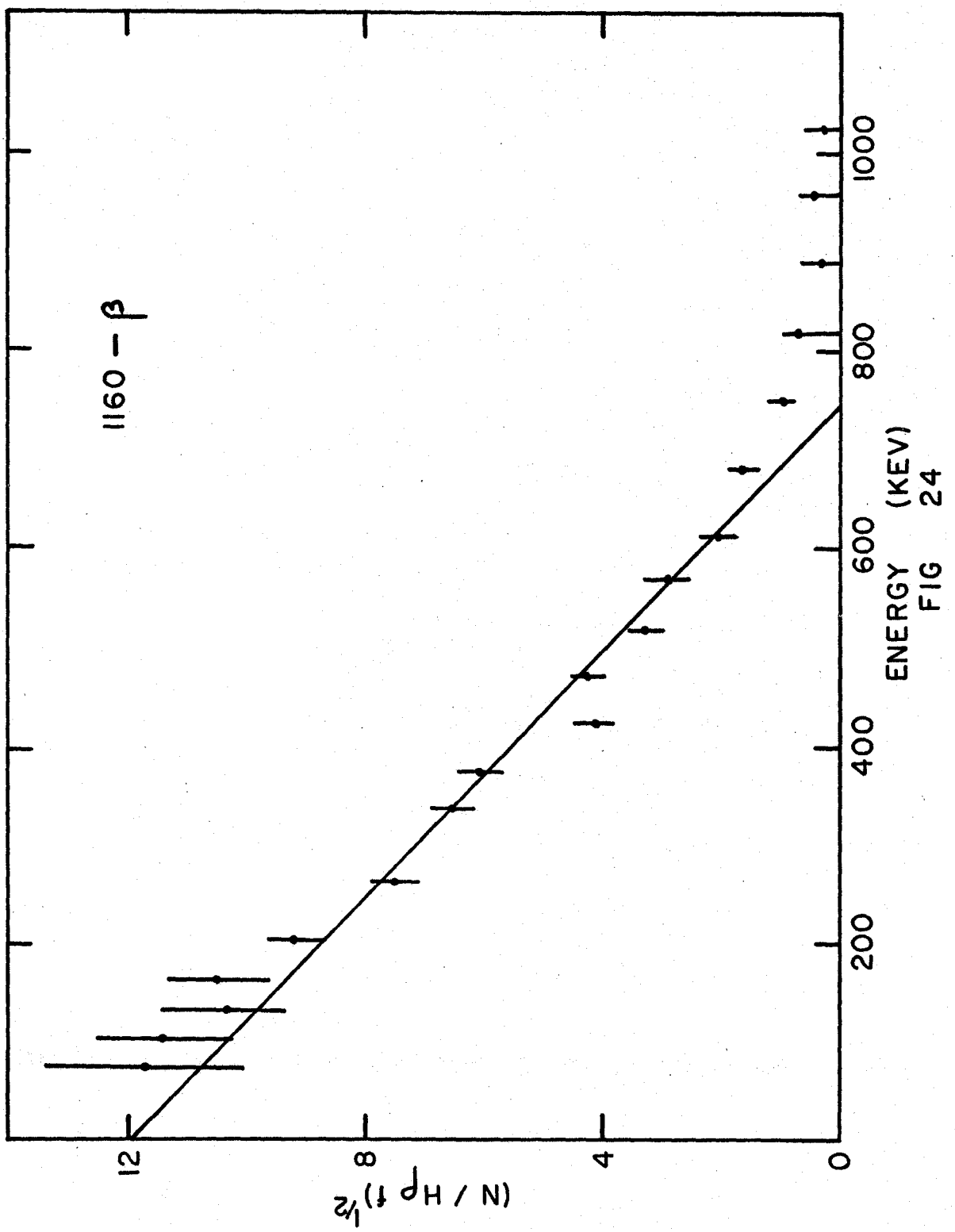

FIG 24

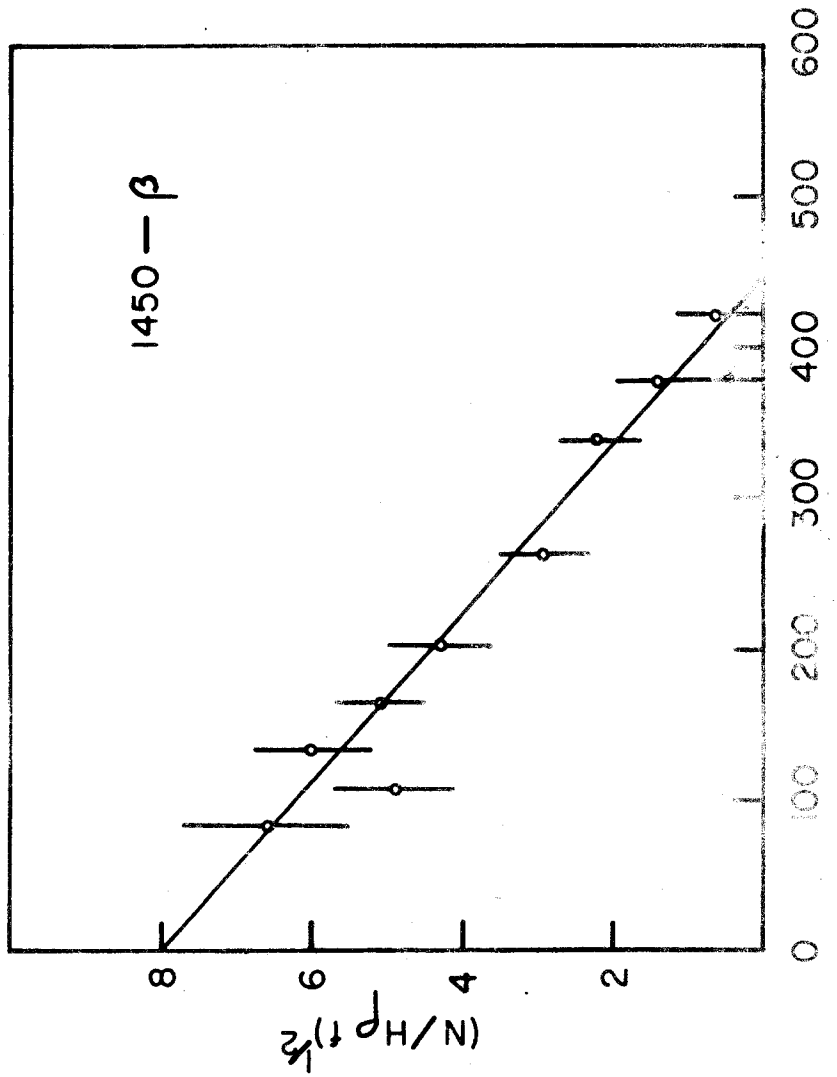

FIG 25

be 0.450 $\pm$ .030. It is of course not certain that these two groups are in fact one and the same since there are so many levels in Pt^{194} at the level of excitation fed by beta rays of this energy.

Beta rays coincident with the 940-kev gamma ray have an end point of 1.00 $\pm$ .03 Mev (Figure 23). Again there is a hint of a second group of lower energy but the analysis was not extended to include this group because the subtraction of the compton distribution for the 1150-kev gamma rays drastically reduced the statistical accuracy of the information below 300 kev.

The analysis of the beta-gamma coincidence rates involving the 1160-kev gamma rays is shown in Figure 24. In addition to the strong beta group with an end-point energy of 0.74 $\pm$ .04 Mev, there seems to be some evidence for a higher energy group extending to approximately 1060 kev. However, the evidence for this group really hinges on two or three points with less than 10 counts in each, and it is therefore impossible to draw any reliable conclusions concerning this group. If this weak component is real, it would necessitate the existence of a level at approximately 1160 kev. Such a level has not been postulated previously. The intensity of this high energy group is so weak that it has little effect on the analysis of the 0.74-Mev group.

The intensity of the various beta groups can be obtained from the straight lines of the Fermi analyses with the aid of the photopeak detection efficiencies obtained in the manner already described. These are displayed in Table IX.

TABLE IX

Intensities (%) of Beta Groups from Beta-Gamma Experiments

Coincident Gamma Rays (kev)	Coincident Beta End Points (Mev) 1.93	1.62	0.97	0.720	0.45
300	5.0 ± 1.0	1.3 ± .4	1.8 ± .4		
600		2.5 ± .4*	1.8 ± .4		5.0 ± 2.0*
940			2.0 ± .4		
1150				1.2 ± .3	
1450					0.45 ± .13

* Greatly dependent on the probability-of-detection factor, which is uncertain.

Since the decay scheme is not well established above 1300 kev, probability-of-detection factors for beta rays feeding levels above this energy cannot be deduced. Therefore, any intensity given in the table outside the boxed area represents the intensity of the beta ray group directly feeding the coincident gamma ray tested in the first column. The total intensity of each of these beta groups is larger than the values quoted. Below 1300 kev, the level structure is better known and the appropriate factors can be deduced. The measured intensity values of column 5, Table IX, in combination with the 622-kev intensity of Kern and Backstrom lead to the following values for these factors:

$$P_{1.92} = 1$$

300 kev - β

$$P_{1.62} = 2b_{293 - 622} = 1.65$$

$$P_{0.97} = b_{940 - 645} + 2b_{645 - 940}\, b_{293 - 622} = 1.38$$

600 kev - β

$$P_{1.62} = b_{622 - 293} = 0.17$$

$$P_{0.97} = b_{645 - 940} + b_{645 - 940}\, b_{622 - 293} = 0.71$$

940 kev - β $\quad P_{0.97} = b_{940 - 645} = 0.39$

It should be noted that $b_{622 - 293}$ is very sensitive to the relative intensities of the 293- and 622-kev transitions, and that there is a considerable discrepancy between the value 0.11 using Kern and Backstrom's data and the value of 0.25 obtained from Johns and Nablo's measurements. The value of 0.17 used above is from Table VIII. The other probability-of-detection factors obtained from either Kern and Backstrom's or Johns and Nablo's data agree quite well with those given above.

The intensity of the 1.93-Mev beta group quoted in Table IX should be very reliable. It is deduced directly from measured counting rates and a known photopeak detection efficiency. Independent confirmation of this 5% value was found in an electron - beta experiment in which one spectrometer was set on the K conversion peak of the 328-kev transition and the other was used to scan the beta continuum. In this experiment, the intensity is determined from counting rates and the known solid angle accepted by the spectrometer focussing the conversion electrons. Although the statistical accuracy

obtained in this experiment was much poorer, the fact that the value obtained was 7 $\pm$ 3% supports the better measurement given in Table IX.

The three different measurements for the intensity of the 0.970-Mev beta group show gratifying consistency. This consistency offers indirect support to the decay scheme from which the probability-of-detection factors were deduced and to the correctness of the photo-peak efficiencies used.

The intensities of the 1.62-Mev and the 0.450-Mev beta groups deduced from the 600-kev gamma ray experiments are rather suspect because of the uncertainty in the probability-of-detection factor discussed above. This is not true for the 0.97-Mev beta group because 85% of the counting rate is due to the 645-kev gamma ray.

The measured intensity of the beta rays feeding the 1150-kev gamma rays is the mean of two determinations obtained in completely separate experiments, and should be quite reliable. In addition, the intensity of the beta group feeding the 1450-kev gamma rays is obtained from a clean reliable experiment.

Discussion The coincidence cascades established in these experiments confirm in nearly all respects the decay scheme of Kern and Backstrom established by energy fit and reference to the decay of Au^{194}. In particular, evidence has been presented to show that the 328-kev level is fed by the gamma rays of energy 293, 940, 1151, 1184, 1294, 1342 and 1786 kev observed by these workers. The present experiments

also show that the 622-kev level is fed by gamma rays of energy 645, 890, 925, 1000 and 1049 kev, and a weak transition near 1180 kev. All of these were placed correctly in the decay scheme by Kern and Backstrom. The differences merit more detailed study.

(a) The 1715-kev transition feeding the 328-kev level de-excites the level at 2044 kev. It has been seen in the Au^{194} decay, and its low intensity in the Ir^{194} decay explains why it was missed in external conversion studies.

(b) The 1184-kev gamma ray was located at two places in the decay scheme by Kern and Backstrom. The present experiments show that it should be described as the 1512-328 kev transition. This conclusion is reached from the gamma-gamma experiments which showed that the intensity of the 1160-kev peak directly in coincidence with the 293-kev line is about the intensity of the 1175-kev gamma ray and much too small to be associated with an 1184-kev transition feeding this level. This view is supported by the fact that the beta rays feeding the 1160-kev gamma rays show no strong component with a 0.44-Mev end point. This assignment agrees with that made by Backstrom et al. in the decay of Au^{194}.

(c) A transition of 1490 kev was found to feed the level at 622 kev. This is undoubtedly the 1493-kev transition reported by Backstrom et al. in Au^{194} and helps to depopulate the 2114-kev level.

(d) Instead of the 1469-kev peak expected from the decay scheme of Kern and Backstrom, a gamma ray of 1450 kev has been found

to feed the 328-kev level. This consistent effect cannot be due to an error in calibration since the calibration was checked over this entire region with the Co^{60} single and sum peaks, and all the other peaks corresponded to known energies in Ir^{194}. Furthermore, the observed 1450-kev transition is considerably weaker than the 1469-kev transition reported by Kern and Backstrom.

Both 1450 and 1469 kev transitions have been observed in Au^{194} with an intensity ratio of 1 : 5. Backstrom et al. looked for coincidences between the stronger of these and the 328-kev transition, but their measurements were inconclusive. These results, combined with the present experiments, suggest that the 1469-kev transition has been wrongly placed in the decay scheme, and that is is probably a ground state transition defining a level at 1469 kev. Support for the existence of this level can be found in the presence of a very weak 1141-kev transition in Au^{194}. This transition has not been placed in the decay scheme, but would be the transition from this level to the 328-kev level. It would certainly have escaped detection in the experiments of Kern and Backstrom and Johns and Nablo.

The 1450-kev transition observed indicates that the level at 1779 kev, which is populated in the decay of Au^{194}, is also fed in the decay of Ir^{194}. However, the possibility cannot be excluded that the 1798-kev level is also real, since even if it is not depopulated by a 1469-kev transition, it is supported by the 1798-kev ground state gamma ray and a weak 1175-kev transition to the 622-kev level.

The results of the beta-gamma experiments confirm the existence of the beta groups seen by Johns and Nablo and Mandeville, Varma and Saraf. In addition, they show that beta transitions occur to the 622-kev level, to one or more of the levels at 1500 kev and to the 1779-kev level. However, the intensities of the beta groups do not agree with those of Johns and Nablo. This is not surprising since the high intensity of the ground state transition makes it very difficult to perform a meaningful Fermi analysis of a singles spectrum.

The intensity of the transition to the first excited state can be used to relate the gamma ray and beta ray intensity scales. However, in order to do this an intensity for the 328-kev transition must be assumed. It is known from both the work of Johns and Nablo and that of Kern and Backstrom that the intensity ratio of the 328- and the 293-kev transition is 5.1:1. Therefore on the MacArthur scale, the intensity of the 328-kev transition is 37.

The total gamma ray intensity into the 328-kev level is about 16 units. Hence the beta group of intensity 5.0% is supplying 21 units and the absolute intensities of the gamma rays can be found from the MacArthur scale by dividing by 4.2. The absolute intensities are presented in Figure 26 (for the stronger radiations).

From the intensity balance, the intensity of the beta group which feeds each level can be predicted. The values predicted from the gamma intensities observed by MacArthur, Kern and Backstom and Johns and Nablo are tabulated in columns 2, 3 and 4 of Figure 26.

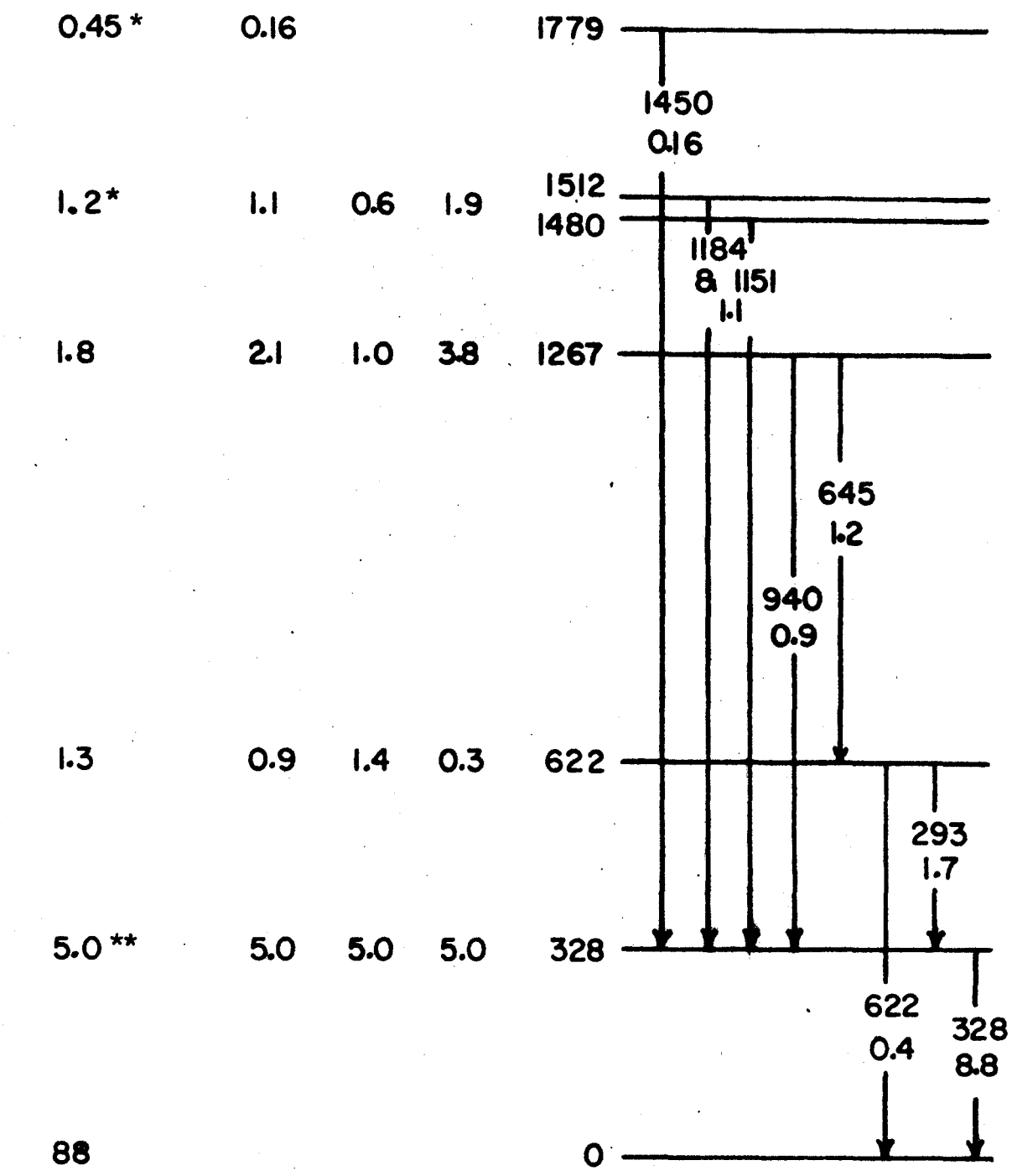

* INTENSITIES IN COINCIDENCE WITH THE GAMMA RAYS SHOWN

** NORMALIZATION

FIG 26

Column 1 represents the experimentally determined beta intensities. The agreement between these and those in column 2 is very gratifying. The lack of agreement with columns 3 and 4 suggests that there are systematic errors involved in the gamma ray intensities measured by external conversion. These errors are probably contained in the intensity measurements of the 293- and 328-kev transitions since these fall in a region where the photoelectron converter efficiencies are difficult to measure. Recent experience in this laboratory (Artna (1961)) suggests that the intensities of the gamma rays of 300 kev are too low. An upward adjustment in the intensity measurements of Johns and Nablo would bring the predicted beta intensities into better agreement with those of MacArthur.

B. DIRECTIONAL CORRELATION EXPERIMENTS

Introduction Several research groups have performed directional correlation experiments on Pt^{194} and have succeeded in identifying the spins of the 328-, 622- and 1267-kev levels.

Mandeville, Varma and Saraf through the correlation of the 293-328 kev cascade assigned a value of 2 to the spins of the first two excited states. These spin assignments were confirmed by the coulomb excitation experiments of McGowan and Stelson (1957).

Johns and MacArthur (1959) and Marklund, Van Nooijen and Grabowski (1960) determined from the strongly anisotropic pattern of the 940-328 kev cascade in Ir^{194} that the spin of the 1267-kev level was zero. Furthermore, in their search for zero spin states, Marklund, Van Nooijen and Grabowski found that the 1160-328 kev cascade was also strongly anisotropic. From the fact that Kern and Backstrom were finding a 1512-kev gamma ray and not a 1480-kev one, they concluded that the state of 1480-kev has a spin of zero. This was subsequently confirmed by Kern and Backstrom in their completed work when an EO transition of 1480 was found.

Butt and Nicholson (1962) have also investigated these cascades. They based their interpretation on the decay scheme of Kern and Backstrom and reached conclusions similar to those of the previous workers except that they considered that the 300-300 kev cascade was actually an average of four different cascades. They therefore were able to assign a spin of 3 or 4 to the 923-kev level.

The experiments described in this section were performed during the period of these publications and duplicate them. However an additional cascade has been studied and the interpretation of the 1160-328 kev cascade has been extended since it is based on the knowledge of the decay scheme gained in Part A.

Experimental Method Sources of iridium metal enriched to 98.7% in Ir^{193} were irradiated for a short time and then centred in the directional correlation table already described. Coincidence counts were recorded for 25 minutes at each of the nine angular positions between 90^{o} and 270^{o} with the electronic arrangement of Figure 4A. This counting interval allowed three runs back and forth through the two quadrants during the two half-lives in which the source was considered workable.

Since the coincidence efficiency of the electronic circuit was known to be quite stable for periods of several days, the angular positions were taken sequentially. However, the gating channel spectrum was observed before and after each count in order to check on the drifts in the energy stability of the counter and to judge the effect of the latter on the coincidence rate. If a drift of 5% or more had occurred, the data was rejected. Finally the decay of the coincidence rate at each angle was measured and any run which did not follow the expected decay curve was discarded.

The six coincidence spectra at each angle were then added together and plotted, and a careful analysis of the underlying compton

distribution of each peak was made with the aid of standard line shapes. The net counting rate due to the cascade for each angle was thus obtained and the rates at the complementary angles compared. If the sets agreed within the statistical limits, they were averaged and the net average rates plotted as a function of the angle. The experimental angular correlation function was determined from this data by the least squares method.

Results

(1) The 940-328 kev Cascade This cascade was examined to determine the spin of the 1267-kev level. Even before the compton distribution from higher energy gamma rays was subtracted, the correlation pattern showed a strong anisotropy. Nevertheless, a careful analysis of this compton distribution was made in order to obtain the true correlation pattern. In addition, a narrow region of the peak was used in determining the coincidence rate in order that nearby gamma rays might be excluded as much as possible. The experimental points and the least squares fit to them are presented in Figure 27. (The statistical errors on each point are only slightly larger than the circles drawn.) The coefficients $A_2 = 0.39 \pm .06$ and $A_4 = 1.04 \pm .10$ are very close to the values 0.36 and 1.14 characteristic of a pure 0-2-0 cascade and permit no other interpretation than that the spin of the 1267-kev level is zero.

(2) The 1450-328 kev Cascade This cascade was examined to establish the spin of the 1779-kev level.

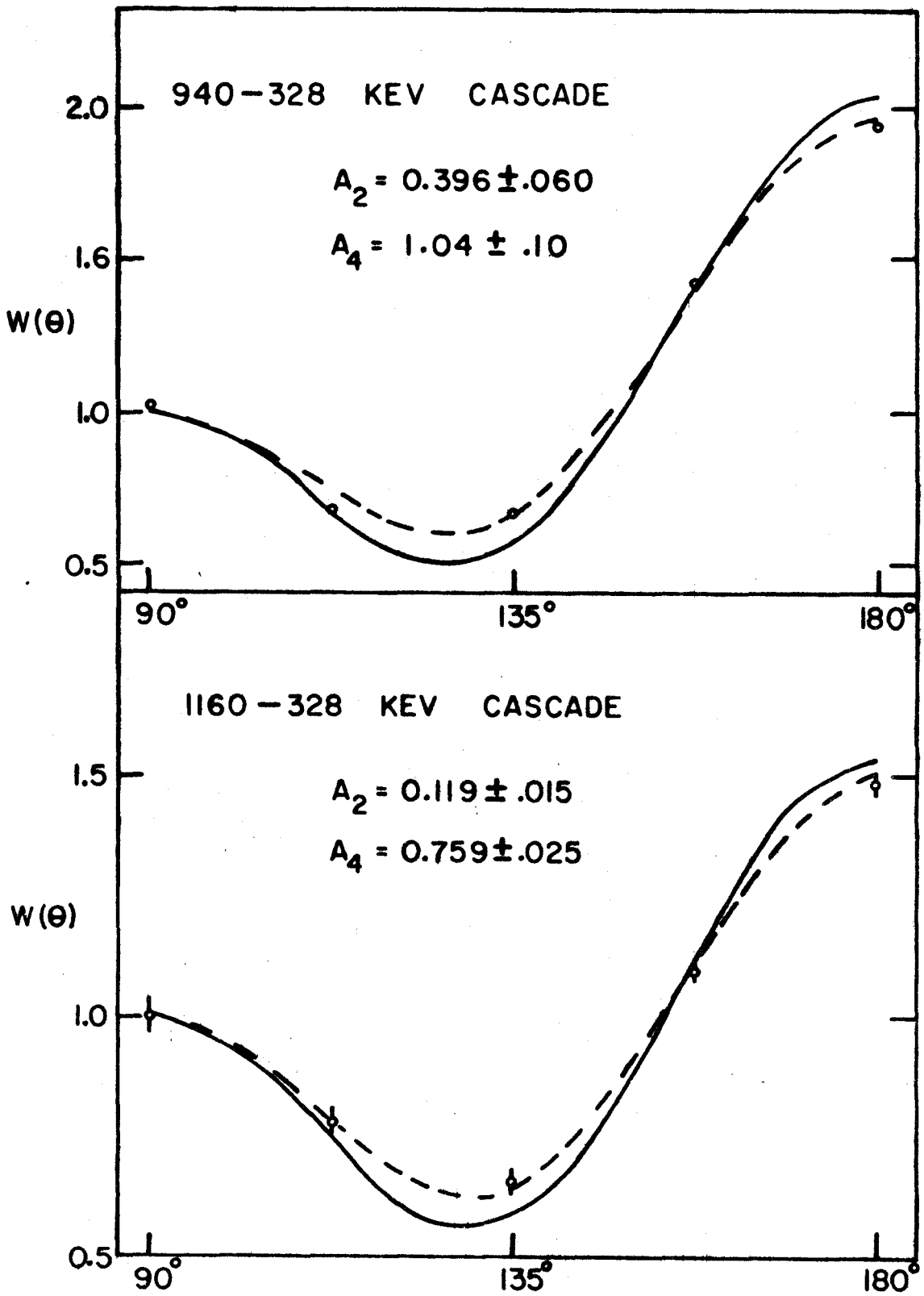
940 – 328 KEV CASCADE
A_2 = 0.396 ± .060
A_4 = 1.04 ± .10
W(θ)
2.0
1.6
1.0
0.5
90°
135°
180°
1160 – 328 KEV CASCADE
A_2 = 0.119 ± .015
A_4 = 0.759 ± .025
W(θ)
1.5
1.0
0.5
90°
135°
180°

FIG 27

The 1450-kev gamma ray does not sit on a large compton distribution and therefore the observed correlation pattern for the cascade is relatively insensitive to other cascades. The correlation pattern shown in Figure 28 was obtained from about 1200 counts per position. The A_2 and A_4 coefficients when transferred to Figure 13 indicate that the possible spin sequences for this cascade are 4-2-0, 3-2-0 and 1-2-0. This experiment would therefore limit the spin of the 1779-kev level to 1, 3 or 4. The spin 4 choice can be rejected at once because it would be impossible to populate this level by beta decay from the 1- ground state of Ir^{194}. The spin 3 choice is also unlikely since the log ft value for the beta transition to the 1779-kev level is 7.9.

Figure 28 presents the analysis of the coefficients for the 1-2-0 cascade. It can be seen that the 1450-kev radiation is almost pure dipole in character. An analysis of the data in terms of a 3-2-0 cascade would also lead to a dipole assignment for the 1450-kev gamma ray.

(3) <u>The 1160-328 kev Cascade</u> In as much as the 1160-kev peak includes many gamma rays, the interpretation of the correlation pattern involving this peak is somewhat complex. It will be recalled that the 1184-kev gamma ray, which had been placed in two positions in the decay scheme by earlier workers, was shown to be entirely in coincidence with the 328-kev transition. Therefore, the 1160-328 kev correlation pattern may be considered as due chiefly to two

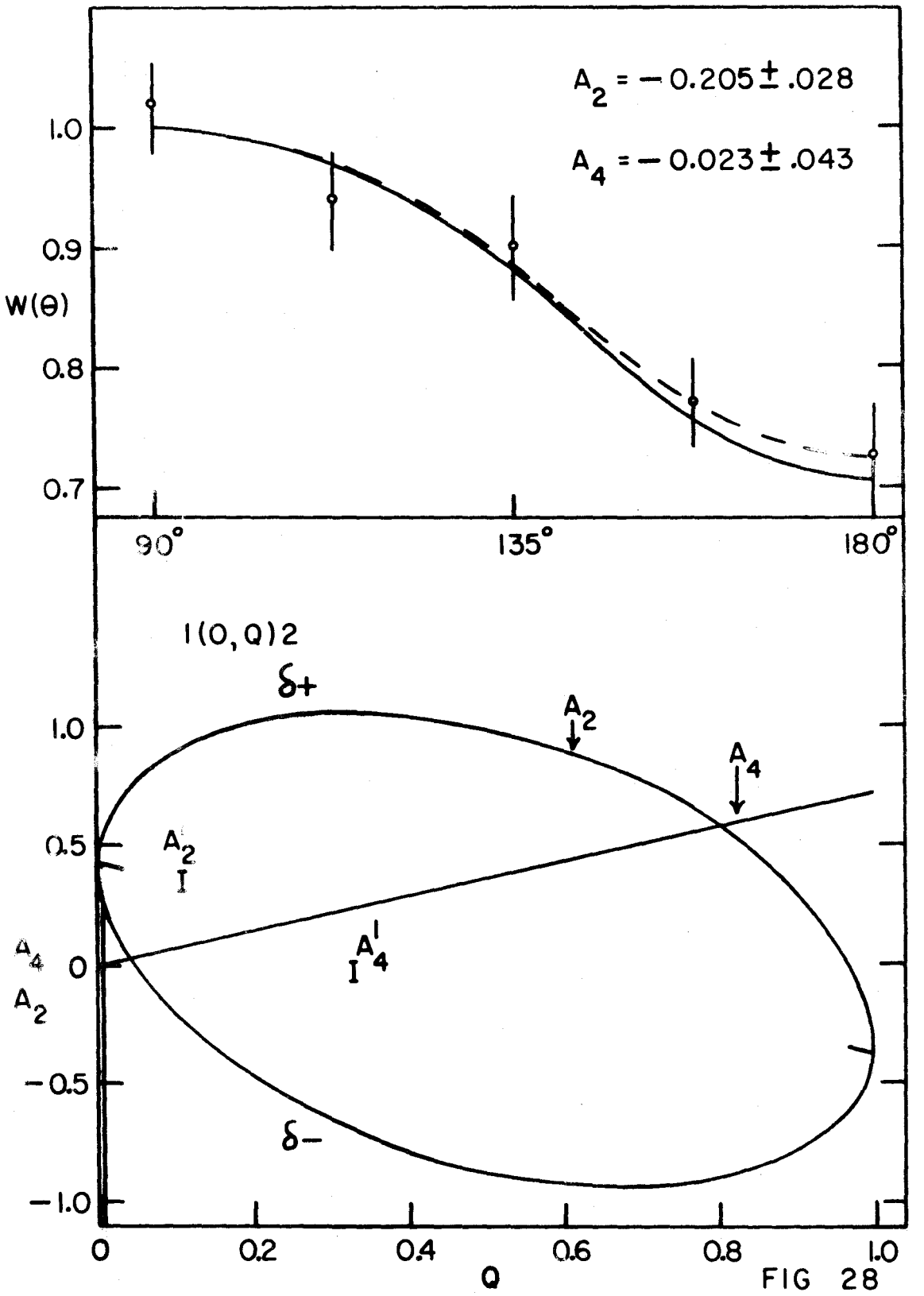
$A_2 = -0.205 \pm .028$
$A_4 = -0.023 \pm .043$
W(θ)
1.0
0.9
0.8
0.7
90°
135°
180°
I(0, Q)2
δ+
δ−
A_2
A_4
A_2 I
A_4' I
A_4 / A_2
0
0.5
−0.5
−1.0
0
0.2
0.4
0.6
0.8
1.0
Q

FIG 28

cascades, 1151-328 kev and 1184-328 kev. The effect of the weaker cascades that are probably present will be dealt with in the discussion.

The 1160-kev peak sits on a compton distribution which can contribute as much as 16% to the total counting rate. However, the compton distribution is known with sufficient accuracy that the error in it does not affect the correlation function significantly. Figure 27 presents the correlation data obtained by amassing 4000 net counts per position. This pattern is so anisotropic that it is at once evident that it contains a 0-2-0 cascade.

It is known from the work of Kern and Backstrom that there is a 1480-kev E0 transition. Therefore, the 1151-328 cascade is the one producing the 0-2-0 pattern. The correlation of the 1184-328 cascade can then be obtained from the measured coefficients.

If a is the probability that the 1184-kev gamma ray is contributing to the 1160-kev peak, the following expressions describe the situation,

$$(1 - a)\ A_2(1151) + a\ A_2(1184) = A_2(\text{exp.})$$

and $$(1 - a)\ A_4(1151) + a\ A_4(1184) = A_4(\text{exp.}) ,$$

where the A coefficients are associated with the gamma rays shown in parentheses.

However, the coefficients $A_2(1151)$ and $A_4(1151)$ have the values 0.36 and 1.14 respectively. In addition, Kern and Backstrom have made a careful measurement of the relative intensities of the

1151- and 1184-kev radiations. These measurements lead to the value of 0.33 $\pm$ .03 for a. With this information and the experimentally measured coefficients $A_2(\text{exp.}) = 0.119 \pm .015$ and $A_4(\text{exp.}) = 0.759 \pm .025$, a straightforward calculation leads to $A_2(1184) = -0.36 \pm .09$ and $A_4(1184) = -0.02 \pm .15$. These coefficients are consistent with the following interpretations (Figure 13).

1-2-0	$-0.2 < \delta < -0.03$
3-2-0	$0.25 < \delta < 0.70$
3-2-0	$3 < \delta < 12$

Again, the spin 3 assignment is unlikely, for the same reasons as given when the 1450-329 cascade was discussed.

Discussion

(1) The 1267-kev Level The spin zero assignment for this level has been obtained by four groups of workers, using the directional correlation method. All groups obtain a large A_4 coefficient which establishes this cascade, but the actual coefficients obtained differ quite markedly. The present work, in which extreme care was taken in correcting for underlying compton distributions, gives the largest value and the one closest to the theoretical coefficient. An earlier investigation in this laboratory (Johns and MacArthur (1959)) gave the lowest value. It is now realized that the compton contribution in the earlier experiments was greatly underestimated.

(2) The 1779-kev Level Evidence for the population of this level in the decay of Ir^{194} was first obtained in the present experiments,

although it was known to exist from the Au^{194} studies. The spin assignment from the directional correlation measurements is 1 or 3. The second choice requires a first forbidden unique transition from Ir^{194} to this level, and no evidence for the unique shape appeared in the beta-gamma experiments described in Part A of this chapter. On these grounds, the spin 3 choice is rejected and the 1779-kev state is assigned a spin of 1. In addition, it is concluded that the 1450-kev transition is predominantly dipole.

The possibility that other cascades are contributing to this correlation pattern cannot be excluded. In fact, it is known that approximately 20% of this 1450-kev peak is due to a gamma ray feeding the 622-kev level. Since its correlation pattern is not known, it is not possible to make a correct allowance for it. However, unless the pattern for it is quite anisotropic, it is not possible to change the directional correlation sufficiently that a spin of 2 for the 1779-kev level is permitted. On the other hand, the mixing ratio for the 1450-kev transition is made somewhat uncertain by the existence of the second transition. Despite this uncertainty, the transition is still likely to be predominantly dipole.

(3) The 1480- and 1512-kev Levels The spins of these two levels have been determined as 0 and 1 respectively. The coefficients obtained for the mixed cascade in this work are intermediate in value between those of Butt and Nicholson (1962) and Marklund,

Van Nooijen and Grabowski (1960). However, all three experimental values are in essential agreement when differences in the widths of the windows used are taken into account. Neither of the other groups of workers attempted to analyse their data for the 1184-328 cascade, nor is it possible from their published data to decide precisely what fraction of the 1151-kev and 1184-kev transitions their window accepted.

Despite the fact that there are several gamma rays contributing to the 1160-kev peak, it has been treated as though it contained only the 1151- and 1184-kev radiations. The decay scheme of Figure 17 indicates that transitions of 1104-, 1175- and 1219-kev would also be included. The effect of these will now be considered.

The 1219-kev transition has the strongest intensity of these and is believed to originate at a level with a spin of zero (Kern and Backstrom). Its correlation pattern would then be the same as that of the 1151-328 cascade. Therefore, the effective contribution of a 0-2-0 cascade to the total pattern would be increased, and the coefficients for the 1184-328 cascade, $A_2(1184)$ and $A_4(1184)$, would become more negative. This effectively pushes the rectangle on Figure 13 further from the ellipse of a 2-2-0 cascade and makes the spin 1 assignment of the 1512-kev level more secure.

The effect of the other cascades is expected to be less

pronounced. Furthermore, any pattern that is going to change the coefficients in the direction necessary to allow a 2-2-0 cascade must have a more negative anisotropy than that of the 1184-328 cascade determined here. Since cascades which can produce such anisotropies are rare and since the gamma rays involved in the cascades are weak, it is difficult to escape the conclusion that the 1512-kev level has a spin of one. The mixing ratio of the 1184-kev transition is, of course, very sensitive to the precise correlation pattern and therefore cannot be well defined. However, the region of the 1-2-0 ellipse contained in the box suggests that it is largely dipole.

Conclusions

The gamma-gamma and beta-gamma coincidence experiments described offer positive support for the energy levels in Pt^{194} proposed on the basis of energy fit by Kern and Backstrom at energies of 0, 328, 622, 1267, 1480, 1512, 1547, 1622, 1671, 2044 and 2114 kev.

A new level at 1469 kev has been proposed to explain the observed coincidence spectra. This level has not been identified in the Au^{194} decay, but transitions required to establish it (1469 and 1141 kev) were observed in the gold spectrum. It has also been found that the level at 1779 kev identified from the Au^{194} studies is populated in the Ir^{194} decay.

No evidence has been obtained to substantiate or disprove the existence of levels at 923, 1432, 1803, 1817, 1830 and 1925 kev

proposed by Kern and Backstrom. Evidence has been found in support of their levels at 1798 kev and/or 1806 kev.

The beta-gamma coincidence experiments have shown that beta rays feed the levels at 328, 622, 1267, 1480 + 1512, and 1779 kev. There may be weaker groups feeding other levels. The absolute intensities of the beta groups feeding the 328-, 622- and 1267-kev levels are 5.0 $\pm$ 1.0%, 1.3 $\pm$ .4% and 1.8 $\pm$ .4% respectively. The ground state transition accounts for about 88% of the disintegrations.

The directional correlation experiments have shown that the spin of the 1267-, 1480- and 1779-kev levels are 0, 0 and 1 respectively, and that the level at 1512 kev probably has a spin of 1.

Several general observations concerning the level structure of Pt^{192} and Pt^{194} can now be made.

(a) The position of the low lying levels in the two nuclides form a strikingly similar pattern although they are populated in different ways. On the other hand, a different set of high energy levels is populated from the decays of Ir^{192} and Ir^{194} because their ground state spins are markedly dissimilar.

(b) Below 1925 kev, identically the same levels in Pt^{194} are populated in the decays of Au^{194} and Ir^{194}. This occurs because the ground state spins of these nuclei are the same. Above 1925 kev, the lower decay energy of Ir^{194} reduces the probability that similar levels will be populated.

(c) Because of the high density of levels above 1300 kev in Pt^{194}, it will be very difficult to make conclusive spin assignments to these levels with the techniques of beta and gamma ray spectroscopy presently available.

APPENDIX I

CATHODE SPUTTERING

Introduction

The success of beta-ray spectroscopy depends to a large extent on the quality of the source preparation. For the investigation of the low energy region of the momentum distribution, the thinness of the source is of the utmost importance because the distribution is distorted when the energy of the electrons is degraded in passing through the source material. Many methods are available for preparing thin sources (Parker, De Croës and Sevier, Jr. (1960). Because of its chemically-inert and refractory nature, iridium is difficult to make into good sources by the normal methods. However, thin films of iridium with high adhesion can be made through the action of cathode sputtering. Several sputtering apparatus have been described (Strong (1938), Novakov and Mladjenovic (1956), Belser and Hicklin (1956)). The one described here is modeled after that built by Belser and Hicklin, but has an electrode structure closer to that of Novakov and Mladjenovic.

The Apparatus

Since cathode sputtering occurs most efficiently at a pressure of about ten microns, an evacuated space must be provided.

In the apparatus of Figure A1, the glass enclosure is a 4" to 1" pipe reducer manufactured by the Corning Glass Company. The small top is closed by an aluminum header through which a half-inch diameter aluminum rod is inserted. The rod carries the anode made of an aluminum disc two inches in diameter. This arrangement allows the electrode separation to be changed. The large end of the pipe reducer sits on a plexiglass base with a large O-ring as a seal. An aluminum tube through the centre of the base serves as the cathode lead and as the exhaust. In order to prevent the discharge from going to this tube, the latter is surrounded by a glass covering.

The cathode supported by the exhaust pipe is a small disc of aluminum on which the material to be deposited is sprinkled. As uniform a deposition as possible is laid down in order that the aluminum, which sputters to a small extent, might be covered.

In order to maintain the pressure at the required value, a Welch Duo-seal backing pump of about 33 litres per min. is used.

The power requirement for the discharge is provided by a simple pi-filtered power supply capable of delivering 70 milliamperes at 4,000 volts. The normal bombarding current is 25 milliamperes.

Sputtering

The name, cathode sputtering, arises because the positive ions that are formed in the discharge are accelerated in the cathode dark space and impinge on the cathode with considerable energy causing cathode material to erupt from the surface. Although the exact

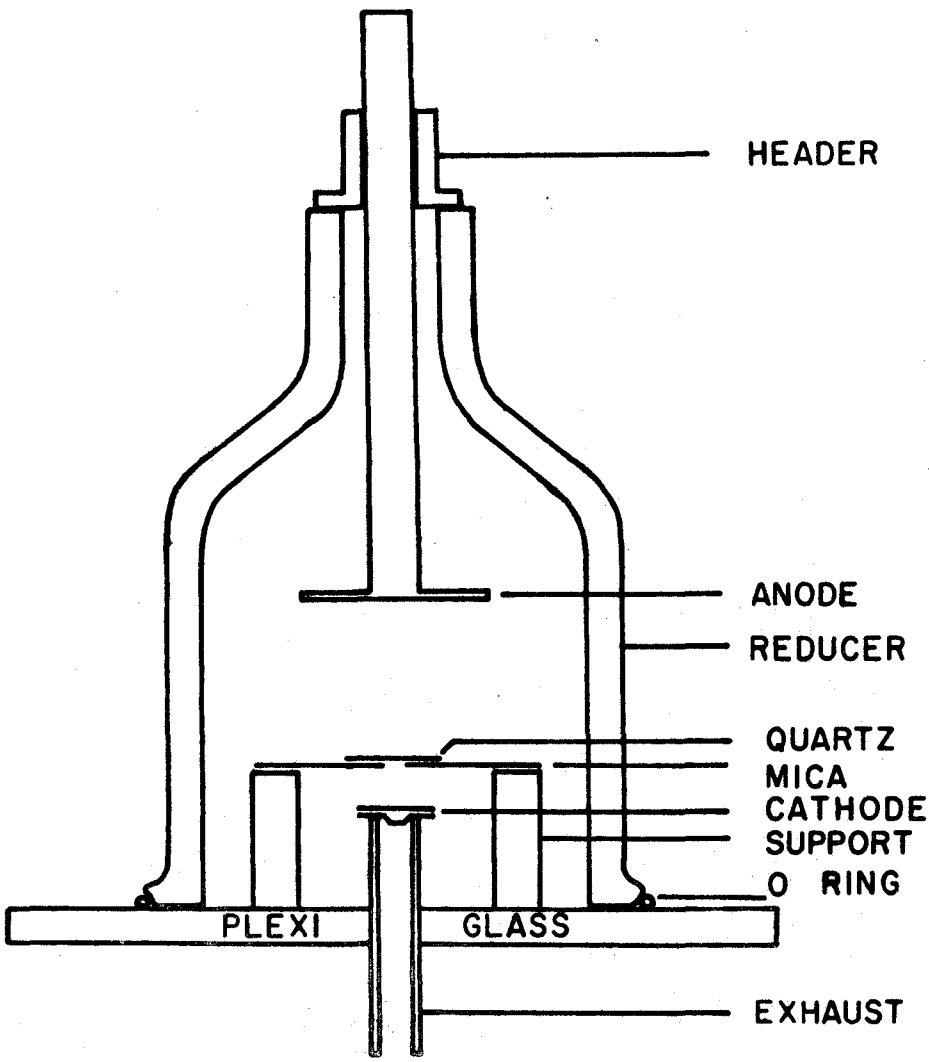
HEADER
ANODE
REDUCER
QUARTZ
MICA
CATHODE
SUPPORT
O RING
PLEXI
GLASS
EXHAUST

FIG AI

mechanism of the cathode sputtering process is not known (Strong (1938), Massey and Burhop (1952)), some experiments have given clues to its nature. At low bombarding energies, Wehner (1954) has shown that the mechanism is one of momentum transfer. However, as the energy is increased, the characteristics of a collision phenomenon are lost, and the model of local heating and evaporation can account for the results. It is probable that sputtering is a result of both processes. Therefore, at the higher bombarding energies, the atoms are emitted from the surface in a distribution which is proportional to the cosine of the angle of emergence.

Source Preparation

Sources which are desirable for the coincidence spectrometer are of small diameter, preferably less than 2 mm. To obtain these, thin films of quartz were shielded with a sheet of mica in which had been punched a hole whose diameter corresponded to the desired size of the source. The mica was supported on ceramic pillars placed out of the directed discharge and just beyond the edge of the cathode dark space. In order to hold the quartz in place behind the hole, a glass plate was rested on the quartz. At a current of 20 milliamperes and a pressure of 20 microns, a uniform deposit of less than 100 $\mu g/cm^2$ was laid in about three hours. This thickness was estimated from the area of the source and the source strength.

The backing material for these experiments had to satisfy two requirements: firstly, it had to be able to withstand the heating during the sputtering process; secondly, it had to be of such a nature that there was no undesirable radioactivity formed in the irradiation process performed after the sputtering. Quartz was found to satisfy these conditions adequately.

Although iridium was the only material sputtered in connection with this work, the method is applicable to those substances which are difficult to handle by evaporation techniques. In addition, the rate of deposition is easily controlled and the thickness of the deposition can be made very uniform.

APPENDIX II

CALIBRATION OF THE NaI(Tl) DETECTORS

A. PHOTOPEAK DETECTION EFFICIENCIES

Introduction As has been stated earlier, the high detection efficiency of a NaI(Tl) crystal for gamma radiation has made the scintillation spectrometer a valuable tool in Nuclear Physics. Unfortunately, both the detection efficiency and the photo-fraction (the number of gamma rays detected in the photopeak to the total number detected) are functions of the energy of the gamma radiation and the source-to-detector distance. Therefore, for quantitative measurements of gamma ray intensities, the variations of the photopeak detection efficiency with these two quantities must be known.

Berger and Doggett (1956) and Miller, Reynolds and Snow (1958) have performed theoretical calculations to determine this variation. However, the sizes of NaI(Tl) crystals and experimental arrangements are many and varied so that each situation should be treated separately. For this reason, a series of coincidence experiments have been performed to determine the variation of the photopeak detection efficiency with the energy of the radiation for a specific experimental arrangement.

Experimental Method In Chapter III, expressions for deducing the intensity of a gamma ray from a gamma-gamma coincidence experiment were set forth with the understanding that information concerning the detection efficiencies $(\omega\epsilon)/1 + \alpha_T$ of the detectors was available. Conversely, if the intensities of the gamma rays are known, these expressions can be used to determine the efficiency factors for the crystals.

The experiment involves the measurement of the coincidence rate between two gamma rays whose single channel counting rates are also available. For the example of a cascade of gamma rays A and B which occur in 100% of the disintegrations, the coincidence rate is

$$N_{A-B} = N_o \delta_B \frac{(\omega\epsilon)_{MB}}{1 + \alpha_B} \frac{(\omega\epsilon)_{FA}}{1 + \alpha_A} \qquad \text{(AII.1)}$$

and the two singles rates are

$$N_A = N_o \delta_A \frac{(\omega\epsilon)_{FA}}{1 + \alpha_A} \qquad \text{(AII.2)}$$

and

$$N_B = N_o \delta_B \frac{(\omega\epsilon)_{MB}}{1 + \alpha_B} \qquad \text{(AII.3)}$$

where F and M have been added to denote the fixed and movable detectors of the coincidence arrangement to be described below.

When the fact that $\delta_A = \delta_B$ is used, $(\omega\epsilon)_{MB}/1 + \alpha_B$ is deduced from AII.1 and AII.2 and $(\omega\epsilon)_{FA}/1 + \alpha_A$ is deduced from AII.1 and AII.3.

From this example, it can be seen that a necessary condition for the utilization of the coincidence technique in the efficiency calibration of the NaI(Tl) detector is firm knowledge of the decay scheme on which the coincidence experiment is performed. For this reason the following nuclei were chosen - In^{114}, Co^{60}, Sc^{46}, Hf^{180m} and La^{140}. Although complete information is not available for the last nucleus, it is known that the 1.60-Mev gamma ray is in coincidence with all of the other transitions. This information is sufficient to permit the use of La^{140} in the calibration of the crystals at 1.60 Mev.

Sources of these nuclei of strength 10-50 μC were placed at the centre of the correlation table (Figure 5). The crystals placed 7 cm. from the source were set at an angle of approximately 120^{o} to each other in order to minimize the effect of directional correlations in the cascades.

The counting circuitry depicted in Figure 4A was used in all of the experiments. The singles counting rate of the fixed counter, which served as the gating channel, was obtained by scanning the spectrum to determine the photopeak position and the amount of underlying compton distribution. The window was then opened to accept pulse heights that corresponded to the photopeak of the gamma ray. Both a singles spectrum and a coincidence spectrum were obtained in the multichannel analyser. For experiments that required more than a few minutes in order to obtain

statistical accuracy, care was taken to check that no drifts in peak positions had occurred.

The data obtained in this way was then treated in a manner outlined earlier after corrections for compton distributions, if any, had been made. In addition, since each crystal detects all of the gamma rays in the spectrum and the source strength can be found from AII.1, 2 and 3, each crystal can be calibrated at the energies of all the gamma rays in the decay scheme. Furthermore, when the roles of the gamma rays in the coincidence arrangement are permuted, i.e. instead of detecting gamma ray A in the gating channel gamma ray B is detected there, a second set of values for the photopeak detection efficiencies can be obtained. The two or more values were then averaged to obtain the final values. Except for the values deduced for the gamma rays of Hf^{180m}, these measurements were taken as the photopeak detection efficiencies ($\omega\epsilon$) of the gamma rays involved. In the case of Hf^{180m}, a correction for the internal conversion process was applied through a knowledge of the type of gamma radiation (E2) and the internal conversion coefficients of Rose (1958).

Further measurements of the photopeak detection efficiencies were made using the standard sources, Ba^{133}, Na^{22}, Cs^{137} and Mn^{54}. The experiments with these consisted of placing the source 7 cm. from the crystal and counting the number of pulses in the photopeak. Because these sources were discs of radioactivity the response of

the crystals to their radiation was not the same as that in the coincidence experiments. However, the photopeak detection efficiencies for these energies did fall near the curve followed by the efficiencies measured in the coincidence experiment, and therefore served as useful checks on the reliability of the measurements.

Results The experimentally determined photopeak detection efficiencies are displayed in Figure A2. They are found to lie on a smooth curve from which the values for the different gamma rays can be determined by interpolation. Since each crystal has its own characteristics, this curve applies only to the movable crystal (Harshaw Chemical Co. No. AS485). A curve, similar in shape but of slightly lower value, resulted for the fixed crystal (Harshaw Chemical Co. No. AL172).

Although no calculations are available for this exact crystal and source-to-detector distance, a comparison of the general shape of this curve with published data can be made. When a comparison is made to the calculations of Miller, Reynolds and Snow, it is found that a curve constructed from their numerical values does not have as much curvature in the region of 500 to 1000 kev. Since the difference is not large and the experimental situation is different from that envisaged in the calculations, the disagreement may not be significant.

Curves such as these were used to provide the relative photopeak detection efficiencies regardless of the source-to-

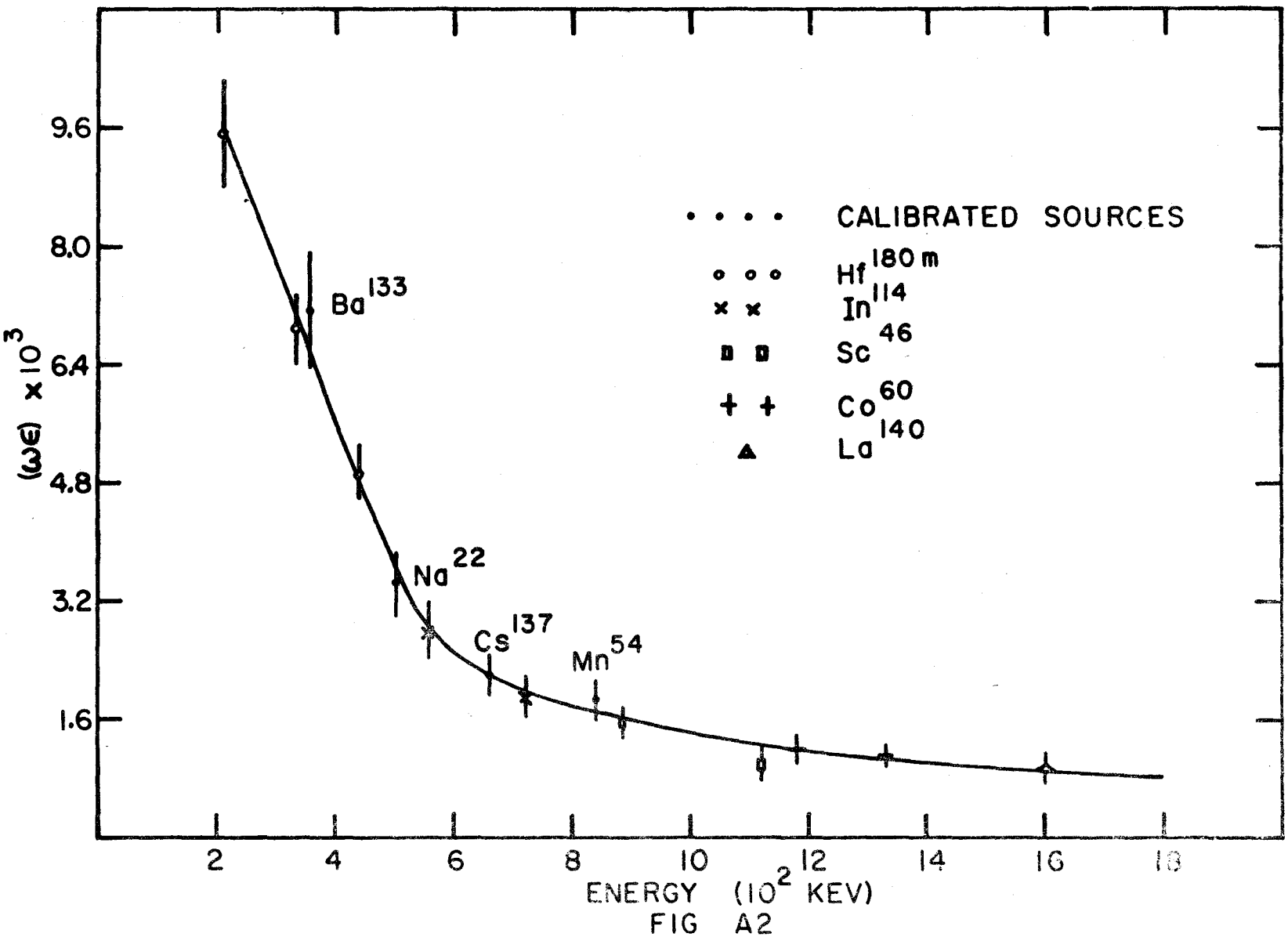
9.6
8.0
6.4
4.8
3.2
1.6
(ωε) x 10^3
Ba^133
Na^22
Cs^137
Mn^54
CALIBRATED SOURCES
Hf^180m
In^114
Sc^46
Co^60
La^140
2
4
6
8
10
12
14
16
18
ENERGY (10^2 KEV)

FIG A2

detector distance. This procedure was felt to be justified since in no experiment designed to measure intensities was the detector closer than 3 cm. to the source. Also the shape of the curve is not a strong function of the source-to-detector distance as is evident from the theoretical calculation.

B. DIRECTIONAL CORRELATION CORRECTION FACTORS

Introduction While the axes of the detectors in a directional correlation experiment are placed at a specific angle in relation to each other, the angles between the directions of the detected radiations vary about this setting because of the finite size of the detectors. The coincidence rate at a particular angle of the counters is therefore the average value of the correlation pattern about the angle. Rose (1953) analysed this problem and showed that by suitable corrections to the coefficients in the correlation functions, the decreased anisotropy because of this averaging process could be removed. He also produced analytical expressions for the correction factors. However, these involve a knowledge of the photopeak detection efficiency as a function of the angle of incidence. This is not available theoretically and must be measured. This section describes the experimental arrangement employed in determining this function.

Experimental Method The angular efficiency of each crystal was determined at a number of gamma ray energies between 100 kev and 1.60 Mev by the method described below (Lawson and Frauenfelder (1953)). A collimated gamma ray beam of width 0.6^{o} at half the

maximum intensity was formed by a lead collimator a foot long. The crystal was then swung through this beam about a centre 7 cm. from the face of the crystal as shown in Figure A3. The relative photopeak detection efficiency of the crystal as a function of the angle between the beam direction and the crystal axis was then determined.

Results The behavior of the angular efficiency of a crystal as a function of energy can be seen in Figure A4. It will be noticed that as the energy of the gamma ray increases, the effective solid angle of the crystal decreases. For energies below 100 kev, the front face of the crystal defines the solid angle, while for energies above 800 kev, the back face of the crystal defines this angle.

The correction factors for the experimentally determined coefficients in a directional correlation can be obtained from these angular efficiency graphs by a numerical integration of the following expressions deduced by Rose (1953);

$$J_0 = \int P_0 \, (1 - \exp - \tau x(\theta)) \, d\cos\theta$$

$$J_2 = \int P_2 \, (1 - \exp - \tau x(\theta)) \, d\cos\theta$$

$$J_4 = \int P_4 \, (1 - \exp - \tau x(\theta)) \, d\cos\theta$$

where P_0, P_2 and P_4 are Legendre polynomials and $(1 - \exp - \tau x(\theta))$ is the efficiency measured in these experiments. This has been done, and the results for the crystal (Harshaw Chemical Co. No. AS485)

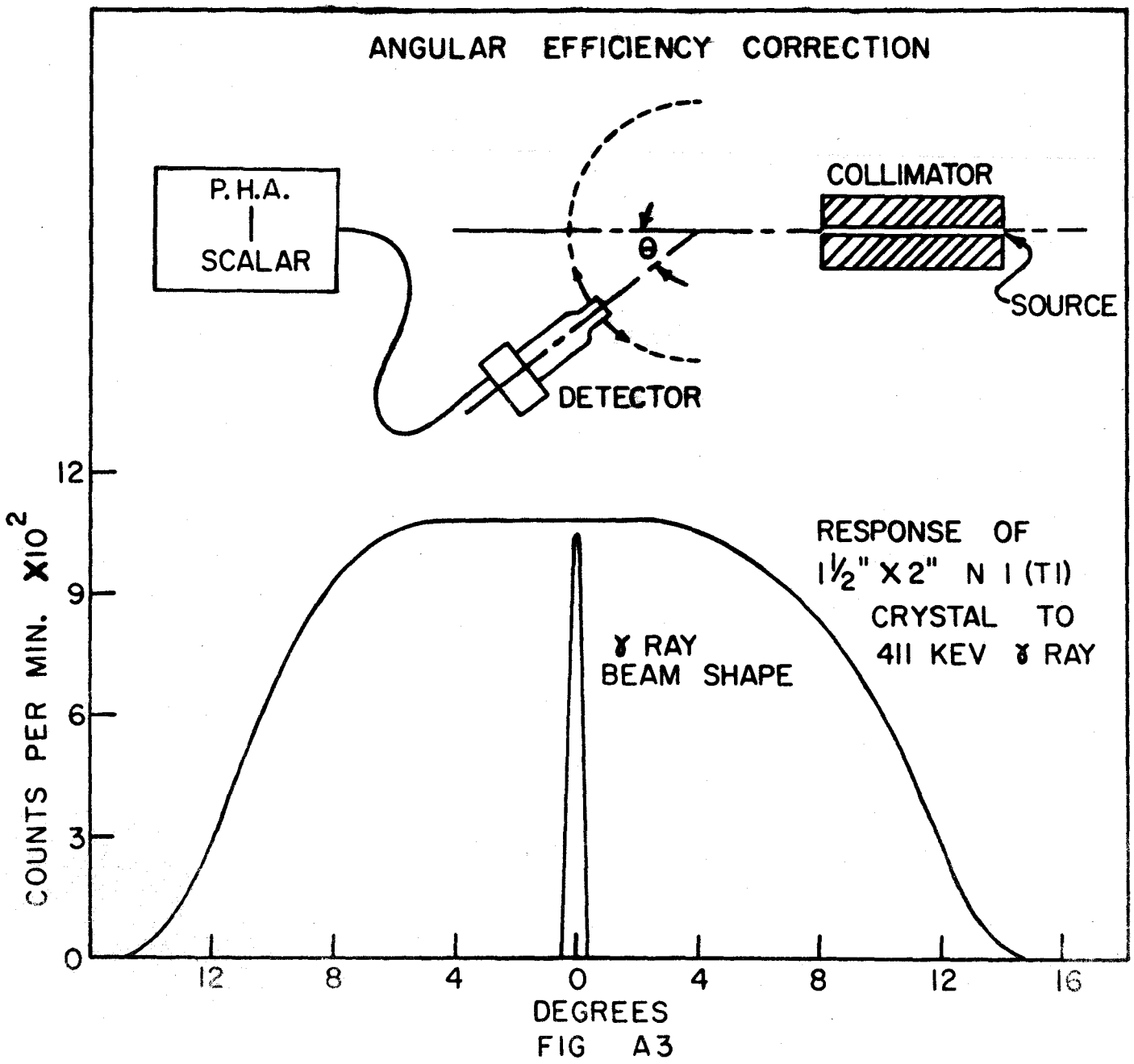
ANGULAR EFFICIENCY CORRECTION
P. H. A.
SCALAR
COLLIMATOR
θ
SOURCE
DETECTOR
COUNTS PER MIN. X10²
12
9
6
3
0
RESPONSE OF
1½" X 2" N I (Tl)
CRYSTAL TO
411 KEV γ RAY
γ RAY
BEAM SHAPE
12
8
4
0
4
8
12
16
DEGREES

FIG A3

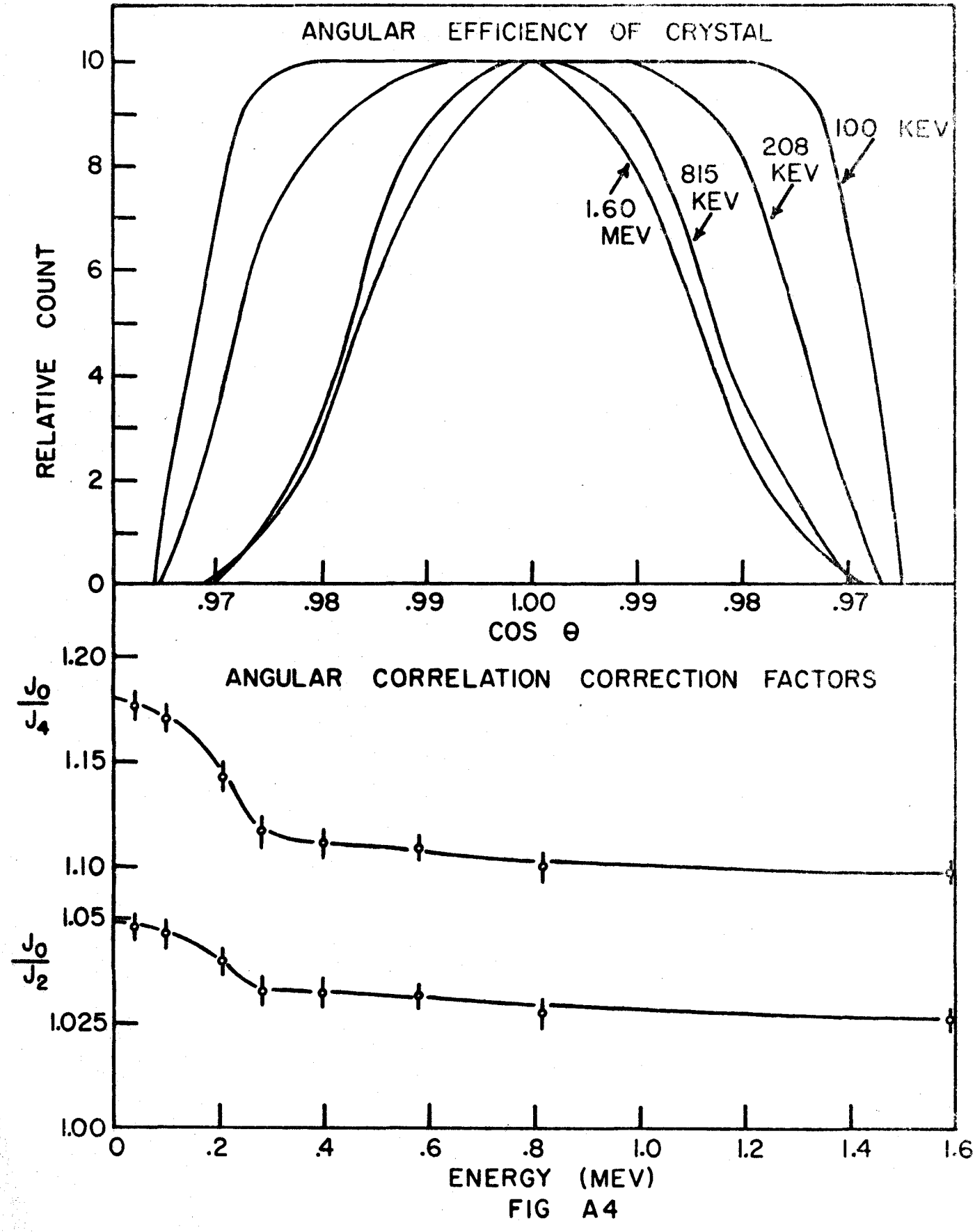
ANGULAR EFFICIENCY OF CRYSTAL
RELATIVE COUNT
10
8
6
4
2
0
100 KEV
208 KEV
815 KEV
1.60 MEV
.97
.98
.99
1.00
.99
.98
.97
COS θ
ANGULAR CORRELATION CORRECTION FACTORS
J4/J0
1.20
1.15
1.10
J2/J0
1.05
1.025
1.00
0
.2
.4
.6
.8
1.0
1.2
1.4
1.6
ENERGY (MEV)

FIG A4

are shown in Figure A4. A similar graph resulted for the other crystal used in the correlation experiments.

From the graphs for the ratio J_2/J_0 of each of the crystals, the correction factor for the coefficient A_2 is found by forming the product of the J_2/J_0 values at the appropriate energies detected in the two detectors. The correction factor for the coefficient A_4 can be similarly determined.

Conclusions

The gamma-gamma coincidence spectrometer has been calibrated for the photopeak detection efficiencies of its crystals over a wide range of gamma ray energies. If an experiment to determine the intensity of a gamma ray is therefore performed when the detectors are 7 cm. from the source, an absolute intensity can be determined. In addition, for experiments conducted with the crystals at some other distance from the source, relative intensity measurements can be made.

The solid angle correction factors for the coefficients of a directional correlation pattern have been experimentally determined for the particular crystals and source-to-detector distance used in this work.

REFERENCES

Alaga, G., Alder, K., Bohr, A., Mottelson, B., (1955); Dan. Mat. Fys. Medd. 29, No. 9.

Alaga, G., (1957); Nucl. Phys. 4, 625.

Alder, K., Bohr, A., Huus, T., Mottelson, B., Winther, A., (1956); Rev. Mod. Phys. 28, 432.

Alder, K., Stech, B., Winther, A., (1957); Phys. Rev. 107, 728.

Arns, R.G., Wiedenbeck, M.L., (1958); Private communication to Beta Spectroscopy Group, McMaster Univ.

Artna, A., (1961); Ph.D. Thesis, McMaster Univ.

Asaro, F., Stephens, F.S., Hollander, J.M., Perlman, I., (1960); Phys. Rev. 117, 492.

Backstrom, G., Bergman, O., Burde, J., Lindfkog, J., (1960); Nucl. Phys. 15, 566.

Baggerly, L.L., Marmier, P., Boehm, F., DuMond, J.W.M., (1955); Phys. Rev. 100, 1364.

Bashilov, A.A., Anton'eva, N.M., Dzhelepov, B.S., (1952); Izvest. Akad. Nauk. SSSR, Ser. Fiz. 16, 264.

Becquerel, H., (1896); Comptes Rendus 122, 1086.

Becquerel, H., (1900); Comptes Rendus 130, 809.

Bell, R.E., Graham, R.L., Petch, H.E., (1952); Can. J. Phys. 30, 35.

Belser, R.B., Hicklin, W.H., (1956); Rev. Sci. Instr. 27, 293.

Berger, M.J., Doggett, J., (1956); Rev. Sci. Instr. 27, 269.

Bethe, H.A., Bacher, R.F., (1936); Rev. Mod. Phys. 8, 82.

Biedenharn, L.C., (1960); "Nuclear Spectroscopy", ed. by F. Ajzenberg-Selove, Academic Press, New York and London.

Bjørnholm, S., Nielsen, O.B., Sheline, R.K., (1959); Phys. Rev. 115, 1613.

Blatt, J.M., Weisskopf, V.F., (1952); "Theoretical Nuclear Physics", John Wiley and Sons, Inc., New York.

Blin-Stoyle, R.S., Grace, M.A., Halban, H., (1955); "Beta- and Gamma-Ray Spectroscopy", ed. by K. Siegbahn, North-Holland Publishing Co., Amsterdam.

Bohr, A., Mottelson, B.R., (1953); Dan. Mat. Fys. Medd. 27, No. 16.

Bohr, A., Mottelson, B.R., (1960); "Nuclear Spectroscopy", ed. by F. Ajzenberg-Selove, Academic Press, New York and London.

Bohr, N., (1913); Phil. Mag. 26, 1.

Brady, E.L., Deutsch, M.I., (1947); Phys. Rev. 72, 870.

Brady, E.L., Deutsch, M.I., (1948); Phys. Rev. 74, 1541.

Brink, D.M., (1960); Progr. in Nucl. Phys. 8, 99.

Butt, D.K., Nicholson, P.W., (1962); Nucl. Phys. 31, 460.

Chadwick, J., (1932); Proc. Roy. Soc. A 136, 692.

Chapman, G.J.S., Gregory, J.M., Hill, R.W., Johns, M.W., (1961); Proc. Roy. Soc. A 262, 541.

Church, E.L., Weneser, J., (1960); Ann. Rev. of Nucl. Sci. 10, 193.

Church, E.L., Weneser, J., (1961); Nucl. Phys. 28, 602.

Dagley, P., Grace, M.A., Hill, J.S., Sowter, C.V., (1958); Phil. Mag. 3, 489.

Davydov, A.S., Fillipov, G.F., (1959); Nucl. Phys. 8, 237.

Davydov, A.S., Chaban, A.A., (1960); Nucl. Phys. 20, 499.

Davydov, A.S., (1961); Nucl. Phys. 24, 682.

DePasquali, G., Frauenfelder, H., Margulies, S., Peacock, R.N., (1960); Phys. Rev. Letters 4, 71.

Deutsch, J.P., Doumont, G., Macq, P.C., (1958); Ann. Soc. Sci. Bruxelles, Ser III, 2, 192.

Devons, S., Goldfarb, L.J.B., (1957); Handbuch der Physik 42, 362.

Ellis, C.D., Wooster, W.A., (1927); Proc. Roy. Soc. A 117, 109.

Fano, U., (1952); "Statistical Matrix Techniques and Their Application to the Directional Correlations of Radiations", National Bureau of Standards Report, U.S. Dept. of Commerce.

Fermi, E., (1934); Z. Phys. 88, 161.

Frauenfelder, H., (1955); "Beta- and Gamma-Ray Spectroscopy", ed. by K. Siegbahn, North-Holland Publishing Co., Amsterdam.

Gallagher Jr., C.J., Thomas, T.D., (1959); Nucl. Phys. 14, 1.

Gamow, G., Teller, E., (1936); Phys. Rev. 49, 895.

Geiger, J., (1962); Private communication to Beta Spectroscopy Group, McMaster Univ.

Gerholm, T.R., (1955); Rev. Sci. Instr. 26, 1069.

Gerholm, T.R., Pettersson, B.G., Van Nooijen, B., Grabowski, Z., (1961); Nucl. Phys. 24, 127.

Goeppert-Mayer, M., (1953); "Beta- and Gamma-Ray Spectroscopy", ed. by K. Siegbahn, North-Holland Publishing Co., Amsterdam.

Goldhaber, M., Sunyar, A.W., (1951); Phys. Rev. 83, 906.

Goldhaber, M., Sunyar, A.W., (1955); "Beta- and Gamma-Ray Spectroscopy", ed. by K. Siegbahn, North-Holland Publishing Co., Amsterdam.

Goldhaber, M., Weneser, J., (1955); Ann. Rev. of Nucl. Sci. 5, 1.

Gray, L.H., (1912); Proc. Roy. Soc. A 87, 489.

Habib, E.E., (1961); Ph. D. Thesis, McMaster Univ., Hamilton.

Hamilton, D.P., (1940); Phys. Rev. 58, 122.

Haxel, O., Jensen, J.H.D., Suess, H.E., (1948); Naturwissenschaften, 35, 376.

Heitler, W., (1947); "The Quantum Theory of Radiation", second edition, Oxford University Press, London.

Hulme, H.R., (1932); Proc. Roy. Soc. A 138, 643.

Johns, M.W., Nablo S.V., (1954); Phys. Rev. 96, 1599.

Johns, M.W., MacArthur, J.D., (1959); Can. J. Phys. 37, 1205.

Kallmann, H., (1947); Natur und Technik July.

Kane, J.V., Pixley, R.E., Schwartz, R.B., Schwarzchild, A., (1960); Phys. Rev. 120, 162.

Kawamura, M., Aoki, A., Hayashi, T., (1958); J. Phys. Soc. Japan 13, 1071.

Kerman, A.K., (1959); "Nuclear Reactions", ed. by P.M. Endt and M. Demeur, North-Holland Publishing Co., Amsterdam.

Kern, J., Backstrom, G., (1960); Nucl. Phys. 19, 461.

Kisslinger, L.S., Sorensen, R.A., (1960); Dan. Mat. Fys. Meed. 32, No. 9.

Kofoed-Hansen, O., (1955); "Beta- and Gamma-Ray Spectroscopy", ed. by K. Siegbahn, North-Holland Publishing Co., Amsterdam.

Konopinski, E.J., Uhlenbeck, G.E., (1941); Phys. Rev. 60, 308.

Konopinski, E.J., (1959); Ann. Rev. of Nucl. Phys. 9, 99.

Kurath, D., (1960); "Nuclear Spectroscopy", ed. by F. Ajzenberg-Selove, Academic Press, New York and London.

Lawson, J.S., Frauenfelder, H., (1953); Phys. Rev. 91, 649.

Lee, T.D., Yang, C.N., (1956); Phys. Rev. 104, 254.

Lide, R.W., Wiedenbeck, M.L., (1959); Phys. Rev. 113, 840.

Mandeville, C.E., Varma, J., Saraf, B., (1955); Phys. Rev. 98, 94.

Marklund, I., Van Nooijen, B., Grabowski, Z., (1960); Nucl. Phys. 15, 533.

Massey, H.S.W., Burhop, E.H.S., (1952); "Electronic and Ionic Impact Phenomena", Oxford University Press, London.

Mayer, M.G., (1948); Phys. Rev. 74, 235.

McGowan, F.K., Stelson, P.H., (1957); Phys. Rev. 106, 522.

Miller, W.F., Reynolds, J., Snow, W.J., (1958); ANL-5902.

Mottelson, B., (1958); "Proceedings of the Rehovoth Conference on Nuclear Structure", ed. by H.J. Lipkin, North-Holland Publishing Co., Amsterdam.

Mraz, J., (1957); Nucl. Phys. 4, 457.

Nathan, O., Hultberg, S., (1958); Nucl. Phys. 10, 118.

Nijgh, G.J., Wapstra, A.H., Van Lieshaut, R., (1959); "Nuclear Spectroscopy Tables", North-Holland Publishing Co., Amsterdam.

Nilsson, S.G., (1955); Dan. Matt. Fys. Medd. 29, No. 16.

Novakov, T., Mladjenovic, M., (1956); Rev. Sci. Instr. 27, 415.

Nuclear Data Tables (1959); N.R.C. 59-2-118, 59-2-121.

Parker, W., DeCroës, M., Sevier Jr., K., (1960); Nucl. Instr. and Methods 7, 22.

Pauli, W., (1925); Z. Phys. 31, 373.

Pauli, W., (1934); Septieme Conseil de Physique Solvay, Noyaux Atomiques, Bruxelles 1933, 324.

Pettersson, B.G., Gerholm, T.R., Grabowski, Z., Van Nooijen, B., (1961); Nucl. Phys. 24, 196.

Post. R.F., Schiff, L.I., (1950); Phys. Rev. 80, 113.

Preston, M.A., (1962); "Physics of the Nucleus", Addison-Wesley, Reading, Mass.

Rainwater, J., (1950); Phys. Rev. 79, 432.

Rose, M.E., Goertzel, G., Spinrad, B., Harr, J., Strong, B., (1949); AECU 550.

Rose, M.E., (1953); Phys. Rev. 91, 610.

Rose, M.E., (1955); "Beta- and Gamma-Ray Spectroscopy", ed. by K. Siegbahn, North-Holland Publishing Co., Amsterdam.

Rose, M.E., (1958); "Internal Conversion Coefficients", North-Holland Publishing Co., Amsterdam.

Rose, M.E., (1960); "Nuclear Spectroscopy", ed. by F. Ajzenberg-Selove, Academic Press, New York and London.

Rossi, B., (1930); Nature 125, 636.

Rutherford, E., Royds, T., (1909); Phil. Mag. 17, 281.

Rutherford, E., (1911); Phil. Mag. 21, 669.

Rutherford, E., Robinson, H., Rawlinson, W.F., (1914); Phil. Mag. 28, 281.

Scharenberg, R.P., Stewart, M.G., Wiedenbeck, M.L., (1956); Phys. Rev. 101, 689.

Schmidt, T., (1937); Z. Phys. 106, 358.

Shiel, V., Wyly, L.D., Braden, C.H., (1957); Phys. Rev. 105, 1521.

Shiel, V., Wyly, L.D., Braden, C.H., (1958); Bull. Am. Phys. Soc. 3, 296.

Simons, L., Spring, E., Wendt, D., (1962); Nucl. Phys. 31, 452.

Sliv, L.A., Band, I.M., (1956), (1958); "Coefficients of Internal Conversion of Gamma Radiation", The Academy of Sciences, Leningrad.

Strong, J., (1938); "Procedures in Experimental Physics", Prentice-Hall, Inc., New York.

Taylor, H.W., Pringle, R.W., (1955); Phys. Rev. 90, 1345.

Taylor, H.W., McPherson, R., (1960), (1961); Private communication to Beta Spectroscopy Group, McMaster Univ.

Von Baeyer, O., Hahn, O., Meitner, L., (1912); Z. Phys. 13, 364.

Wehner, G.K., (1954); J. Appl. Phys. 25, 270.

Weisskopf, V.F., (1951); Phys. Rev. 83, 1073.

Wilkinson, D.H., (1960); "Nuclear Spectroscopy", ed. by F. Ajzenberg-Selove, Academic Press, New York and London.

Wu, C.S., (1955); "Beta- and Gamma-Ray Spectroscopy", ed. by K. Siegbahn, North-Holland Publishing Co., Amsterdam.

Wu, C.S., Ambler, E., Hayward, R.W., Hoppes, D.D., Hudson, R.D., (1957); Phys. Rev. 105, 1413.